FROM CO_2 EMISSIONS TO FUELS AND CHEMICALS: CURRENT DEVELOPMENT, CHALLENGES AND PERSPECTIVES

EDITED BY: Adele Brunetti, Simon Roussanaly, Juliana Monteiro, Claudio Pistidda and Rahul Anantharaman

PUBLISHED IN: Frontiers in Chemical Engineering

frontiers Research Topics

frontiers

ISSN 1664-8714
ISBN 978-2-88974-035-2
DOI 10.3389/978-2-88974-035-2

About Frontiers

Frontiers is more than just an open-access publisher of scholarly articles: it is a pioneering approach to the world of academia, radically improving the way scholarly research is managed. The grand vision of Frontiers is a world where all people have an equal opportunity to seek, share and generate knowledge. Frontiers provides immediate and permanent online open access to all its publications, but this alone is not enough to realize our grand goals.

Frontiers Journal Series

The Frontiers Journal Series is a multi-tier and interdisciplinary set of open-access, online journals, promising a paradigm shift from the current review, selection and dissemination processes in academic publishing. All Frontiers journals are driven by researchers for researchers; therefore, they constitute a service to the scholarly community. At the same time, the Frontiers Journal Series operates on a revolutionary invention, the tiered publishing system, initially addressing specific communities of scholars, and gradually climbing up to broader public understanding, thus serving the interests of the lay society, too.

Dedication to Quality

Each Frontiers article is a landmark of the highest quality, thanks to genuinely collaborative interactions between authors and review editors, who include some of the world's best academicians. Research must be certified by peers before entering a stream of knowledge that may eventually reach the public - and shape society; therefore, Frontiers only applies the most rigorous and unbiased reviews.
Frontiers revolutionizes research publishing by freely delivering the most outstanding research, evaluated with no bias from both the academic and social point of view. By applying the most advanced information technologies, Frontiers is catapulting scholarly publishing into a new generation.

What are Frontiers Research Topics?

Frontiers Research Topics are very popular trademarks of the Frontiers Journals Series: they are collections of at least ten articles, all centered on a particular subject. With their unique mix of varied contributions from Original Research to Review Articles, Frontiers Research Topics unify the most influential researchers, the latest key findings and historical advances in a hot research area! Find out more on how to host your own Frontiers Research Topic or contribute to one as an author by contacting the Frontiers Editorial Office: frontiersin.org/about/contact

FROM CO_2 EMISSIONS TO FUELS AND CHEMICALS: CURRENT DEVELOPMENT, CHALLENGES AND PERSPECTIVES

Topic Editors:
Adele Brunetti, National Research Council (CNR), Italy
Simon Roussanaly, SINTEF Energy Research, Norway
Juliana Monteiro, Netherlands Organisation for Applied Scientific Research, Netherlands
Claudio Pistidda, Helmholtz-Zentrum hereon GmbH, Institute of Hydrogen Technology, Department of Materials Design, Max-Planck-Straße 1, 21502, Geesthacht, Germany
Rahul Anantharaman, SINTEF Energy Research, Norway

Citation: Brunetti, A., Roussanaly, S., Monteiro, J., Pistidda, C., Anantharaman, R., eds. (2021). From CO_2 Emissions to Fuels and Chemicals: Current Development, Challenges and Perspectives. Lausanne: Frontiers Media SA.
doi: 10.3389/978-2-88974-035-2

Table of Contents

frontiers in Chemical Engineering

EDITORIAL
published: 09 August 2021
doi: 10.3389/fceng.2021.747399

Editorial: From CO_2 Emissions to Fuels and Chemicals: Current Development, Challenges and Perspectives

Adele Brunetti[1]*, *Simon Roussanaly*[2], *Juliana Monteiro*[3], *Rahul Anantharaman*[2] and *Claudio Pistidda*[4]

[1]National Research Council—Institute on Membrane Technology (ITM-CNR), Rende, Italy, [2]Gas Technology Department, SINTEF Energy Research, Trondheim, Norway, [3]TNO, Amsterdam, Netherlands, [4]Department of Materials Design, Institute of Hydrogen Technology, Helmholtz-Zentrum Hereon GmbH, Geesthacht, Germany

Keywords: CO_2, Separation, conversion, capture, emission reduction

Editorial on Research Topic

From CO_2 Emissions to Fuels and Chemicals: Current Development, Challenges and Perspectives

Carbon capture and utilization (CCU) is attracting considerable attention as a new way to reduce release of greenhouse gases to the atmosphere while valorising CO_2 through the production of fuels and green chemical intermediates [1].

Over the past decades, significant effort has been targeted at developing and demonstrating at large-scale CO_2 capture from power and industrial sources [2]. To accelerate deployment, further efforts are taking place to reduce energy penalties and costs of such a process, as well as scale-up promising solutions. However, one of the key hurdles for implementation remains the destination of these huge CO_2 streams. While CO_2 storage has been shown to be, by far, the main option to ensure permanent sequestration of the amount of CO_2 to be captured [3], integrating CO_2 capture and storage can be challenging, especially in the near term, due to the distances between sources and sinks, the time required to develop such geological sinks, scale mismatches, etc. While it is expected to play a smaller role than CO_2 storage, CO_2 utilization remains an interesting sink for captured CO_2 as it creates opportunities for new revenue streams. Furthermore, CO_2 utilization can also be considered for small capture flowrates which make it an interesting solution in the case of early deployment. There are many potential routes to convert CO_2 into useful and, hopefully, more sustainable chemicals and fuels. For example, converting CO_2 into polyols could enable the production of more sustainable elastomers, fibers, flexible foam, adhesives, sealants, inks, paints, and coatings. Another route that can be considered is the conversion of CO_2 in valuable energy carriers such as methane, methanol, etc., which could be an attractive CCU solution while simultaneously addressing global warming and storing of hydrogen energy or renewable energy in commonly used dense energy carriers [4–6]. However, for all the routes and targeted products, it is important to ensure that CCU pathways deliver the three following aspects: 1) sustainable cradle-to-grave solutions 2) economically viable solutions 3) scalable solutions.

In this Research Topic, we aimed to make a picture of the knowledge of the current progress in the area of CO_2 capture and conversion techniques.

In particular, Skoricova et al. proposed the techno-economic assessment of the sorption-enhanced dimethyl-ether (DME) synthesis process, as an innovative way for producing fuel-grade DME from carbon dioxide and green H_2. They found that the production cost for DME was ~€1.3 per kg for a relatively small-scale production plant of 23 kt/year. Although higher than the current market price for fossil-based DME, the results showed the potential of this route as more

OPEN ACCESS

Edited and reviewed by:
Eric Favre,
Université de Lorraine, Nancy, France

***Correspondence:**
Adele Brunetti
a.brunetti@itm.cnr.it

Received: *26 July 2021*
Accepted: *28 July 2021*
Published: *09 August 2021*

Citation:
Brunetti A, Roussanaly S, Monteiro J, Anantharaman R and Pistidda C (2021) Editorial: From CO_2 Emissions to Fuels and Chemicals: Current Development, Challenges and Perspectives. Front. Chem. Eng. 3:747399. doi: 10.3389/fceng.2021.747399

promising than other studies on DME production from CO_2 by conventional DME synthesis processes.

Biermann et al. discussed the effects of carbon allocation on the emission intensities of low-carbon products cogenerated in facilities that co-process biogenic and fossil feedstocks and apply the carbon capture utilization and storage technology. They considered an integrated steel mill that injects biomass into the blast furnace, captures CO_2 for storage, and ferments CO into ethanol from the blast furnace gas, obtaining an overall emissions saving up to 27 and 47% in the near-term and long-term future, respectively, and confirming that the choice of the allocation scheme greatly affects the emissions intensities of cogenerated products.

Fu et al. proposed an investigation of calcium looping capture for the Natural Gas Combined Cycle through a techno-economic study evaluating one simple and one advanced calcium looping processes for CO_2 capture. The analysis demonstrated that the calcium looping processes are not competitive with the reference MEA-based CO_2 capture process for this application, and would require significant improvements in terms of equipment capital cost, plant efficiency and sorbent annual cost.

Schellevis et al. investigated the CO_2 capture from the atmosphere *via* Direct Air Capture using solid supported-amine sorbents, evaluating the possibility of a continuous adsorption process in a radial flow contactor, using both batch and continuous modes of operation. A 15–25% lower capture efficiency was found for the continuous process, confirming that the batch process is preferred in most of the operating conditions.

The Research Topic ends with the study of Castel et al. who proposed interesting guidelines on the possibilities and limitations of the use of membrane technology for Direct Carbon Dioxide Capture from air. They found that a fundamental requirement to make this technology competitive is the use of highly selective membranes that can assure higher productivity levels, even if the specific energy requirement is globally higher than that of the adsorption and absorption processes.

The guest editors wish to thank all the authors for their valuable contributions, as well as, all the reviewers for the tremendous efforts given to guarantee a high-quality review process required to achieve the most appropriate decisions on the evaluated manuscripts. Finally, we would like to sincerely express our gratitude to Prof. Eric Favre and the whole editorial team of Frontiers in Chemical Engineering for their continuous support.

AUTHOR CONTRIBUTIONS

All authors listed have made a substantial, direct, and intellectual contribution to the work and approved it for publication.

REFERENCES

1. IEA (2019). *Putting CO_2 to Use*. Paris: IEA. Available at: https://www.iea.org/reports/putting-co2-to-use (Accessed July 14, 2021).
2. IEA (2020). *CCUS in Clean Energy Transitions*. Paris: IEA. Available at: https://www.iea.org/reports/ccus-in-clean-energy-transitions (Accessed July 14, 2021).
3. Mac Dowell, N., Fennell, P. S., Shah, N., and Maitland, G. C. (2017). The Role of CO2 Capture and Utilization in Mitigating Climate Change. *Nat. Clim Change* 7, 243–249. doi:10.1038/nclimate3231
4. Mazari, S. A., Hossain, N., Basirun, W. J., Mubarak, N. M., Abro, R., Sabzoi, N., et al. (2021). An Overview of Catalytic Conversion of CO2 into Fuels and Chemicals Using Metal Organic Frameworks. *Process Saf. Environ. Prot.* 149, 67–92. doi:10.1016/j.psep.2020.10.025
5. Monteiro, J., Goetheer, E., Schols, E., van Os, P., Perez Calvo, J. F., Hoppe, H., et al. (2018). H2020 CEMCAP D5.1 Post-capture CO_2 Management: Options for the Cement Industry. Zenodo. doi:10.5281/zenodo.2597056
6. Peng, W., Chuong Nguyen, T. H., Nguyen, D. L. T., Wang, T., Van Thi Tran, T., Le, T. H., et al. (2021). A Roadmap Towards the Development of Superior Photocatalysts for Solar- Driven CO2-to-Fuels Production. *Renew. Sustain. Energ. Rev.* 148, 111298. doi:10.1016/j.rser.2021.111298

Conflict of Interest: The authors declare that the research was conducted in the absence of any commercial or financial relationships that could be construed as a potential conflict of interest.

frontiers in Chemical Engineering

ORIGINAL RESEARCH
published: 20 November 2020
doi: 10.3389/fceng.2020.596555

CO_2 Capture From Air in a Radial Flow Contactor: Batch or Continuous Operation?

Michel Schellevis, Tim Jacobs and Wim Brilman*

Sustainable Process Technology, Faculty of Science and Technology, University of Twente, Enschede, Netherlands

The capture of CO_2 from the atmosphere via Direct Air Capture using solid supported-amine sorbents is an important option to reduce the atmospheric concentration of CO_2. It addresses CO_2 emissions from dispersed sources and delivers a location independent, sustainable carbon source. This study evaluates the possibility for a continuous adsorption process for direct air capture in a radial flow contactor, using both batch and continuous mode of operation. Gas and solid flow were varied to determine hydrodynamic feasible operating conditions. The operation modes are compared by their capture efficiencies in the optimal adsorption time range of 0.5 t^B_{sto} and 1.5 t^B_{sto}. A 15–25% lower capture efficiency is found for a continuous process compared to a batch process in the relevant range for direct air capture. This decline in gas-solid contact efficiency is more pronounced at longer adsorption time and higher superficial gas velocity. Overall, a batch process is preferred over a continuous process in the majority of operating conditions.

Keywords: direct air capture, radial flow adsorber, supported amine sorbents, adsorption, moving bed adsorber

OPEN ACCESS

Edited by:
Adele Brunetti,
National Research Council (CNR), Italy

Reviewed by:
Mohammad Younas,
University of Engineering & Technology Peshawar, Pakistan
Jun Gao,
Shandong University of Science and Technology, China

****Correspondence:***
Michel Schellevis
h.m.schellevis@utwente.nl

Specialty section:
This article was submitted to Separation Processes, a section of the journal Frontiers in Chemical Engineering

Received: *19 August 2020*
Accepted: *14 October 2020*
Published: *20 November 2020*

Citation:
Schellevis M, Jacobs T and Brilman W (2020) CO_2 Capture From Air in a Radial Flow Contactor: Batch or Continuous Operation?. Front. Chem. Eng. 2:596555. doi: 10.3389/fceng.2020.596555

INTRODUCTION

Direct air capture (DAC) is the extraction of CO_2 directly from the atmosphere. It is considered a core element in reducing global CO_2 emissions (Lackner et al., 2012). Capturing CO_2 from air has the ability to: 1) mitigate CO_2 emissions from dispersed sources, which contribute for approximately 45% of the total CO_2 emissions in the US (USEPA, 2018), 2) deliver, anywhere, a renewable carbon source for carbon-neutral processes and 3) enable other carbon-negative products/technologies.

Even though we consider the CO_2 concentration in air to be (too) high, it is very low regarding separation purposes. Therefore, a highly selective separation process is required. Adsorption is among the most promising technologies to capture CO_2 from air (Goeppert et al., 2012; Brilman and Veneman, 2013; Lu et al., 2013; Sanz-Pérez et al., 2016; Yang et al., 2019; Stampi-Bombelli et al., 2020). Research on the development of adsorption materials is widely available in literature (Choi et al., 2009; D'Alessandro et al., 2010; Shekhah et al., 2014; Kumar et al., 2015; Sanz-Pérez et al., 2016; Gelles et al., 2020; Singh et al., 2020). Selective adsorption of CO_2 onto the sorbent is usually based on a chemical reaction of CO_2 with functional groups on the sorbents internal surface. Amines in particular are suitable for CO_2 capture, as is evident from the benchmark CO_2 absorption process using an aqueous ethanolamine solution (Topham et al., 2014). Caplow (1968), and later Danckwerts (1979), proposed a two-step reaction mechanism for reaction of amines with CO_2 via the formation of a zwitterion (Caplow, 1968; Danckwerts, 1979). The zwitterion is then deprotonated by a base. On the other hand, Crooks and Donnellan (1989) proposed a termolecular mechanism where the reaction occurs in a single step. CO_2 reacts simultaneously with the amine and with a base. They claim the termolecular mechanism is more likely than the zwitterion mechanism. Experimental

results from Mukherjee et al. (2018) support this statement for the reaction of CO_2 with benzylamine in an aqueous environment.

The sorbent used in this study has a polystyrene backbone with above mentioned benzylamine as functional group attached. The sorbent is able to capture CO_2 at both dry and humid conditions. At humid conditions, depending on humidity, the CO_2 capacity is up to 50% higher, suggesting that both carbamate formation and bicarbonate formation play a role.

A complete adsorption process cycle consists of two steps. The first step is the adsorption of CO_2 onto the surface of the sorbent. This is preferred at ambient conditions, since large volumes are processed (at least 1,400 m^3 for 1 kg of CO_2) and a pre-treatment would be energy intensive. The second step is the regeneration of the sorbent. In this latter phase, the product gas is collected and lean sorbent is obtained for reuse in the adsorption step. The reaction of CO_2 with the amine can be reversed by a temperature and/or pressure swing (Bos et al., 2018; Elfving et al., 2021). In this research, we focus on the adsorption step of a sorbent-based DAC process.

Efficient gas-solid contacting is an important aspect of the DAC process, especially for the adsorption phase. Contactors for DAC include monolith (Kulkarni and Sholl, 2012), fluidized bed (Zhang et al., 2014) and fixed bed (Wurzbacher et al., 2012; Bajamundi et al., 2019; Yu and Brilman, 2020), of which the latter one is the most common. During adsorption, the sorbent material remains fixed in the reactor during the process. In the systems of Bajamundi et al. (2019) and Wurzbacher et al. (2012), sorbent regeneration occurs in the same reactor where the operating conditions are changed. As alternative, the sorbent itself can be transported between separate adsorption and desorption units, as utilized in the study of Yu and Brilman (2020). This limits the energy penalty for temperature swing regeneration as only the sorbent material needs to be heated, instead of the whole contactor.

Yu and Brilman (2020) designed a direct air capture system using a radial flow contactor with the option of sorbent circulation. Adsorption was performed in batches, where the complete sorbent batch was transported to the regeneration section at once. Freshly regenerated sorbent was then loaded to the radial flow contactor. This system also allows for full continuous operation as a cross-flow moving bed. In that study, a single run demonstrated the technical feasibility, but also a significant reduction in capture efficiency. In this work, we revisit this option to investigate opportunities for performance improvement.

Moving bed contactors are well suitable for processes with a rapid, but reversible decay in activity of the solid material. In chemical reaction technology, this situation is encountered when dealing with rapid catalyst deactivation (Ginestra and Jackson, 1985; Pilcher and Bridgwater, 1990; Shirzad et al., 2019). In adsorption technology, like here for DAC, a similar rapid decrease in activity occurs due to saturation of the sorbent. Moving bed contactors are already considered for post-combustion CO_2 capture (Kim et al., 2013; Grande et al., 2017; Mondino et al., 2019). However, these employ a counter-current moving bed, whereas this study concerns a cross-flow moving bed. In a cross-flow moving bed contactor, the gas flow is perpendicular to the solid flow, which results in a drag force that acts upon the particles. Under certain process conditions this leads to undesired hydrodynamic phenomena known as "pinning" and "cavity" (Ginestra and Jackson, 1985; Doyle et al., 1986; Pilcher and Bridgwater, 1990; Long et al., 2015; Wang et al., 2020). The drag force exerted by the cross flow gas stream on the particles results in a friction force of the solids on the downstream (with respect to the gas flow) porous wall. At a sufficiently high gas velocity, this (partially or completely) prevents the solids from moving downwards. This phenomenon is known as "pinning". A "cavity" may form between the upstream porous wall and the solids, thus reducing the effective bed length. As a result local gas bypassing will occur, which lowers the efficiency of the process.

Research into the hydrodynamics of a moving bed contactor started in the 1980s where Ginestra and Jackson (1985) analyzed the mechanism of "pinning" and "cavity" of a rectangular cross flow moving bed. Doyle et al. (1986) extended this analysis to a radial flow moving bed, since this configuration is more common for industrial applications. Pilcher and Bridgwater (1990) further investigated the mechanism of "pinning" by varying particle size and bed thickness and observed four distinct modes of pinning. In addition, they mention several other parameters that can influence the flow pattern of the solids such as solid distribution at the inlet and packing structure near the porous walls. Long et al. (2015) proposes a trapezoidal cross-flow moving bed, which significantly increases the critical gas velocity for "pinning" compared to a rectangular configuration. Another optimization is proposed by Wang et al. (2020), in which gas-solid baffles are placed in the middle of the bed that reduces pinning and cavity. However, the effect of the before mentioned phenomena on the actual performance and potential of the moving bed system is not discussed. In this study, we assess the possibility of performing direct air capture in a radial flow moving bed contactor. This is done by comparing the capture efficiency of this continuous system with that of the corresponding batch wise operated system. Therefore, we do not investigate whether phenomena like "pinning" and "cavity" occur. Instead, we investigate the magnitude of their influence within the desired operating range of direct air capture on the capture performance.

MATERIALS AND METHODS

Materials

The sorbent material used in this study is Lewatit® VP OC 1065 (Lanxess). This is a polymeric, amine-functionalized sorbent with polystyrene-divinylbenzene copolymer as support and primary benzyl amines as functional groups. Using energy-dispersive X-ray spectroscopy, Alesi et al. (Alesi and Kitchin, 2012) determined the concentration of these functional groups at 7.5 mol/kg. Other physical properties of the sorbent can be found in **Table 1**. The sorbent was prepared in a two-step process, which is only required upon first use of the sorbent. In the first step, excess water is removed, since the sorbent originally, as purchased, contains up to 50 wt% water. For this, the sorbent is placed in an oven (80°C) under nitrogen flow for at least 16 h. Approximately 98% of the adsorbed water is removed. In the second step, a small amount of graphite (~0.3 wt%) is

TABLE 1 | Physical properties of Lewatit® VP OC 1065.

Property	Value		Ref
Particle size (average)	668	μm	(Driessen et al., 2020a)
Bulk density	533	$kg_s\ m_r^{-3}$	(Driessen et al., 2020b)
Particle density	861	$kg_s\ m_s^{-3}$	(Driessen et al., 2020b)
BET surface area	50	m^2g^{-1}	(Lanxess, 2017)
Pore volume	0.27	cm^3g^{-1}	(Lanxess, 2017)
Pore size	25	nm	(Lanxess, 2017)
Heat capacity	1.5	kJ $kg^{-1}K^{-1}$	(Alesi and Kitchin, 2012)

mixed with the sorbent to reduces the static effects during sorbent handling.

The stability of the sorbent is validated to make sure that the quality of the sorbent does not decrease over time. A sample is taken at several time intervals during the experiments and the capacity is determined by thermogravimetric analysis. The CO_2 capacity of the sorbent is measured at 1.76 ± 0.04 mol/kg at 40°C and 15% CO_2 in N_2. The performance of the sorbent did not decrease over time (**Figure 1**).

In all adsorption experiments, air is sucked in directly from the laboratory. The air composition (CO_2 concentration and humidity) is affected by weather conditions, lab use and air ventilation. In all desorption experiments, high purity N_2 is used.

Batch Experiments

Batch (or fixed bed) experiments are used as reference point for the continuous experiments. The experimental set-up is shown in **Figure 2**. The gas-solid contactor is a π-type radial flow contactor with inwards flow. The sorbent is contained between two porous faces with a mesh size of 400 μm. Yu and Brilman (2017) designed this contactor specifically for direct air capture. In this respect, a bed length of 40 cm and bed thickness of only 1.5 cm is selected, which enables operation at a low pressure drop. This results in an effective sorbent mass of 1.72 kg. Also, some sorbent is present in the volume between the radial flow part of the reactor and the rotary valve, which results in a total sorbent mass of approximately 2 kg. During adsorption, the air flow is controlled by a centrifugal fan (ER 120, Itho Daalderop). The CO_2 concentration, temperature and pressure drop are measured. Two CO_2 analyzers (LI-COR LI840A) determine the CO_2 concentration in the inlet and outlet of the contactor, the temperature is monitored at three location in the sorbent bed (4, 19, and 36 cm from sorbent inlet) and in the ingoing air and, finally, the pressure drop between the inner and outer channel is measured with a differential pressure transmitter (DMD 341 from DB SENSORS).

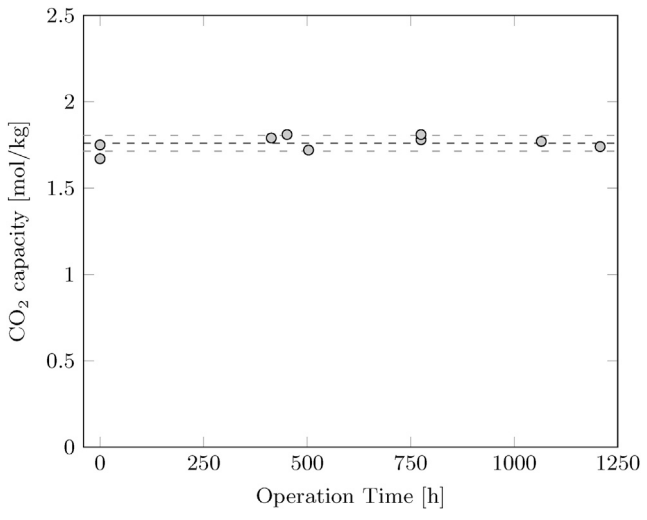

FIGURE 1 | CO_2 capacity of the sorbent as function of operation time. The capacity is determined by thermogravimetric analysis at 40°C and 15% CO_2 in N_2. The average CO_2 capacity is 1.76 mol/kg with a standard deviation of 0.04 mol/kg.

Adsorption and sorbent regeneration is performed in the radial flow contactor, so the same sorbent batch is used for all batch experiments. The sorbent is regenerated before all adsorption experiments. For this, a temperature of 100°C and a nitrogen flow of 70 NL/min (0.55 cm/s) is used. Regeneration is continued until the CO_2 concentration in the outlet is below 10 ppm. This corresponds to an equilibrium capacity of approximately 2 mmol/kg. Batch adsorption experiments are performed for a superficial gas velocity of 0.10–0.40 m/s, corresponding to a Reynolds number of 4.2–17.8. Adsorption is continued until equilibrium is reached.

Continuous Experiments

Continuous (or moving bed) experiments are carried out in the same set-up as batch experiments (**Figure 2**). The experiments are very similar to ones in the batch mode of operation, except that the solid particles are continuously added to and withdrawn from the contactor. The solid flux is driven by gravity and controlled with a rotary valve by adjusting the motor voltage. Steady-state operation is expected to begin after all sorbent in the contactor is replaced once with freshly added (regenerated) sorbent and this steady-state was maintained for another sorbent residence time. This procedure thus requires an available amount of sorbent of at least three times the sorbent hold-up of the contactor (hence, around 6 kg). The experiments are continued until all sorbent passed the contactor through the rotary valve. The performance of the moving bed configuration is evaluated between $t = \tau_s^C$, the average sorbent residence time, and $2\tau_s^C$. The solid flux is varied between 60 and 275 $g/m^2/s$. Regeneration follows the same procedure as for the fixed bed experiments, to ensure a fair comparison between the different types of experiments. The regeneration was carried out in three batches, since three times as much sorbent is required here. The regenerated sorbent is stored in a closed container under nitrogen atmosphere, to avoid adsorption of CO_2 during storage.

Methodology

The basis of this study is to compare the performance of the continuous operation with batch operation. Therefore, a methodology is required to fairly compare these results. As performance indicators, the gas- and solid efficiencies are used. The gas efficiency is defined as the fraction of CO_2 that is captured from the air that is supplied (**Eq. 1**) and the solid

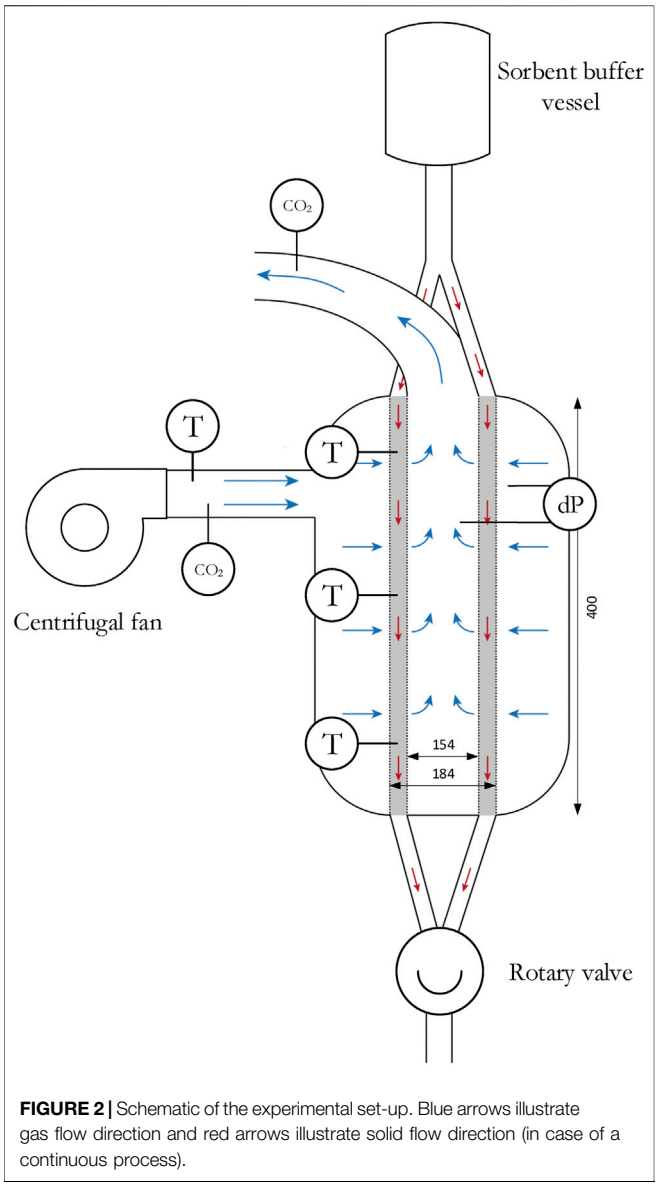

FIGURE 2 | Schematic of the experimental set-up. Blue arrows illustrate gas flow direction and red arrows illustrate solid flow direction (in case of a continuous process).

efficiency is defined as the saturation level of the sorbent (**Eq. 2**). In both **Eqs 1** and **2**, we neglect the effect of the reduced CO_2 concentration on the total gas flow rate. For batch operation, these are a function of time, since the sorbents get saturated as the adsorption progresses. Therefore, the solid efficiency increases with time. This results in a lower driving force for adsorption and, hence, a lower adsorption rate and decreasing gas efficiency over time. During continuous operation, on the other hand, a steady state situation is reached. Therefore, the continuous operated system results in a single gas and solid efficiency (**Eqs 3** and **4**, again, neglecting the effect of reduced CO_2 concentration on the total gas flow rate).

$$\eta_g^B = \frac{\int_0^{t_{\text{ads}}^B} \left(C_{\text{CO}_2}^{\text{in}} - C_{\text{CO}_2}^{\text{out}}\right) dt}{\int_0^{t_{\text{ads}}^B} C_{\text{CO}_2}^{\text{in}}\, dt} \tag{1}$$

$$\eta_s^B = \frac{q(t)}{q_{\text{eq}}} = \frac{\phi_{V,g} \int_0^{t_{\text{ads}}^B} \left(C_{\text{CO}_2}^{\text{in}} - C_{\text{CO}_2}^{\text{out}}\right) dt}{m_s\, q_{\text{eq}}} \tag{2}$$

$$\eta_g^C = 1 - \frac{C_{\text{CO}_2}^{\text{out}}}{C_{\text{CO}_2}^{\text{in}}} \tag{3}$$

$$\eta_s^C = \frac{\phi_{V,g}\left(C_{\text{CO}_2}^{\text{in}} - C_{\text{CO}_2}^{\text{out}}\right)}{\phi_{M,s}\, q_{\text{eq}}} \tag{4}$$

A comprehensible method is required to compare both operation modes. The approach selected here is to process the same amount of sorbent for a given amount of time. In batch operation always the same amount of sorbent is used, whereas for the continuous operation this depends on the solid flux. To compare both process operating modes, the same gas-sorbent contact time is applied, which is calculated with **Eq. 5**. Note that this is not necessarily the real average residence time of the solid sorbent in the contactor since the value of M_s is taken constant, based on the sorbent hold-up during fixed bed operation. The actual sorbent residence time during moving bed operation may therefore be somewhat lower due to a lower solid hold-up.

$$t_{\text{ads}}^B = \tau_s^C = \frac{M_s}{\phi_{M,s}} \tag{5}$$

The adsorption time is normalized by the stoichiometric time. This is the point when the amount of CO_2 fed is equal to the maximum amount of CO_2 that can be adsorbed. The stoichiometric time concept was shown to be very useful for the optimization of a direct air capture process (Yu and Brilman, 2017).

For a batch process the stoichiometric time is calculated by **Eq. 6**. For a continuous process it is not possible to define a stoichiometric time, but is merely operating at a certain normalized adsorption time. This is found by combining **Eqs. 5** and **6** to obtain **Eq. 7**. This is the ratio of the CO_2 supply rate and the maximum CO_2 removal rate.

$$t_{\text{sto}}^B = \frac{M_s q_e}{\phi_{V,g} C_{\text{CO}_2}^{\text{in}}} \tag{6}$$

$$\frac{\tau_s^C}{t_{\text{sto}}^B} = \frac{\phi_{V,g} C_{\text{CO}_2}^{\text{in}}}{\phi_{M,s} q_{\text{eq}}} \tag{7}$$

By combining **Eqs 1**–**7**, the following relation is found:

$$\frac{t_{\text{ads}}^B}{t_{\text{sto}}^B} = \frac{\eta_s^B}{\eta_g^B} = \frac{\tau_s^C}{t_{\text{sto}}^B} = \frac{\eta_s^C}{\eta_g^C} \tag{8}$$

RESULTS

Batch Operation

Batchwise adsorption experiments were performed in the radial flow contactor for a superficial velocity of 0.10–0.40 m/s. **Figure 3**

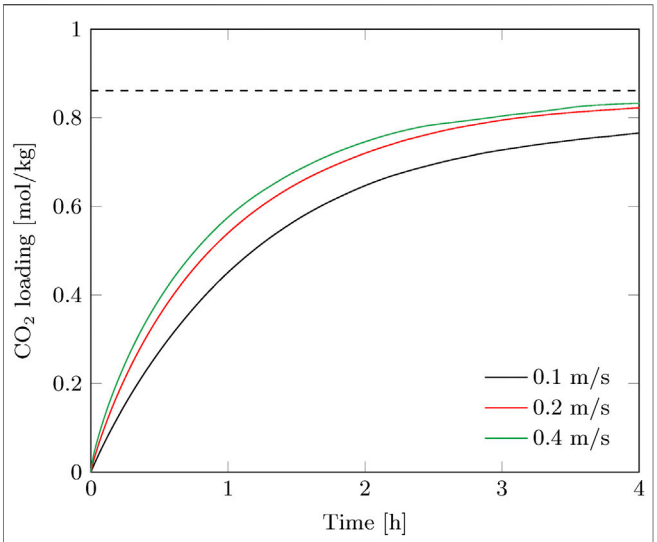

FIGURE 3 | Breakthrough curves of the batch experiments for various superficial gas velocities. The equilibrium capacity at direct air capture conditions under the prevailing lab conditions is indicated as well.

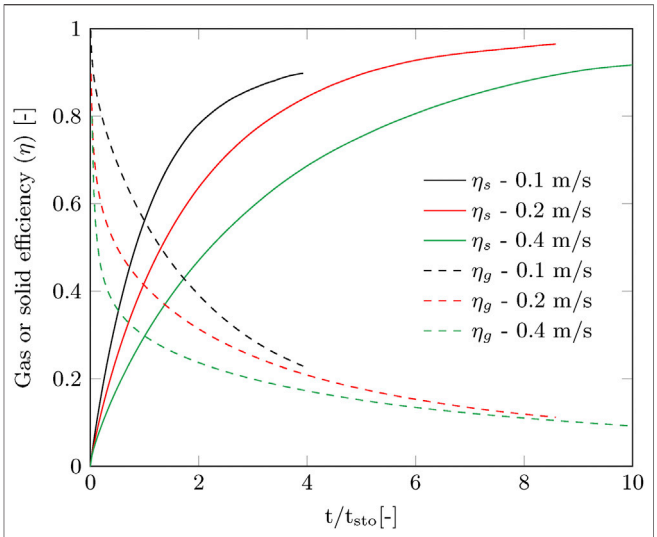

FIGURE 4 | Gas and solid efficiencies as function of stoichiometric time corresponding to the measured breakthrough curves from **Figure 3**.

shows the CO_2 loading of the sorbent over time. Faster adsorption is observed at increasing flowrate due to the higher average bulk concentration over the radial length of the adsorption bed. External mass transfer and feed rate limitations are negligible above 0.20 m/s, hence internal mass transfer resistance and reaction rate limitations control the sorbent saturation rate. A flowrate above 0.20 m/s is therefore not preferred and the experiments at 0.10 and 0.20 m/s are used as basis for comparison between batch and continuous operation.

The contact time of the gas phase with the sorbent is very short (0.04–0.15 s), therefore immediate breakthrough is observed. This is visible in the gas efficiency, which immediately drops considerably at the start of the adsorption, especially for the higher gas velocity (**Figure 4**). The capture efficiency decreases strongly with the gas velocity when going from 0.2 to 0.4 m/s, but the productivity increases to a much lesser extent (**Figure 3**). This effectively means that more compression power is spend for a faster adsorption of CO_2. On the other hand, for the envisioned thermal swing adsorption process, this will save energy during desorption as more CO_2 is produced with the same energy penalty. The time of adsorption is therefore a trade-off between compression duty and thermal energy duty. For this specific adsorption process using a radial flow contactor, circulating sorbent batches and the considered gas velocity range, the optimal adsorption time was found between 0.5 t^B_{sto} and 1.5 t^B_{sto} (Yu and Brilman, 2017).

Moving Bed

Operation Window

The operation window of a radial flow moving bed contactor in terms of gas velocity and solid flux is specific to each design. Phenomena as pinning and cavity limit the possible operating range of such a contactor (Ginestra and Jackson, 1985; Doyle et al., 1986; Chen et al., 2007). General parameters such as particle size, bed thickness and Reynolds number affect this operation range. However, other aspects are very specific such as the location of gas inlet, the distribution of solid particles and mesh size of the porous faces. To determine whether it is possible to operate this contactor at the desired process conditions, its hydrodynamic operation window with respect to gas and solids flow is determined. The solid flux is measured for gas velocities ranging from 0–0.5 m/s. For this, the solids are collected after the reactor and solid flux is determined by measuring the mass of the sorbent collected in a certain amount of time.

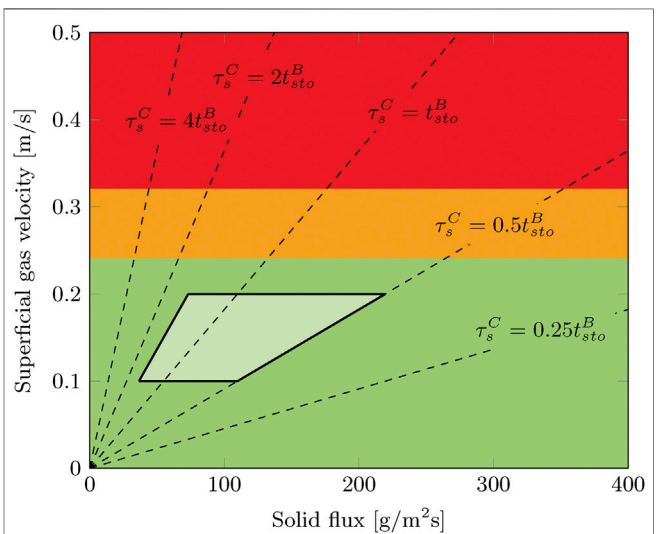

FIGURE 5 | Operation window for moving bed operation in the radial flow contactor. The solid flow is either good (green, $u_g < 0.24$ m/s), irregular (orange, $0.24 < u_g < 0.32$ m/s) or blocked (red, $u_g > 0.32$ m/s).

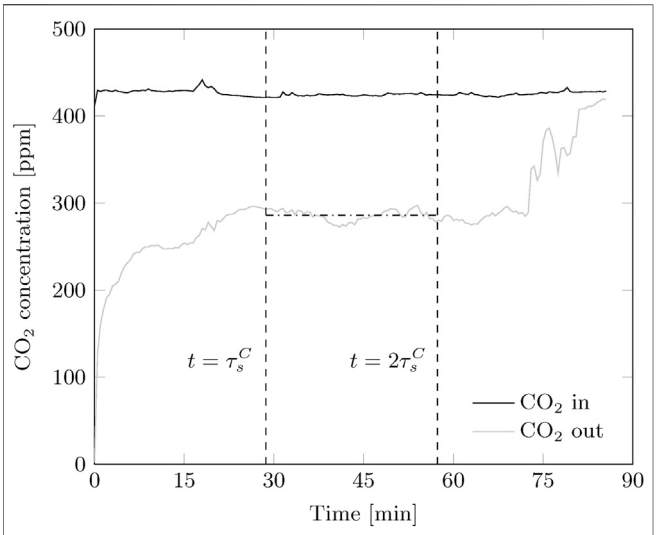

FIGURE 6 | Typical CO_2 concentration profiles for a continuous adsorption experiment. A steady-state is observed after the sorbent is refreshed once. The experiment ends when all sorbent left the reactor.

It was found that only the gas velocity affects the hydrodynamic operation range. No limitations are observed in terms of solid flux, at least up to 400 g/m^2/s (**Figure 5**). This is in line with the investigation of Chen et al. (2007) for a comparable operation window in terms of gas velocity and solid flux. Above approximately 0.3 m/s the solid flux stops completely due to the effects of cavity formation and pinning. Irregularities in solid flux are sometimes observed below this threshold gas velocity down to approximately 0.25 m/s. In this range, the total solid flux is as expected. However, by visual observation it was found that the solid flow is either not continuous over time or not evenly distributed across the radial cross section. At gas velocities up to 0.2 m/s, this radial flow moving bed contactor can be operated without any notable disturbances in solid flow. These critical values for the gas velocity are much lower than reported by Chen et al. (2007), 0.3 m/s and 0.84 m/s respectively. This is caused by the smaller particle size (0.67 mm vs. 1.96 mm) and smaller bed thickness (15 mm vs. 105 mm).

The optimal adsorption time, or solid residence time, for a DAC process (0.5 t^B_{sto} to 1.5 t^B_{sto}) corresponds to a combination of gas velocity (CO_2 supply) and solid flux (CO_2 removal). This is also derived in **Eq. 7** and is visualized in **Figure 5** by the addition of the (dashed) working lines. Since the gas and solid flow are normalized to the corresponding surface areas, the slope of these lines are a function of the dimensions of the contactor. The desired operating window (for optimum performance in view of solid and gas efficiency) lies well within the range of hydrodynamic feasible operating conditions, therefore continuous adsorption is possible with this cross flow moving bed contactor and the process conditions optimization is not hindered by constraints imposed by hydrodynamics.

Breakthrough Experiments

Continuous adsorption experiments reach a steady state situation. Since adsorption is started with lean sorbent, this is observed after the bed is fully refreshed (**Figure 6**). The experiment runs until no more sorbent is available, hence the outlet CO_2 concentration equals the inlet. After one sorbent refreshment, the CO_2 concentration remains stable, however some fluctuations are present in all experiments. This indicates that some disturbances in either solid flux of gas distribution are always present.

The experimental conditions and results for the continuous adsorption experiments are given in **Table 2**. Air is extracted from the laboratory, hence some variation in the experimental (inlet-) conditions is unavoidable. The differences in temperature and CO_2 concentration result in an equilibrium loading between 0.82 and 0.87 mol/kg. With this, the standard deviation in reaction rate remains within 4%. Relative humidity is another (weather) condition that is known to influence the equilibrium loading. The spread in the humidity (40–60% RH) is larger than the variation in the temperature and CO_2 concentration in the current set of (indoor) experiments. However, we do not see a clear effect of this variation in relative humidity in the results. Overall, we conclude that within this dataset the fluctuations in experimental conditions do not influence the results significantly.

It is expected that the sorbent loading increases with sorbent residence time and gas velocity, similar to the batch process. This is indeed also observed for the continuous process. However, the influence of gas velocity seems less pronounced. Especially for a solid flux of 60 g/m^2/s there is barely any increase in sorbent loading when the gas velocity increases from 0.10 to 0.22 m/s. For the gas efficiency there is a significant difference in efficiency noticeable. This indicates that also at 0.22 m/s some influence of cavity formation or pinning is present that is more prominent at a lower solid flux.

TABLE 2 | Experimental conditions and results for moving bed experiments.

u_g [m/s]	$\Phi_{M,s}$ [g/m^{2}s]	T_{in} [K]	RH [%]	τ_s^C [min]	CO_2^{in} [ppm]	CO_2^{out} [ppm]	τ_s^C/t_{sto}^B [−]	q^C [mol/kg]	Φ_{CO_2} [mmol/s]	η_s^C [−]	η_g^C [−]
0.22	63.8	22.4	60	57.3	435	335	1.94	0.38	0.19	0.47	0.23
0.22	126	20.5	42	28.7	424	286	0.96	0.27	0.27	0.31	0.32
0.22	246	20.6	51	14.6	438	267	0.51	0.17	0.34	0.20	0.39
0.10	60.2	20.2	61	59.7	431	232	0.92	0.36	0.18	0.42	0.46
0.10	126	20.2	46	28.7	426	166	0.43	0.23	0.23	0.26	0.61
0.10	276	22.0	59	13.0	421	106	0.19	0.12	0.27	0.14	0.75

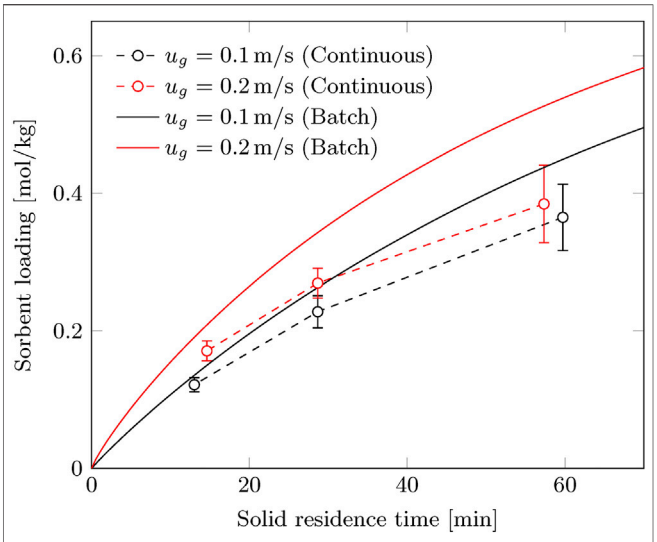

FIGURE 7 | Working capacity of the continuous process compared to the batch process at corresponding solid residence time.

There is a clear trade-off between solid efficiency (η_s^C) and productivity (Φ_{CO_2}). The productivity is proportional to the difference in CO_2 concentration of inlet and outlet. Increase in productivity can be achieved by increasing the solid flux. Consequently, a lower saturation level of the sorbent is obtained due to the reduced solid residence time.

Comparison

Capture Efficiency

The CO_2 capacity of the sorbent (q^C) in the continuous process (**Table 2**) is compared to that obtained in the batch process, evaluated at the solid residence time in the gas-solid contactor (**Figure 7**). From this, a decrease in process performance is evident. For an adsorption time of approximately an hour, the CO_2 loading of a batch process at 0.10 m/s is even higher than for a continuous process at 0.20 m/s. The reduced performance points toward a serious drop in gas-solid contacting efficiency.

Furthermore, we compare the batch and continuous processes by their gas and solid efficiencies. The adsorption time and solid residence time are normalized to their stoichiometric times and plotted in **Figure 8A** together with the dimensionless curves for the batch process. This allows for a fair comparison between gas velocities and reduces the influence of slightly different operation conditions as well. Batch operation is in all cases more efficient than a continuous process in terms of capture efficiency. A reduction of 15–25% is observed within the desired operation range of 0.5 t^B_{sto} to 1.5 t^B_{sto}(**Figure 8B**). We identify here two trends. Firstly, the performance (efficiency) declines when the solid flux is lowered or, in other words, for a longer adsorption phase. Secondly, the performance declines for a higher gas velocity.

Although we operate in the "green" area of the operating window, we observe a decrease in performance of the continuous process compared to the batch process. We propose two effects that contribute to this. The first effect is the reduced solid hold-up in the radial flow contactor during continuous operation, which was briefly mentioned before. This reduces the residence time of the sorbent and lowers the adsorption rate. To give an idea, the solid hold-up for this sorbent at minimum fluidization is about 17% lower than for a fixed bed. In a cross-flow moving bed the reduction in solid hold-up is most likely not that large, but can still be significant. This may explain the decrease in capture efficiency for an increasing gas flow. However, this will not explain the decreased efficiency over time. The second effect that may play a role is the possible occurrence of non-homogeneous sorbent flow inside the contactor. Possible

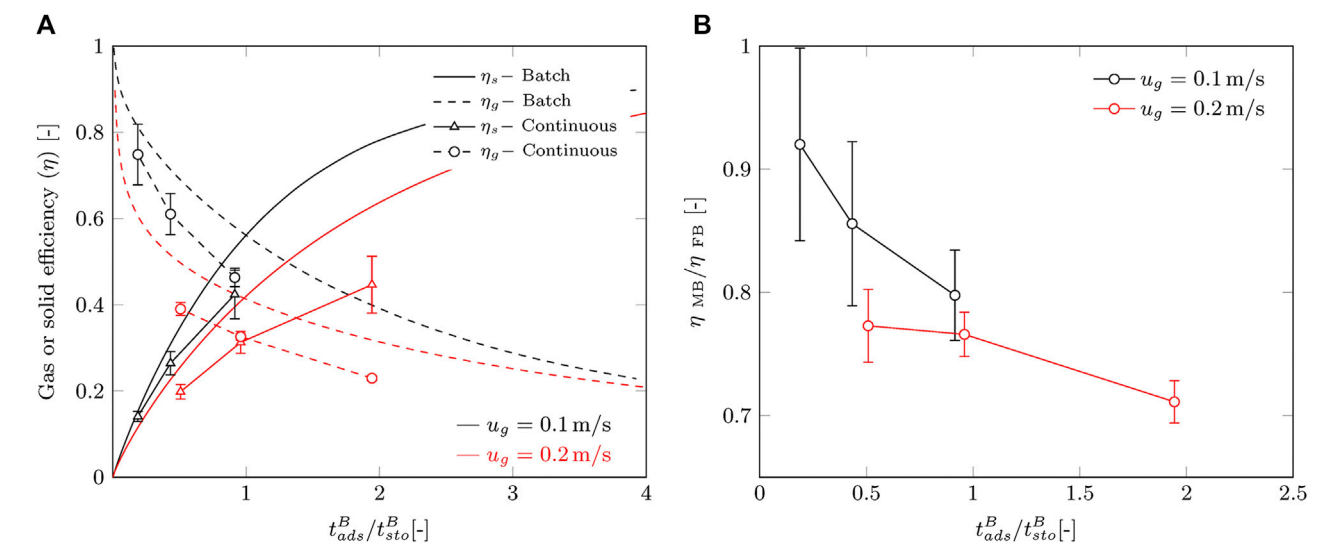

FIGURE 8 | Comparison of the continuous process with the batch process. Error margins represent the standard deviation by error propagation. **(A)** Gas and solid efficiency according to **Eqs (1)–(4)** and **(B)** the ratio of the efficiency between batch and continuous.

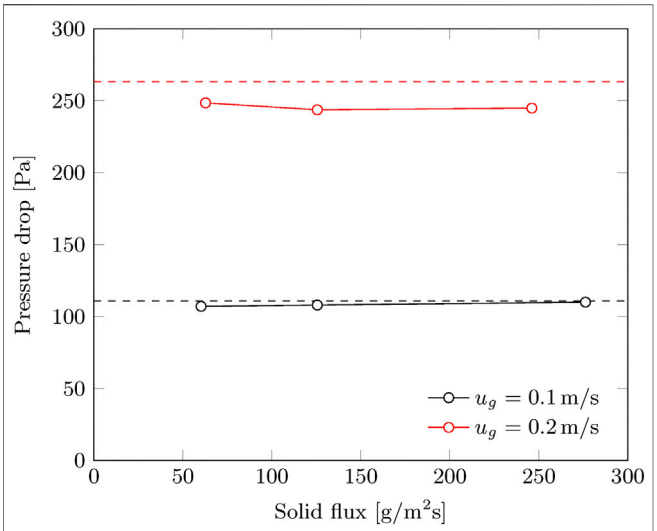

FIGURE 9 | Pressure drop over the radial flow moving bed contactor as function of solid flow.

causes are the formation and collapse of cavities or deviation from plug flow behavior due to shear forces on the porous faces. This will contribute to a lower solid hold-up, as well as a wider residence time distribution of solid material.

Pressure Drop

Reduced gas-solid contacting is expected to give rise to a reduction in pressure drop. The pressure drop is measured between the inner channel and the outer channel. This is only measured at a single vertical position, but is confirmed to be constant along the axial length of the contactor. Along the azimuth angle we were not able to validate this, but it might vary due to the location of the gas inlet.

For a superficial gas velocity of 0.20 m/s, a small (some 10%) reduction in pressure drop is observed for the continuous operation in comparison to batch operation. This is in contrast with the results at a gas velocity of 0.10 m/s. The pressure drop is found to be independent of the solid flux (within the experimental range), and consequently the gas-solid contacting is also not likely to be affected by the solid flux. The difference in results between 0.10 and 0.20 m/s gas velocity in **Figure 9**, might indicate the formation of cavities in the radial bed and a (slightly) reduced sorbent hold-up.

Temperature Profile

During the adsorption process a temperature profile may develop. The reactive adsorption of CO_2 on the surface of the sorbent is an exothermic process and the specific heat of the sorbent is low. However, the adsorbing particles are cooled by a large convective air flow. Since the saturation level of the sorbent negatively effects the reaction rate, a temperature profile as function of time or axial length of the contactor is expected for respectively the batch and continuous process. A possible gradient in temperature can affect the local reaction rate and hence capture efficiency. The temperature is measured at three locations in the bed (at a height of 4, 19 and 36 cm) and in the air inlet. For all experiments, the air inlet has a slightly different temperature due to temporal variations in the ambient temperature. For that reason, the temperature *increase* with respect to air inlet temperature is used for comparison and not the absolute temperature.

The temperature profiles in **Figure 10A** do not show large surprises. Convective cooling is very significant, as the temperature excursion is lower for 0.2 m/s while the average CO_2 uptake rate is higher. One could argue that the higher temperature causes a higher reaction rate and that this is the difference observed in capture efficiency. However, the difference between continuous and batch processes, shown in **Figure 8**, is present for both gas velocities. In order to compare the temperature profiles to the batch process, the temperature should be described as a function of sorbent residence time. For example at 19 cm, the residence time of the sorbent is 27.2, 13.6 and 6.8 min for 0.5, 1 and 2 g/s (or 63, 125 and 250 g/m^2/s) respectively. The temperature for the batch process is taken as the average temperature of the three locations.

With this transformation, the temperature profile is nearly identical for the batch and continuous process (**Figure 10B**). For the continuous process, the peak temperature seems slightly lower. This might be related to heat dispersion by the moving solids. Considering the reduced reaction rate during continuous operation, the temperature is actually expected to be lower than during batch operation. This is not the case, if any the temperature is higher for the continuous process. Therefore, convective cooling is less efficient in a continuous process, which indicates to a decrease in gas-solid contacting.

Discussion

The capture efficiency of a continuous adsorption process in a radial flow moving bed contactor is significantly lower compared to the corresponding batch process. This efficiency decreases with 1) the increasing superficial gas velocity and 2) increasing adsorption time. The contacting of gas and solid becomes less effective for a moving bed. Temperature profiles support this statement, where a decline in convective cooling is observed. Also, the pressure drop is slightly lower, especially for 0.20 m/s. Since the pressure drop is only measured at a single location, local variations cannot be observed, but are most likely present. A reduced solid hold-up and irregularities in solid flow are identified as possible sources of the decrease in gas-solid contacting. The solid hold-up in the gas-solid contactor during a continuous process is estimated to be at most 17% lower than for a batch process. How the solids hold-up is affected by solid flux and gas velocity is not known and requires further study. Irregularities in solid flow give rise to a wider residence time distribution for the sorbent phase. A detailed and dedicated hydrodynamics study of this gas-solid contactor is therefore recommended and required to investigate the magnitude of these phenomena.

The reproducibility is validated for a batch operation experiment. Although weather conditions do not allow for an exact replication of the experiment, the deviation in loading after 4 h was only 2%. Continuous experiments are not

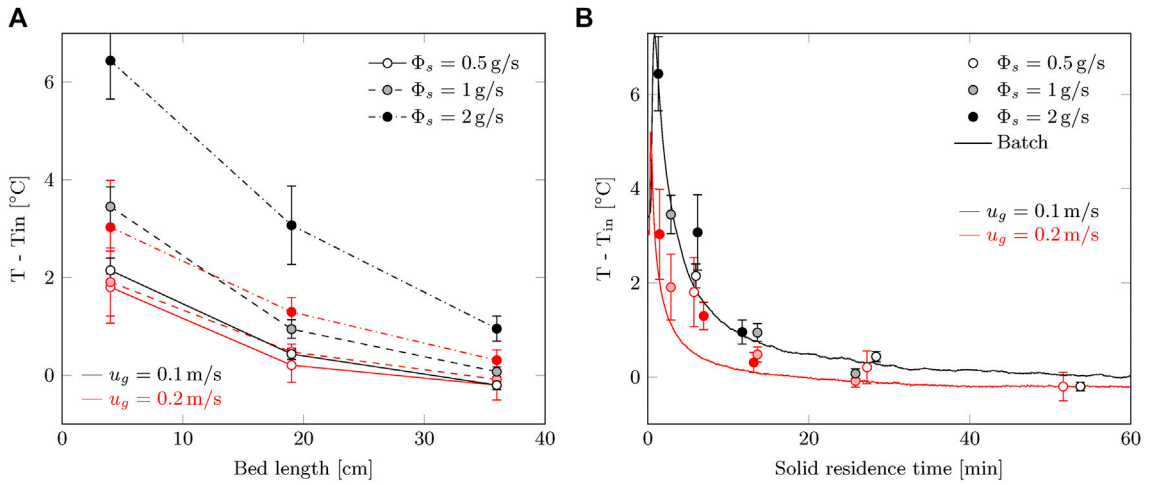

FIGURE 10 | Temperature increase during the steady-state phase of the radial flow moving bed experiments as function of: **(A)** axial location of the contactor (0 = top; 40 cm = bottom) and **(B)** solid residence time (batch process data is added for comparison). The error margins represent the standard deviation in the steady-state temperature.

reproduced due to the time consuming desorption procedure. However, for each and every experiment, the gas and solid flows are checked. Also, the performance of the sorbent itself is verified and found to be stable throughout the measurement campaign. Therefore, the results are considered reproducible and trends to be reliable.

All experiments started with nearly completely regenerated sorbents, since this ensures an equal starting point for all experiments. In an actual process with sorbent circulation, full regeneration is not likely because it takes too much time to reach such a high regeneration level. Since the required adsorption time is then also a bit shorter, the difference between continuous and batch may become smaller.

Two other factors diminish the difference between the performance of batchwise operation and continuous operation. These will be related to the process economics for both energy consumption as well as the effective use of invested capital on equipment. Firstly, in continuous operation, the availability of the gas-solid contactor is full time, whereas for batch wise operation the loading and unloading of the contactor must be accounted for. For the contactor in this study, the down time is about 4 min per cycle, but can vary widely for other configurations. The reduction in equipment availability can be as high as 30% (0.22 m/s and $\tau^c_{\text{sto}} = 0.5\, t^B_{\text{sto}}$). Secondly, the total amount of sorbent differs between batch and continuous operation. During batch operation, around 15% of the sorbent in the gas-solid contactor is required to fill the feed- and exit pipes. This sorbent fraction did not participate in the adsorption process, but is still transported, without loading, to the regenerator, where it is heated to regeneration conditions. A recent study by Bos et al. (2020) estimates sorbent heating to account for 45% of the operating costs. Therefore, around 10% of total operating costs can be saved in the continuous process. Another important issue regarding total sorbent inventory is the cost contribution by the (initial) sorbent mass required. The afore mentioned study showed that for a fixed bed process almost 70% of the capital cost is related to the sorbent costs. When operating the gas-solid contactor in a continuous manner, sorbent hold-up in the entire process (adsorber, desorber and intermediate storage) can be reduced by some 30%. This stems from the required intermediate storage in a batch process, in contrast to a continuous process where all sorbent material participates in either adsorption or regeneration. Overall, the investment costs for sorbents can be reduced by 20–25% for a continuous process. With these considerations, a continuous process can be on par or even become more beneficial than a batch process, especially for short adsorption time and low gas velocity. For example, for a continuous process operating at $0.5 t^B_{\text{sto}}$ and 0.1 m/s, the efficiency is 15% lower than for the batch process. In this case, only a 4 min transition phase between batches is available for the batch process to remain more efficient.

CONCLUSION

This study compares the performance of a radial flow moving bed adsorption process with a batch process. The process is tailored for Direct Air Capture using a supported amine sorbent. In the desired operating regime for DAC, the capture efficiency of a continuous process is lowered by 15–25% compared to a batch process. This decrease in gas-solid contacting efficiency is higher with increasing superficial gas velocity, which indicates the occurrence of pinning and cavity even at these low Reynolds numbers. In addition, the continuous process performs increasingly worse as the adsorption progresses. Nonetheless, a continuous process can still become more profitable is case of a low gas velocity combined with a short adsorption phase, due to the time penalty for sorbent replacement during batch operation.

DATA AVAILABILITY STATEMENT

The raw data supporting the conclusions of this article will be made available by the authors, without undue reservation

AUTHOR CONTRIBUTIONS

MS and TJ designed this study and the methodology. TJ performed the experiments. MS, TJ, and WB were involved in the data analysis and data interpretation. MS wrote the manuscript under supervision of WB Methodology: MS and TJ, Data collection: TJ, Data analysis and interpretation: MS, TJ and WB, Writing: MS, Supervision: WB.

FUNDING

This research was funded by NORTH-WEST EUROPE INTERREG, grant number NWE 639 as part of the IDEA project (Implementation and development of economic viable algae-based value chains in North-West Europe).

REFERENCES

Alesi, W. R., and Kitchin, J. R. (2012). Evaluation of a primary amine-functionalized ion-exchange resin for CO_2 capture. *Ind. Eng. Chem. Res.* 51 (19), 6907–6915. doi:10.1021/ie300452c

Bajamundi, C. J. E., Koponen, J., Ruuskanen, V., Elfving, J., Kosonen, A., Kauppinen, J., et al. (2019). Capturing CO_2 from air: technical performance and process control improvement. *J. of CO_2 Utilization.* 30, 232–239. doi:10.1016/j.jcou.2019.02.002

Bos, M. J., Kersten, S. R. A., and Brilman, D. W. F. (2020). Wind power to methanol: renewable methanol production using electricity, electrolysis of water and CO_2 air capture. *Appl. Energy* 264, 114672. doi:10.1016/j.apenergy.2020.114672

Bos, M. J., Kroeze, V., Sutanto, S., and Brilman, D. W. F. (2018). Evaluating regeneration options for bulk CO_2 removal from biogas using solid amine sorbents. *Ind. Eng. Chem.* 57, 11141–11153. doi:10.1021/acs.iecr.8b00768

Brilman, D. W. F., and Veneman, R. (2013). Capturing atmospheric CO_2 using supported amine sorbents. *Energy Procedia.* 37, 6070–6078. doi:10.1016/j.egypro.2013.06.536

Caplow, M. (1968). Kinetics of carbamate formation and breakdown. *J. Am. Chem. Soc.* 90 (24), 6795–6803. doi:10.1021/ja01026a041

Chen, Y., Zhu, X., Wu, Y., and Zhu, Z. (2007). The investigation of pressure drop in moving-beds. *Front. Chem. Eng. China.* 1 (2), 184–189. doi:10.1007/s11705-007-0034-4

Choi, S., Drese, J. H., and Jones, C. W. (2009). Adsorbent materials for carbon dioxide capture from large anthropogenic point sources. *ChemSusChem.* 2 (9), 796–854. doi:10.1002/cssc.200900036

Crooks, J. E., and Donnellan, J. P. (1989). Kinetics and mechanism of the reaction between carbon dioxide and amines in aqueous solution. *J. Chem. Soc., Perkin Trans.* 2 (4), 331–333. doi:10.1039/P29890000331

D'Alessandro, D. M., Smit, B., and Long, J. R. (2010). Carbon dioxide capture: prospects for new materials. *Angew. Chem. Int. Ed.* 49 (35), 6058–6082. doi:10.1002/anie.201000431

Danckwerts, P. V. (1979). The reaction of CO_2 with ethanolamines. *Chem. Eng. Sci.* 34 (4), 443–446. doi:10.1016/0009-2509(79)85087-3

Doyle, F. J., Jackson, R., and Ginestra, J. C. (1986). The phenomenon of pinning in an annular moving bed reactor with crossflow of gas. *Chem. Eng. Sci.* 41 (6), 1485–1495. doi:10.1016/0009-2509(86)85233-2

Driessen, R. T., Knaken, B., Buzink, T., Jacobs, D. A. F., Hrstka, J., and Brilman, D. W. F. (2020a). Design and proof of concept of a continuous pressurized multi-stage fluidized bed setup for deep sour gas removal using adsorption. *Powder Technol.* 366, 859–872. doi:10.1016/j.powtec.2020.03.013

Driessen, R. T., van der Linden, J. J. Q., Kersten, S. R. A., Bos, M. J., and Brilman, D. W. F. (2020b). Characterization of mass transfer in a shallow fluidized bed for adsorption processes: modeling and supporting experiments. *Chem. Eng. J.* 388, 123931. doi:10.1016/j.cej.2019.123931

Elfving, J., Kauppinen, J., Jegoroff, M., Ruuskanen, V., Järvinen, L., and Sainio, T. (2021). Experimental comparison of regeneration methods for CO_2 concentration from air using amine-based adsorbent. *Chem. Eng. J.* 404, 126337. doi:10.1016/j.cej.2020.126337

Gelles, T., Lawson, S., Rownaghi, A. A., and Rezaei, F. (2020). Recent advances in development of amine functionalized adsorbents for CO_2 capture. *Adsorption.* 26 (1), 5–50. doi:10.1007/s10450-019-00151-0

Ginestra, J. C., and Jackson, R. (1985). Pinning of a bed of particles in a vertical channel by a cross flow of gas. *Ind. Eng. Chem. Fund.* 24 (2), 121–128. doi:10.1021/i100018a001

Goeppert, A., Czaun, M., Surya Prakash, G. K., and Olah, G. A. (2012). Air as the renewable carbon source of the future: an overview of CO_2 capture from the atmosphere. *Energy Environ. Sci.* 5 (7), 7833–7853. doi:10.1039/C2EE21586A

Grande, C. A., Kvamsdal, H., Mondino, G., and Blom, R. (2017). Development of moving bed temperature swing adsorption (MBTSA) process for post-combustion CO_2 capture: initial benchmarking in a NGCC context. *Energy Procedia.* 114, 2203–2210. doi:10.1016/j.egypro.2017.03.1357

Kim, K., Son, Y., Lee, W. B., and Lee, K. S. (2013). Moving bed adsorption process with internal heat integration for carbon dioxide capture. *International Journal of Greenhouse Gas Control.* 17, 13–24. doi:10.1016/j.ijggc.2013.04.005

Kulkarni, A. R., and Sholl, D. S. (2012). Analysis of equilibrium-based TSA processes for direct capture of CO_2 from air. *Ind. Eng. Chem. Res.* 51 (25), 8631–8645. doi:10.1021/ie300691c

Kumar, A., Madden, D. G., Lusi, M., Chen, K.-J., Daniels, E. A., Curtin, T., et al. (2015). Direct air capture of CO_2 by physisorbent materials. *Angew. Chem. Int. Ed.* 54 (48), 14372–14377. doi:10.1002/anie.201506952

Lackner, K. S., Brennan, S., Matter, J. M., Park, A. H. A., Wright, A., and van der Zwaan, B. (2012). The urgency of the development of CO2 capture from ambient air. *Proc. Natl. Acad. Sci. Unit. States Am.* 109 (33), 13156–13162. doi:10.1073/pnas.1108765109

Lanxess (2017). Product information Lewatit VP OC 1065. [Online]. Available at https://products.lanxess.com/ (Accessed September 20, 2020).

Long, W., Xu, J., Fan, Y., and Lu, C. (2015). Pinning and cavity in two types of cross-flow moving beds. *Powder Technol.* 269, 66–74. doi:10.1016/j.powtec.2014.09.013

Lu, W., Sculley, J. P., Yuan, D., Krishna, R., and Zhou, H.-C. (2013). Carbon dioxide capture from air using amine-grafted porous polymer networks. *J. Phys. Chem. C.* 117 (8), 4057–4061. doi:10.1021/jp311512q

Mondino, G., Grande, C. A., Blom, R., and Nord, L. O. (2019). Moving bed temperature swing adsorption for CO_2 capture from a natural gas combined cycle power plant. *Int. J. Greenh. Gas Control.* 85, 58–70. doi:10.1016/j.ijggc.2019.03.021

Mukherjee, S., Bandyopadhyay, S. S., and Samanta, A. N. (2018). Kinetic study of CO_2 absorption in aqueous benzylamine solvent using a stirred cell reaction calorimeter. *Energy Fuels.* 32 (3), 3668–3680. doi:10.1021/acs.energyfuels.7b03743

Pilcher, K. A., and Bridgwater, J. (1990). Pinning in a rectangular moving bed reactor with gas cross-flow. *Chem. Eng. Sci.* 45 (8), 2535–2542. doi:10.1016/0009-2509(90)80139-6

Sanz-Pérez, E. S., Murdock, C. R., Didas, S. A., and Jones, C. W. (2016). Direct capture of CO_2 from ambient air. *Chem. Rev.* 116 (19), 11840–11876. doi:10.1021/acs.chemrev.6b00173

Shekhah, O., Belmabkhout, Y., Chen, Z., Guillerm, V., Cairns, A., Adil, K., et al. (2014). Made-to-order metal-organic frameworks for trace carbon dioxide removal and air capture. *Nat. Commun.* 5, 4228. doi:10.1038/ncomms5228

Shirzad, M., Karimi, M., Silva, J. A. C., and Rodrigues, A. E. (2019). Moving bed reactors: challenges and progress of experimental and theoretical studies in a century of research. *Ind. Eng. Chem. Res.* 58 (22), 9179–9198. doi:10.1021/acs.iecr.9b01136

Singh, G., Lee, J., Karakoti, A., Bahadur, R., Yi, J., Zhao, D., et al. (2020). Emerging trends in porous materials for CO2 capture and conversion. *Chem. Soc. Rev.* 49 (13), 4360–4404. doi:10.1039/d0cs00075b

Stampi-Bombelli, V., van der Spek, M., and Mazzotti, M. (2020). Analysis of direct capture of CO_2 from ambient air via steam-assisted temperature-vacuum swing adsorption. *Adsorption.*, 26, 1183. doi:10.1007/s10450-020-00249-w

Topham, S., Bazzanella, A., Schiebahn, S., Luhr, S., Zhao, L., Otto, A., et al. (2014). "Carbon dioxide," in *Ullmann's encyclopedia of industrial chemistry*. (Weinheim, Germany: Wiley-VCH Verlag GmbH), 1–43.

USEPA (2018). Carbon dioxide emissions. [Online]. Available at https://www.epa.gov/ghgemissions/overview-greenhouse-gases#carbon-dioxide (Accessed August 18, 2020).

Wang, R., Wang, D., Fan, Y., Lu, C., Hu, B., and Zhang, S. (2020). Cavity, pinning and air lock in both rectangular and radial cross-flow moving beds with a gas-solid baffle. *Powder Technol.* 374, 449–461. doi:10.1016/j.powtec.2020.07.021

Wurzbacher, J. A., Gebald, C., Piatkowski, N., and Steinfeld, A. (2012). Concurrent separation of CO_2 and H_2O from air by a temperature-vacuum swing adsorption/desorption cycle. *Environ. Sci. Technol.* 46 (16), 9191–9198. doi:10.1021/es301953k

Yang, M., Ma, C., Xu, M.-m., Wang, S., and Xu, L. (2019). Recent advances in CO_2 adsorption from air: a review. *Curr. Pollut. Reports.* 5, 272–293.

Yu, Q., and Brilman, D. W. F. (2017). Design strategy for CO_2 adsorption from ambient air using a supported amine based sorbent in a fixed bed reactor. *Energy Procedia.* 114, 6102–6114. doi:10.1016/j.egypro.2017.03.1747

Yu, Q., and Brilman, W. (2020). A radial flow contactor for ambient air CO_2 capture. *Appl. Sci.* 10 (3), 1080. doi:10.3390/app10031080

Zhang, W., Liu, H., Sun, C., Drage, T. C., and Snape, C. E. (2014). Capturing CO_2 from ambient air using a polyethyleneimine-silica adsorbent in fluidized beds. *Chem. Eng. Sci.* 116, 306–316. doi:10.1016/j.ces.2014.05.018

Conflict of Interest: The authors declare that the research was conducted in the absence of any commercial or financial relationships that could be construed as a potential conflict of interest.

frontiers in Chemical Engineering

ORIGINAL RESEARCH
published: 09 December 2020
doi: 10.3389/fceng.2020.596279

Carbon Allocation in Multi-Product Steel Mills That Co-process Biogenic and Fossil Feedstocks and Adopt Carbon Capture Utilization and Storage Technologies

Maximilian Biermann, Rubén M. Montañés, Fredrik Normann and Filip Johnsson*

Division of Energy Technology, Department of Space, Earth, and Environment, Chalmers University of Technology, Gothenburg, Sweden

This work investigates the effects of carbon allocation on the emission intensities of low-carbon products cogenerated in facilities that co-process biogenic and fossil feedstocks and apply the carbon capture utilization and storage technology. Thus, these plants simultaneously sequester CO_2 and synthesize fuels or chemicals. We consider an integrated steel mill that injects biomass into the blast furnace, captures CO_2 for storage, and ferments CO into ethanol from the blast furnace gas. We examine two schemes to allocate the CO_2 emissions avoided [due to the renewable feedstock share (biomass) and CO_2 capture and storage (CCS)] to the products of steel, ethanol, and electricity (generated through the combustion of steel mill waste gases): 1) allocation by (carbon) mass, which represents actual carbon flows, and 2) a free-choice attribution that maximizes the renewable content allocated to electricity and ethanol. With respect to the chosen assumptions on process performance and heat integration, we find that allocation by mass favors steel and is unlikely to yield an ethanol product that fulfills the Renewable Energy Directive (RED) biofuel criterion (65% emission reduction relative to a fossil comparator), even when using renewable electricity and applying CCS to the blast furnace gas prior to CO conversion into ethanol and electricity. In contrast, attribution fulfills the criterion and yields bioethanol for electricity grid intensities <180 gCO_2/kWh_{el} without CCS and yields bioethanol for grid intensities up to 800 gCO_2/kWh_{el} with CCS. The overall emissions savings are up to 27 and 47% in the near-term and long-term future, respectively. The choice of the allocation scheme greatly affects the emissions intensities of cogenerated products. Thus, the set of valid allocation schemes determines the extent of flexibility that manufacturers have in producing low-carbon products, which is relevant for industries whose product target sectors that value emissions differently. We recommend that policymakers consider the emerging relevance of co-processing in nonrefining facilities. Provided there is no double-accounting of emissions, policies should contain a reasonable degree of freedom in the allocation of emissions savings to low-carbon products, so as to promote the sale of these savings, thereby making investments in mitigation technologies more attractive to stakeholders.

Keywords: low-carbon products, allocation, integrated steel mill, co-processing, carbon capture utilization and storage, pulverized coal injection, syngas fermentation, biofuels

OPEN ACCESS

Edited by:
Juliana Monteiro, Netherlands Organisation for Applied Scientific Research, Netherlands

Reviewed by:
Qingchun Yang, Hefei University of Technology, China
Juan Gabriel Segovia Hernandez, University of Guanajuato, Mexico

****Correspondence:***
Maximilian Biermann
max.biermann@chalmers.se

Specialty section:
This article was submitted to Separation Processes, a section of the journal Frontiers in Chemical Engineering

Received: *18 August 2020*
Accepted: *08 October 2020*
Published: *09 December 2020*

Citation:
Biermann M, Montañés RM, Normann F and Johnsson F (2020) Carbon Allocation in Multi-Product Steel Mills That Co-process Biogenic and Fossil Feedstocks and Adopt Carbon Capture Utilization and Storage Technologies. Front. Chem. Eng. 2:596279. doi: 10.3389/fceng.2020.596279

INTRODUCTION

To limit the global temperature increase to 1.5°C, global net anthropogenic CO_2 emissions will have to fall rapidly over the coming decades and—depending on the trajectory, approach zero by year 2050 (Masson-Delmotte et al., 2018). This is in line with the European Green Deal (European Commission, 2019c) proposed by the European Commission (EC), which aims for a climate-neutral EU by year 2050. To reach climate neutrality, a series of mitigation options, such as material and energy efficiencies, carbon capture utilization and/or storage (CCUS), and the use of renewable energy sources such as wind, solar, and biomass, must be deployed across all sectors, including the base materials industry (Energy Transition Commission, 2018; Agora Energiewende and Wuppertal Institut, 2019). All emission-intensive sectors will experience dramatic changes, including increased sector-coupling and implementation of solutions that involve alignment with circular economy principles (ArcelorMittal, 2020). Within some sectors, several mitigation options are available. In the steel industry, for example, a portfolio of the abovementioned mitigation technologies is available today, but it must be evaluated also against the prospect of breakthrough technologies, such as electrowinning hydrogen direct reduction (Vogl et al., 2018), relying on renewable electricity. Steel mills located in countries with an ample supply of renewable energy will experience favorable conditions to implement such breakthrough technologies or direct reduction with natural gas as an intermediate step (Vogl and Åhman, 2019). Although a first large-scale demonstration of hydrogen direct reduction steel is expected in year 2026 (SSAB, 2019), fossil-based processes will continue to emit until a complete transition to such carbon direct avoidance technologies becomes commercially available and feasible for countries in central Europe with electricity systems that are still reliant on fossil fuels. There is also competition between sectors for renewable biomass and electricity. Given the urgency of climate change and that many of the existing industrial processes will not be immediately made carbon-neutral via breakthrough technologies or shutdown, there is a need to implement a combination of already available technologies for partial mitigation, for example, fuel shifting to biomass and the application of CCS (Biermann et al., 2018; Berghout et al., 2019; Mandova et al., 2019).

When multi-product industrial facilities apply partial mitigation measures, the allocation of emissions or emission savings to the different products becomes important. Schemes for funding or subsidizing mitigation options must be sufficiently precise and robust to reach the desired target, to ensure that emissions savings are only accounted for once (i.e., in one sector), and that there is accounting for all the emissions in affected sectors. Importantly, the principles by which emission savings are allocated to the products determine which low-carbon products are formed and can be sold on existing or emerging markets. An example of this is the renewable content when co-processing renewable, for example, biogenic, and fossil feedstocks in refineries, which is currently allocated to the formed fuel products by various allocation principles applied in the so-called voluntary schemes that are approved by the EC (European Commission, 2020) and adhere to the current Renewable Energy Directive (RED II) (European Parliament and Council of the European Union, 2018a). RED II and associated regulations state that the overall quantity of renewables must reflect the energy balance and efficiency of the co-processing (Annex I, Part 1, paragraph 3(c) (ii) of Directive (EU) 2015/652) but leave the definition of valid allocation principles for co-processing to a so-called "Delegated Act," which is to be implemented in December 2021 (Hawighorst, 2019). Although discrepancies exist in terms of verifiability, accuracy, and cost (van Dyk et al., 2019), most of these allocation principles lead to a proportional allocation of renewable content to all the products of a refinery (Schimmel et al., 2018). However, companies will have an interest in having flexibility in the allocation to selected, high-revenue products when possible from the technical point of view (Schimmel et al., 2018).

The described current co-processing regulations are tailored to refinery operations. However, other industries that have nonfuel main products and are also engaging in fuel production should be considered when defining the set of valid allocation principles. A representative example of this is the "TORefying wood with Ethanol as a Renewable Output" (Torero) project for the co-processing of fossil and biogenic feedstocks in the blast furnace (Torero Consortium, 2017), with subsequent fuel synthesis from the steel mill gases (Steelanol Consortium, 2015). The injection of biomass into the blast furnace has been extensively studied (Mousa et al., 2016; Suopajärvi et al., 2017, Suopajärvi et al., 2018), as has been the application of CCS to steel mill gases (Ho et al., 2013; IEAGHG, 2013; Ramírez-Santos et al., 2018; Sundqvist et al., 2018). Although studies of the life cycle emissions of fuel from steel mill gases have been performed (Ou et al., 2013; Handler et al., 2016), quantification of the renewable content of cogenerated fuel and steel product due to a preceding biomass injection according to the abovementioned allocation principles is unprecedented and explored in detail in this study. The theoretical potential of achieving net-zero emissions in the European steel industry through a strategy of biomass introduction at multiple locations in the blast furnace route combined with CCS has been described by Mandova et al. (2019). Tanzer et al. (2020) have compared all the major primary steel production routes to estimate the bioenergy with carbon capture and storage (BECCS) potential and concluded that supply chain emissions for biomass, and CO_2 capture throughout steel and bioenergy production, as well as rigorous monitoring of CO_2 storage, are all required to achieve CO_2-negative steel. Toktarova et al. (2020) have investigated mitigation pathways toward zero carbon emissions, comparing hydrogen direct reduction and top-gas recycling blast furnaces with biochar injection and CCS in a Swedish context. Yet, their study does not use any detailed energy and mass balances but evaluates techno-economic pathways from data on the annual energy consumption for steel production. However, there is a lack of a more detailed process evaluation of the near-term potential for emissions reductions considering practical and technical limitations of biochar injection and CCS, also in combination with carbon utilization, which we seek to address with this article.

Therefore, this work assesses the implications of different carbon allocation principles for the generation of low-carbon products. The work evaluates the potential for reducing CO_2 emissions and the emissions intensities of the products, in a European setting, by implementing CCS and/or bio-substitution of pulverized coal injection (Bio-PCI) at an integrated steel mill that produces a transport fuel or electricity in addition to steel. More specifically, the present work assesses the following:

- The technical (level of bio-substitution) and regulatory (allocation in co-processing) conditions under which ethanol produced from steel mill off-gases, subsequent to biochar injection into the blast furnace, can be regarded as bioethanol in accordance with current EU regulations;
- The CO_2 emissions reduction achievable by CCS and the ethanol synthesis from blast furnace gas as an example of CCUS considering both the near-term feasibility and the theoretical potential for future developments; and
- The energy and emissions intensities of steel, ethanol, and electricity produced in an integrated steel mill that applies CCS and/or Bio-PCI and ethanol synthesis, given selected carbon allocation schemes.

The remainder of this article is organized as follows. The selected mitigation technologies are briefly reviewed in Chapter 2, followed by an overview of relevant EU regulations and guidelines in Chapter 3. Chapter 4 describes the system investigated and the principles of allocation of avoided emissions due to renewable content (due to Bio-PCI) and due to CCS to the final products of steel, ethanol, or electricity. The results in Chapter 5 focus on the impacts of allocation on the flow pathways of carbon, as well as the emissions intensities of the final products. In addition, both the near-term and potential future reductions in emissions brought about by the combined application of the selected mitigation technologies are quantified. Chapter 6 discusses the technical challenges for deep mitigation and the value for producers (in creating low-carbon products) that is generated by the potential flexible allocation of biogenic inputs and avoided CO_2 emissions.

NEAR-TERM MITIGATION TECHNOLOGIES

Integrated steel mills that apply the best-available technology in Europe have achieved carbon intensity levels that are close to technical and theoretical limits (Kirschen et al., 2011). Thus, further reductions will require significant investments in new technologies, as well as a shift toward using renewable fuels. This article focuses on CCS (represented by amine absorption of CO_2) and fuel switching from coal to biomass (represented by Bio-PCI), as well as the synthesis of ethanol via fermentation from blast furnace gases. Ethanol is chosen as product since it represents a valuable low-carbon product that is already traded globally at high volumes. However, the discussion in this article should be applicable also to other hydrocarbon products. It is reasonable to assume that these technologies can be implemented within 5 years (FEED, detailed engineering, construction, and commissioning), as both postcombustion capture and the use of biomass have been proven to be feasible, albeit not demonstrated at scale in the steel industry.

Pulverized Biochar Injection

Coke is the primary fuel and reducing agent in blast furnaces, and its replacement comes with both technical and economic challenges. Usually, pulverized coal is injected to reduce significantly the amount of coke, leading to an increase in energy efficiency. However, top-fed coke cannot be replaced completely, given its essential mechanical function in supporting the burden material (Suopajärvi 2018). Replacing pulverized coal injection is the easiest way to introduce biomass (Wang et al., 2015) into an integrated steel mill, and 23%–28% emissions can be mitigated by fully substituting pulverized coal in the blast furnace (Ng et al., 2010; Mathieson et al., 2011; Wang et al., 2015). The most extensively studied biogenic feedstock for iron-making is woody biomass (Suopajärvi et al., 2013). However, the properties of raw biomass differ from those of coal (Shankar Tumuluru et al., 2011) to such an extent that pretreatment is required. Wang and colleagues have estimated the maximum replacement rate potential of coal in a blast furnace with pretreated woody biomass for three pretreatment processes involving wood pellets, torrefied wood, and charcoal (Wang et al., 2015). The low energy density of biomass is explained by its high content oxygen, which, in turns, increases the need for O_2-enrichment of the blast, so as to maintain the race-away adiabatic flame temperature in the blast furnace. According to a previous report (Wang et al., 2015), charcoal from pyrolysis can fully replace, while torrefied wood and wood pellets can replace pulverized coal by 22.8% and 20.0%, respectively. The four main technical limitations associated with biomass injection in a blast furnace (BF) are lower calorific value of the biomass, porosity, broader distribution of particle size for injection, and higher levels of alkalis in some biomass products (Suopajärvi 2018). According to a previous study (Ng et al., 2010), charcoal injection affects only weakly the operating conditions of the furnace, and the desirable chemical compositions of the slag and hot metal can be maintained by adjusting the fluxing rate.

Wiklund et al. (2017) have concluded that slow pyrolysis is the most promising pretreatment technology from a techno-economic perspective. Technical and economic constraints may still be linked to logistic challenges within the supply chain (biomass availability) or quality aspects of the produced iron when increasing significantly Bio-PCI injection (Wang et al., 2015; Suopajärvi et al., 2017). This needs to be tested in blast furnaces on a case-by-case basis. Increasing the biomass feed could increase the price of biomass, especially if other industries are interested in also using more biomass. Thus, the economic feasibility of using biomass as a reducing agent in blast furnaces may be affected (Wang et al., 2015).

CO_2 Capture From Steel Mill Gases

CCS implies the capture of CO_2 from flue gases [stacks of combined heat and power (CHP) plants, hot stoves, lime kilns,

sinter plants, and coke ovens] or from the blast furnace gas (BFG) prior to its combustion in other steel units or in the CHP plant. Captured CO_2 is compressed or liquefied for transport to a designated geologic storage site (often located offshore beneath the seabed). The most extensively studied and most suitable system for retrofitting (Gardarsdottir et al., 2019; Voldsund et al., 2019) is end-of-pipe capture, often achieved through the chemical absorption of CO_2 using aqueous amine solutions. Amine absorption is commercially available and has been evaluated as the most mature CO_2 capture technology, at a technology readiness level (TRL) of 9 (Bui et al., 2018; IChemE Energy Centre, 2018). Gas separation via amine absorption typically implies energy penalties of ~3–4 GJ/tCO_2-captured for solvent regeneration (heat) and ~0.3–0.6 GJ/tCO_2-captured for compression/liquefaction of CO_2 (power). Many studies have evaluated CCS from steel mill off-gases (Kuramochi et al., 2012; Arasto et al., 2013; Ho et al., 2013; IEAGHG, 2013; Tsupari et al., 2013; Cormos, 2016; Biermann et al., 2019; Martinez Castilla et al., 2019). In summary, those studies have reported CO_2 avoidance levels of 50%–80% if the CO_2 is captured from the largest direct emissions point onsite and depending on the number of flue gas stacks included. Applying amine absorption to the BFG alone could reduce emissions by 19%–39% (Kuramochi et al., 2012; Ho et al., 2013; Biermann et al., 2019). Other technologies undergoing development include the sorption-enhanced Water-Gas Shift technology (Gazzani et al., 2015; ECN, 2019) with a TRL of 3–6 (Gazzani et al., 2015; Axelson et al., 2018), and Top-Gas-Recycling Blast Furnace (Meijer et al., 2009; Birat, 2020), which involves the recirculation of the BFG as a reducing gas. The choice of BFG over flue gases as the source of CO_2 for partial capture is advantageous in the techno-economic sense due to the higher CO_2 partial pressures (Sundqvist et al., 2018; Biermann et al., 2019) and the absence of oxygen (Dreillard et al., 2017) in the BFG. Near-term efforts will focus on partial CO_2 capture from one or a few stacks, to minimize the absolute and specific (per tCO_2-captured) costs by avoiding the high integration costs linked to having several stacks and to utilize excess heat as a low-cost heat source (Ali et al., 2018; Biermann et al., 2018, 2019). As of June 2020, globally, one CCUS project involving steel mill off-gases utilizes 0.8 $MtCO_2$ annually for enhanced oil recovery in Abu Dhabi (Global CCS Institute, 2019), and one CCS project ("3D") is in early development in France (Dreillard et al., 2017; Birat, 2020; CORDIS, 2020) with a potential capacity of ~1.5 $MtCO_2$ to be stored annually.

Fermentation of Steel Mill Waste Gases to Ethanol

Bioethanol from sugar crops dominates global biofuel production (>60% share) and is used as drop-in fuel at lower blend levels (5%–-22%) (World Bioenergy Association, 2019) in combination with gasoline. To meet the Paris Agreement, the IEA recommends, *inter alia*, the commercialization of advanced biofuels from, for example, lignocellulosic biomass (IEA, 2019). Ethanol produced from lignocellulosic biomass via enzymatic hydrolysis and fermentation (Robak and Balcerek, 2018) requires expensive pretreatment and leaves the lignin fraction unconverted (Liew et al., 2016). Alternatively, the entirety of the biomass can be gasified followed by either catalytic Fischer–Tropsch (FT) synthesis or fermentation by acetogenic bacteria. Although associated with slower conversion rates and limited substrate solubility, syngas fermentation occurs at ambient conditions, is more flexible in terms of the substrate's H_2:CO ratio, and has a higher conversion rate and product selectivity than FT processes (Liew et al., 2016). After fermentation, the ethanol is separated from water by distillation and dehydration (Pardo-planas et al., 2017), or via extraction (Phillips et al., 2017). The energy intensity of the distillation is in the range of 5–12 MJ/kgEtOH for concentrations of ethanol in the fermenter effluent of 6–2 wt.% (Molitor et al., 2016).

Steel mill gases that contain fossil-derived CO and H_2 are attractive for ongoing carbon capture and utilization (CCU) projects to form ammonia, methanol, polymers, and polyaclohols ("Carbon2Chem"; Federal Ministry of Education and Research of Germany, 2016), methanol for transport ("FReSME"; CORDIS, 2016), polyurethane for isolation ("Carbon4Pur"; CORDIS, 2017), and ethanol for transport ("Steelanol"; Steelanol Consortium, 2015). All steel mill gases can be used for syngas fermentation (Handler et al., 2016; Molitor et al., 2016). However, the basic oxygen furnace gas has the highest CO content, followed by the BFG. Life cycle assessments of ethanol fermented from steel mill gas have found a 40%–60% and 56%–70% reduction in greenhouse gas (GHG) emissions compared to conventional gasoline for on-road vehicles in Chinese (Ou et al., 2013) and US (Handler et al., 2016) contexts, respectively. In comparison, converting 100% biogenic feedstocks to ethanol by gasification and subsequent fermentation could lead to reductions in GHG emissions of 92%-98% compared to gasoline for on-road vehicles depending on feedstock (Handler et al., 2016). Syngas fermentation is being commercialized, mainly by LanzaTech. The first large-scale plant producing 46,000 tEtOH/year from steel mill gases was commissioned in 2018 (LanzaTech, 2018). The planned capacity of Steelanol (also LanzaTech) is 63,000 tEtOH/year, to be commissioned in 2022 (Steelanol Consortium, 2015).

OVERVIEW OVER ALLOCATION AND REGULATIONS APPLIED IN EU

Allocation is here defined as the partitioning of input or output flows of a process or a product system between the product system under study and one or more other product systems (ISO, 2006). Allocation should be dictated by the physical and quantitative relationships between inputs/outputs and the co-products, such as mass or energy content of product/intermediate streams, and energy or exergy consumption. Alternatively, the allocation can be based on the economic value of the products. Concerning a conventional, fossil-based, integrated steel mill, allocation methods have been studied to determine the CO_2 intensity of the electricity produced from the steel mill off-gases (Messagie et al., 2013), as well as to determine the emissions intensities of the blast furnace products of pig iron and slag (World Steel Association, 2014). A life cycle assessment

TABLE 1 | Regulations and guidelines relevant to this work and the applicable allocation schemes/methodologies that they incorporate. This list is not exhaustive and is based solely on a literature search.

Regulation/guideline	Mass content	Energy content	^{14}C-analysis	Other	Reference
Allocation of GHG emissions between fuel and coproducts					
RED II and FQD	—	LHV basis	—	—	(European Parliament and Council of the European Union, 2018a; European Parliament and Council of the European Union, 2018b)
Allocation scheme (Schimmel et al., 2018) for fuels co-processed from biogenic and fossil feedstocks					
DIN 51637 (Germany)	—	—	✓	—	(Schimmel et al., 2018)
Department for Transport: RTFO (UK)	—	✓	—	—	(Schimmel et al., 2018)
ISCC GmbH	✓	✓	✓	(attribution - ?)	(ISCC, 2017; Schimmel et al., 2018)
KRZ INIG System	—	✓	—	—	(Schimmel et al., 2018)
CARB (California)	✓	✓ (in draft)	✓ (in draft)	—	(Schimmel et al., 2018)
EU 2015/652	—	—	—	High-level principle of energy balance and efficiency	(European Commission, 2015)
Allocation rules for free allowances in the EU ETS					
Waste gases and process emissions subinstallation	—	—	—	Split of emissions between consumer/ producer of waste gas	(European Commission, 2019b)

of the carbon footprint of captured CO_2 for CCU purposes found that allocation based on a physical relationship between the amounts of captured CO_2 and the main product perform as well as substitution, although such allocation is superior in terms of obtaining product-specific emissions to allocation based on the mass or economic value of CO_2 and the main product (Müller et al., 2020).

Table 1 lists the EU regulations and guidelines applicable to the allocation schemes relevant to this work. Concerning fuel production processes, in general, the Renewable Energy Directive (RED II, Directive 2018/2001) (European Parliament and Council of the European Union, 2018a) and the Fuel Quality Directive (FQD, Directive 98/70/EC) (European Parliament and Council of the European Union, 2018b) mandate that the GHG emissions be divided between the fuel or its intermediate product and the coproducts in proportion to their energy contents (determined by the lower heating value, LHV).

Allocation for co-processing of biogenic and fossil feedstocks

The voluntary schemes applied in the EU (*cf.* **Table 1**) base the allocation of a biogenic feedstock to a certain process and to the corresponding biogenic products on one of the following:

(1) The energy content of cogenerated products;
(2) A (carbon) mass balance; and
(3) A C^{14}-analysis, that is, an actual physical measurement downstream of the co-processing unit.

Thus, the level of biogenic output and the allocation to the cogenerated products may vary depending on the adopted approach. Flexible allocations (e.g., economically motivated) outside these approaches have been described as incompatible with a previous draft of RED II (which was not implemented) (Schimmel et al., 2018). The guidelines issued by the certification company ISCC (ISCC, 2017) refer implicitly to such flexible allocation: *the determined sustainable bio-output can be attributed to the respective products. If 12C- or 14C-analyses [a] are conducted for a specific product, only the determined bio-content of this product can be sold as such.* Flexible allocation is beneficial to fuel-/chemical-producing companies for economic reasons because products that generate high levels of revenue on the market can be favored (Schimmel et al., 2018). As a compromise, Schimmel and colleagues have suggested allocating different shares of biogenic carbon within products ("within-product" allocation). This means, for example, the sale of an amount y of a fuel with 0% biogenic content and the sale of an amount x of the same fuel with 100% biogenic content, with x and y being limited by the total share of biogenic carbon that is allocated to each fuel produced in the same unit (Schimmel et al., 2018).

Free allowances for electricity and heat produced from steel mill waste gases

In the EU Emissions Trading System (EU ETS), sectors other than power generation are gradually transitioning to 100%

auctioning, although they continue to receive free allowances (EUAs) to prevent carbon leakage. Relevant to this work is the free allocation of EUAs for the production and consumption of waste gases, as laid out in the guidance document (European Commission, 2019b). In this system, a consumer of waste gas (e.g., a CHP plant operated on blast furnace off-gases) that produces electricity does not receive any free EUAs and must therefore pay for the CO_2 emissions from electricity production. Importantly, not all of the carbon in the waste gas that leaves the electricity generation unit is allocated to electricity. Instead, the carbon is split so that the inert CO_2 in the waste gas, which merely passes through the electricity generation unit, is an emission that is allocated to the producer of the waste gas (e.g., steel mill units and BF/BOF). Only those species (hydrocarbons and CO) that have a heating value for the electricity generation unit and are converted to CO_2 are allocated to electricity as an emission. In contrast, free allowances are received for the share of the waste gases that is consumed to produce heat and that is sold to produce a nonbenchmarked product or sold to a consumer outside of the EU ETS (e.g., district heating) (European Commission, 2019a).

Production of Biofuels

In the EU, the GHG emissions of biofuels for transport are regulated by the RED II and the FQD. Biofuels that do not meet the sustainability and GHG saving criteria are counted as fossil fuels. Biofuels from waste and residues other than those from, *inter alia*, agricultural and forestry sources must only meet the GHG-saving criteria. The sustainability criteria (art. 29 §2-7) consider, *inter alia*, restrictions on the usage of land areas with high biodiversity or high-carbon stock (wetlands and peatland) for agricultural biomass, and consider sustainability and land use, land-use change, and forestry (LULUCF) criteria for forestry biomass. For transport biofuels, a GHG emissions-saving criterion is defined as 65% relative to a fossil comparator emitting 94 gCO_{2eq}/MJ. Biomass is regarded as CO_2-neutral when combusted, that is, the CO_2 released originates from the atmosphere and has accumulated during the growth phase of the biomass, that is, assuming the net growth in carbon stock is equal to, or larger than, the outtake over a sufficiently long time, such as the case in Sweden. The biogenic carbon balance should include the upstream/life cycle GHG emissions, such as those encountered during cultivation, extraction, and processing, and during the transport and distribution of feedstock and products. Potential savings from CCS or CCU can be claimed according to the accounting methodology (Annex V, RED II), as described in **Supplementary Material Section 1**. Of importance is the role of electricity in producing alternative fuels. Concerning the production of renewable fuels of nonbiologic origin, RED II foresees that the electricity used is of renewable origin (for details, see paragraph 90 and article 27.3), whereas the Joint Research Centre suggests to use the average GHG intensity of electricity supplied in a member state or in the EU (Joint Research Centre, 2016). Similarly, for transport fuels, biofuels, and bioliquids, the GHG intensity of imported electricity can represent either a defined region or a source not connected to the grid (RED II, Annex V, C.1).

METHOD

This theoretical work builds upon well-documented mass and energy balances of a model of a typical European integrated steel mill validated against real process data (IEAGHG). Changes to these concerning energy demand and carbon (mass) flows with the integration of mitigation technologies are quantified by simple spreadsheet calculations based on published information about these technologies (see *Investigated Systems and Cases of Applied CO_2-Mitigation Technologies*). Examined technologies are Bio-PCI using biochar from the slow pyrolysis of wood waste type B collected from construction and demolition sites, ethanol synthesis from BFG via syngas fermentation of mainly CO and H_2, and CCS from BFG using amine absorption. Note that commercial stakeholders, including technology providers, might claim process performances exceeding those assumed here for the syngas fermentation and for amine-based CO_2 capture. The changes in carbon mass flows and energy balances are calculated for four configurations of the integrated steel mill:

C1: Reference mill with excess electricity production;
C2: Bio-PCI and electricity production;
C3: Bio-PCI and ethanol production; and
C4: Bio-PCI, ethanol production, and CCS.

These four technical configurations are examined concerning the emission intensity of their products depending on allocation schemes of avoided emissions due to shares of biogenic carbon and due to CCS (see *Investigated Systems and Cases of Applied CO_2-Mitigation Technologies, Allocation and Attribution Schemes in Co-Processing, andCO_2 Emission Intensities of Low-Carbon Products and Avoided CO_2 Emissions*). A sensitivity analysis on the resulting emission intensities is conducted with respect to indirect emissions from imported grid electricity and the extent of possible heat integration between the processes. In addition, the potential reduction in emissions of configuration C4 (Bio-PCI, ethanol, and CCS) is assessed for varying the extent of biochar injection and CO_2 capture from the BFG to represent both a near-term implementation and the potential future development.

Investigated Systems and Cases of Applied CO_2-Mitigation Technologies

Figure 1 presents an overview of the studied integrated steel mill and associated product systems, comprising the steel product system, the electricity grid system, and the transport fuel system. The allocation of avoided emissions due to shares of renewable carbon in the process streams and due to CCS is studied in the subsystem downstream of the blast furnace (indicated by the blue line in **Figure 1**), here termed the *carbon allocation system* (CAS). Process streams receive biogenic and/or fossil carbon via a selected allocation scheme (presented in *Allocation and attribution schemes in co-processing*), in line with the voluntary schemes for co-processing applied in the EU (*cf.* **Table 1** and *Allocation for Co-Processing of Biogenic and Fossil Feedstocks*), and move it through process units until the carbon is either emitted or captured as CO_2 or ends up physically in a product (steel and

ethanol). All the carbon in the streams, captured CO_2, and emissions leaving the CAS are allocated to the formed products (ethanol, steel, and electricity) such that all the direct CO_2 emissions of the steel mill are considered. In principle, the carbon flowing into each process unit that is emitted as CO_2, captured for storage, or ends up in the product is allocated to the product that is processed within that unit. While this is trivial for most units, it is nontrivial for CO_2 capture from intermediate streams associated with several products (which require the allocation of avoided emissions, see *Allocation and attribution schemes in co-processing*) or for units that consume steel mill waste gases, for which we adopt a methodology in line with the EU ETS emissions split (see *Allocation and Attribution Schemes in Co-Processing*). The direct emissions of the CAS are augmented by the indirect emissions that arise from the three product systems with the implementation of mitigation technologies, as compared to a reference mill. For this, an expanded system is defined (indicated by the red line in **Figure 1**), here termed the *total emissions system* (TES). This is instead of adopting the terminology of scope 1, 2, and 3 emissions, which is nontrivial for a circular, non–end product such as steel. Indirect emissions consider changes to the electricity grid's emissions that occur due to the import or export of electricity. The transport fuel system considers the transport and distribution of wood waste and ethanol, as well as the (fossil) emissions arising from combustion in a vehicle. Thus, TES quantifies the overall reduction of CO_2 emissions, as well as the CO_2 emission (equivalents) intensity for each product (see *Allocation and Attribution Schemes in Co-Processing*). Importantly, no reduction in the emission of carbon molecules to the atmosphere is counted double, which means that it can only be ascribed to one of the three product systems. The calculation of the emission intensity of the transport fuel (ethanol) and the criteria for biofuels are based on the RED II accounting methodology and emissions saving targets for biofuels used for transport (*cf. Production of Biofuels* and **Supplementary Material Section 1**).

Reference Integrated Steel Mill

To represent a typical European integrated steel mill, a reference mill with a production capacity of 4 Mt hot-rolled coil (HRC) per year and direct fossil emissions of 8,377 kt CO_2 per year (2,094 kg CO_2/t HRC) is studied. The mass flows are adopted from the IEAGHG CCS study (IEAGHG, 2013). **Figure 2** shows the carbon balance over the studied CAS subsystem (**Figure 1**) in the reference steel mill, with the underlying material flows listed in **Supplementary Table S1**. Approximately 30% of the carbon input into the CAS is PCI-coal, and around 87% of the carbon leaves the CAS in the form of CO_2 emissions, whereas only ~0.2% remains in the solid phase in the steel product. The remaining carbon is sent to other steel mill units (sinter plant and coking plant). The energy balance of the steel mill shown in **Figure 3** is modified from (IEAGHG, 2013) to model an excess electricity generation of 10%, as compared to the required electricity for steel mill operations. In addition, export of excess heat to industrial or municipal district heating is assumed in order to reflect more accurately a typical steel mill, since the IEAGHG study assumed a steel mill with no energy export. In the reference mill, the CHP plant receives its thermal inputs from BFG (63%), BOFG (18%), COG (2%), and NG (18%) and operates with electric and total efficiencies of 32.2% and 80.2%, respectively.

Pulverized Biochar Injection (Bio-PCI)

Pretreated biomass enters the blast furnace in the form of biochar (the upgrading process is outside the scope of the present work), as indicated in **Figure 1**. The biochar resembles woody biomass that is upgraded via slow pyrolysis with a carbon content of ~80 $wt.\%_{wet}$. The slow pyrolysis process is chosen due to its techno-economic performance (Wiklund et al., 2017) and the possibility to apply high replacement rates (up to 100%) of the fossil-based PCI. According to Wang et al. (2015), a greater mass of biomass must be injected in relation to the reference PCI-coal to achieve the same level of blast furnace operation. The amount of additional biochar is determined by the substitution ratio $\phi_{subst.}$ [see **Eq. 1**], which is adopted from the publication of Wang et al. (2015) and applied to the reductants specified in this work (see **Supplementary Table S2**). The biochar used here, $\phi_{subst.}$ is 0.9067. The share $r_{bio\text{-}PCI}$ of pulverized coal that is replaced by biochar [see **Eq. 2**] is set to 10% to resemble a replacement rate that is deemed to be practically feasible for an initial near-term implementation. Other items that are injected, such as coke and oxygen, as well as the gas distribution between the steel units are kept constant when introducing biochar. Thus, the total amount of BFG generated increases slightly. Changes in the composition of the BFG are neglected, since they are assumed to be negligible.

$$\phi_{\text{subst.}} = \frac{\dot{m}_{\text{PC}}}{\dot{m}_{\text{biochar}}} \left[\frac{\text{kg}}{\text{kg}}\right] \tag{1}$$

$$r_{\text{bioPCI}} = \frac{\dot{m}_{\text{PC, replaced}}}{\dot{m}_{\text{PCI}_{\text{REF}}}} = \frac{\dot{m}_{\text{biochar}} \cdot \phi_{\text{subst.}}}{\dot{m}_{\text{PCI}_{\text{REF}}}} \left[\frac{\text{kg}}{\text{kg}}\right] \tag{2}$$

Syngas Fermentation

A simplified syngas fermentation process is assumed (**Figure 4**). The size of the plant (production rate of ethanol) is chosen to match the biomass input into the blast furnace so that the input of biogenic carbon matches the output of carbon in ethanol (independent of the biomass share). The feed gas is assumed to be BFG. This choice allows one to study the effects of a combined implementation of CCS and ethanol production from the same intermediate stream, the BFG. The key assumptions made for the syngas fermentation plant are listed in **Supplementary Table S3**. The electricity consumption is 3.7 MJ/kgEtOH (Piccolo and Bezzo, 2009). The BFG conversion rate is determined according to the reactions defined by others (Piccolo and Bezzo, 2009), and assumed conversion rates for CO and H_2 of 80% and 40%, respectively, are similar to the values reported previously (Pardo-planas et al., 2017). The fractional conversions and the reactions implemented are listed in **Supplementary Table S4**. The steam demand for the distillation is determined as 10.3 MJ/kgEtOH, which is similar to values (9.8–12.0 MJ/kgEtOH) reported previously (Piccolo and

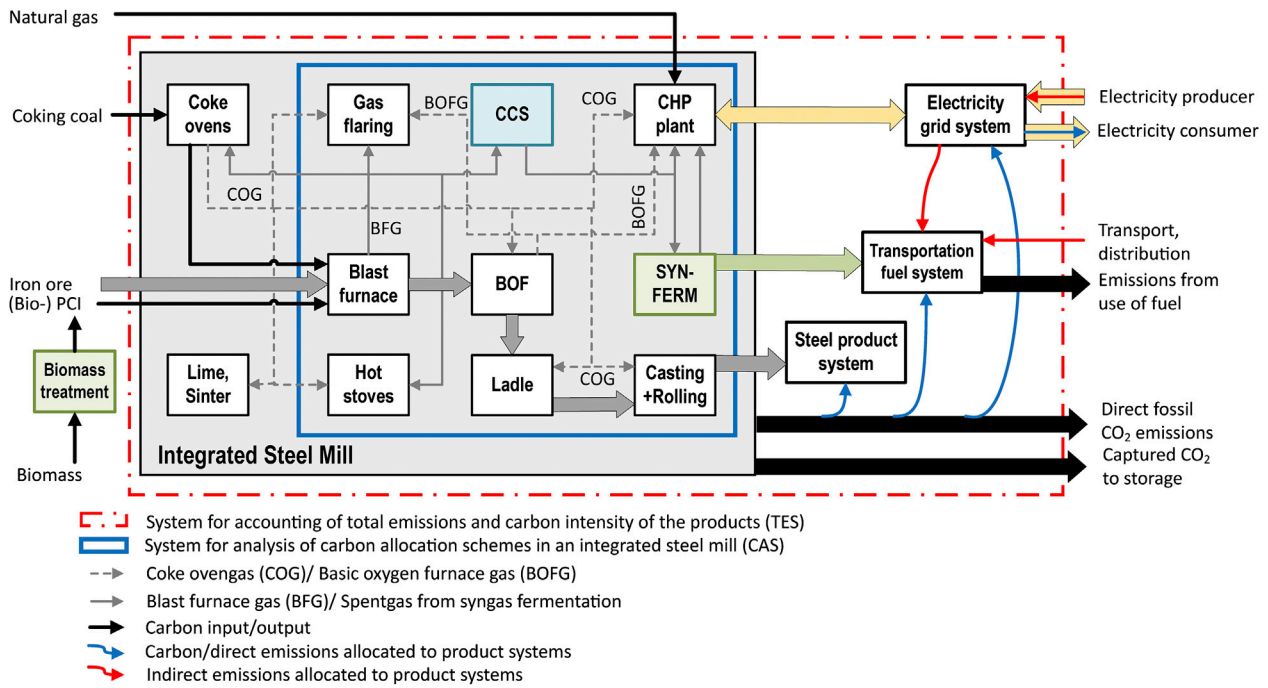

FIGURE 1 | Overview of the systems considered in the present study. An integrated steel mill with major process units (white boxes), its carbon-rich streams (black and grey), and its products, which are supplied to three product systems (thick arrows). The considered mitigation technologies of CCS, biochar injection (Bio-PCI) and syngas fermentation (SYNFERM) are highlighted in color. The CAS and TES are used for the study of carbon allocation schemes and emissions accounting, respectively. Abbreviations: BFG, blast furnace gas; BOF(G), basic oxygen furnace (gas); CAS, carbon allocation system; CHP, combined heat and power plant; COG, coke oven gas; TES, total emissions system.

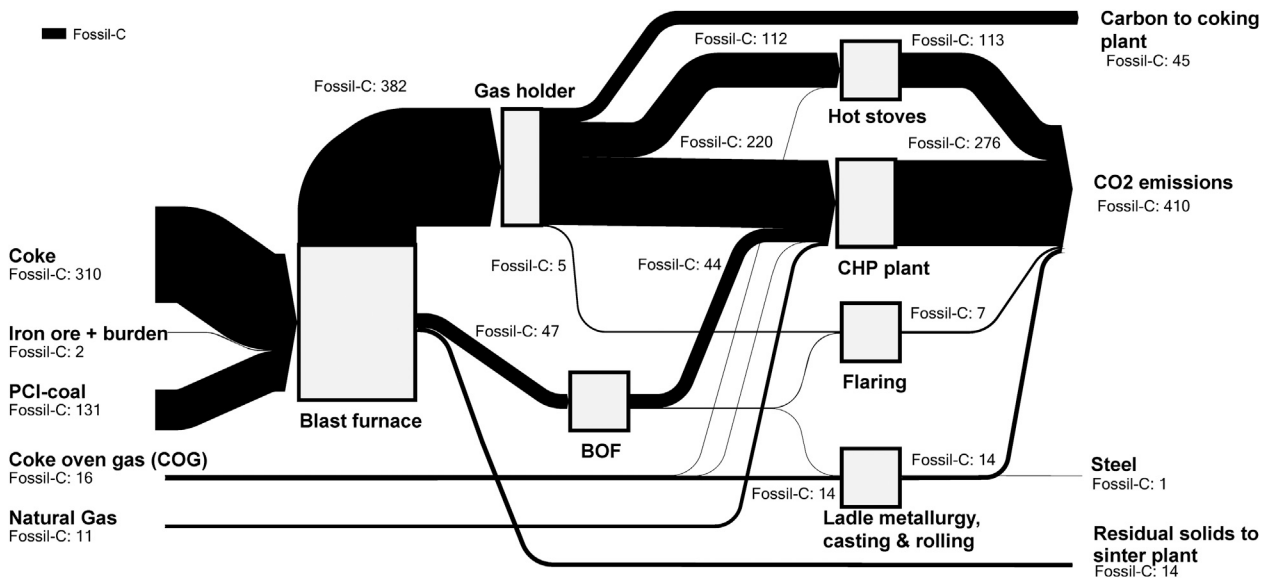

FIGURE 2 | Carbon balance of the reference integrated steel mill excluding units upstream of the blast furnace (coke ovens, lime kiln, sinter plant) according to the blue system boundary in **Figure 1**. The mass balances are derived from previous paper (IEAGHG, 2013). The values shown are presented in kilograms of carbon per ton of hot-rolled coil (HRC).

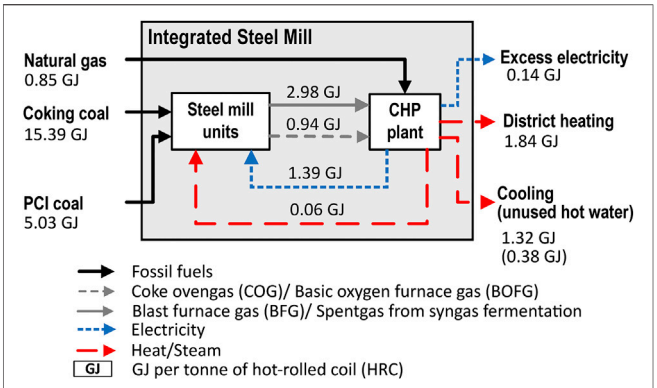

FIGURE 3 | Energy flows for the reference steel mill with a production of 4 Mt HRC per year; adapted from (IEAGHG, 2013; Lulekraft, 2018). The values shown are per ton of HRC.

Bezzo, 2009; Molitor et al., 2016; Pardo-planas et al., 2017). The spent gas from the fermentation is sent back to the CHP plant.

Amine Absorption of CO_2

The CO_2 capture process uses an amine solvent, that is, aqueous 30 wt.% monoethanolamine (MEA) to reflect the most commonly applied capture technology. The chosen feed gas is the BFG because its techno-economic performance is superior to those of other CO_2 sources at a steel mill viable for near-term implementation (Biermann et al., 2019). The capture unit is placed after the BFG cleaning unit and before the BFG holder. Thereafter, the gas is distributed to the hot stoves, coking plant, and CHP plant, or it is flared in case of excessive amounts. The heat requirement, based on a previous work (Sundqvist et al., 2018), together with the power consumption, including compression at 7 bar for ship transportation (Deng et al., 2019), and the BFG composition are listed for various capture rates in **Supplementary Table S5**. As a default value, a capture rate of 90% is assumed, which is within the range of capture rates associated with the lowest investment cost per captured ton of CO_2 (Rao and Rubin, 2006; Biermann et al., 2018). Extension of the capture rate to 99% is carried out to explore the maximal mitigation that can be achieved with CCS and Bio-PCI.

Allocation and Attribution Schemes in Co-processing

We apply the common definition of allocation as described in *Overview Over Allocation and Regulations Applied in EU.* Thus, the biogenic content is allocated to any formed (intermediate) coproduct in the process or intermediate process into which the biomass was introduced with respect to consistent physical principles (e.g., the carbon (mass) or energy content of the product). In addition, we define "*attribution*" as a free-choice allocation of biogenic content to any (intermediate) coproduct formed in the process or intermediate process into which the biomass was introduced. In this context, CO_2 is explicitly not automatically regarded as a loss/waste of biogenic carbon, but instead as a potential product.

For the steel mill, the differences in the allocation schemes are of great importance to the blast furnace, as illustrated for these four selected schemes (**Figure 5**):

- The allocation by mass of carbon (top-left panel in **Figure 5**) gives each effluent stream of the blast furnace the same share of biogenic carbon $f_{bio,BF,mass}$ corresponding to the mass fraction of total carbon $w_{C,i,total}$ in that stream. In all of the carbon-containing effluent streams, each carbon-containing species (including CO_2) is assigned the same share of biogenic carbon $f_{bio,BF,mass}$, as described by **Eq. 3**. This share is determined by the weighted ratio of the biogenic and fossil inputs into the process according to **Eq. 4**. For the calculation of $f_{bio,BF,mass}$, the pretreated biochar (Bio-PCI) is considered as a biogenic input, whereas the remaining PCI-coal and the coke are fossil inputs.
- For the allocation by energy content (top-right panel in **Figure 5**), the share of biogenic carbon/content in the inputs to the blast furnace is based on an energetic weighting factor $f_{bio,BF,LHV}$ according to **Eq. 5**. The biogenic output of the blast furnace, which is the total output amount (mass) multiplied by $f_{bio,BF,LHV}$ is allocated to the effluent streams based on the ratio of their energy content, that is, the mass flow multiplied by the LHV. The share of biogenic content $w_{bio,i,LHV}$ in each effluent stream is calculated accordingly, as in **Eq. 6**. This allocation scheme based on energy content implies a 100% allocation of biogenic content to CO (88%) and H_2 (12%) in the BFG, since pig iron, the blast furnace slag, and the CO_2 in the BFG have an LHV value of zero. Note that the fossil carbon is allocated in a corresponding manner, that is, it does not necessarily follow the actual mass flows of carbon, as compared to the allocation by mass. An example of this is the dissolved carbon in pig iron.
- The third allocation scheme is termed *physical partitioning* (bottom-left panel in **Figure 5**). It allocates (biogenic) carbon to the energy consumed for the formation of the coproducts, that is, the effluent streams of the blast furnace. Adapting exemplary values from **Supplementary Table S6** (World Steel Association, 2014) implies that 61.7% of the biogenic carbon is allocated to the hot metal (HM) (10,032 MJ/t HM);

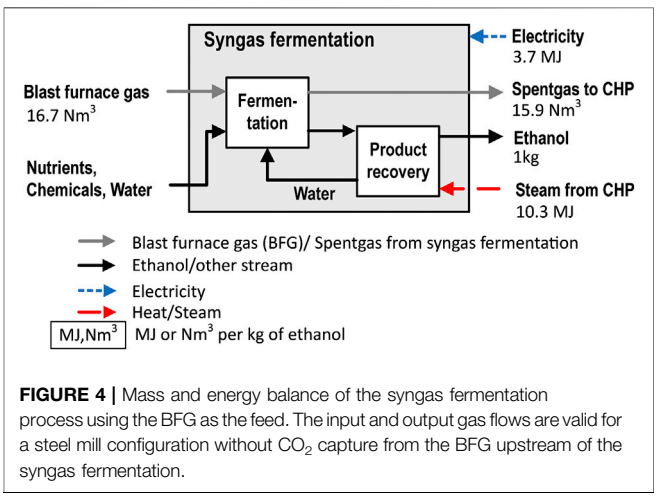

FIGURE 4 | Mass and energy balance of the syngas fermentation process using the BFG as the feed. The input and output gas flows are valid for a steel mill configuration without CO_2 capture from the BFG upstream of the syngas fermentation.

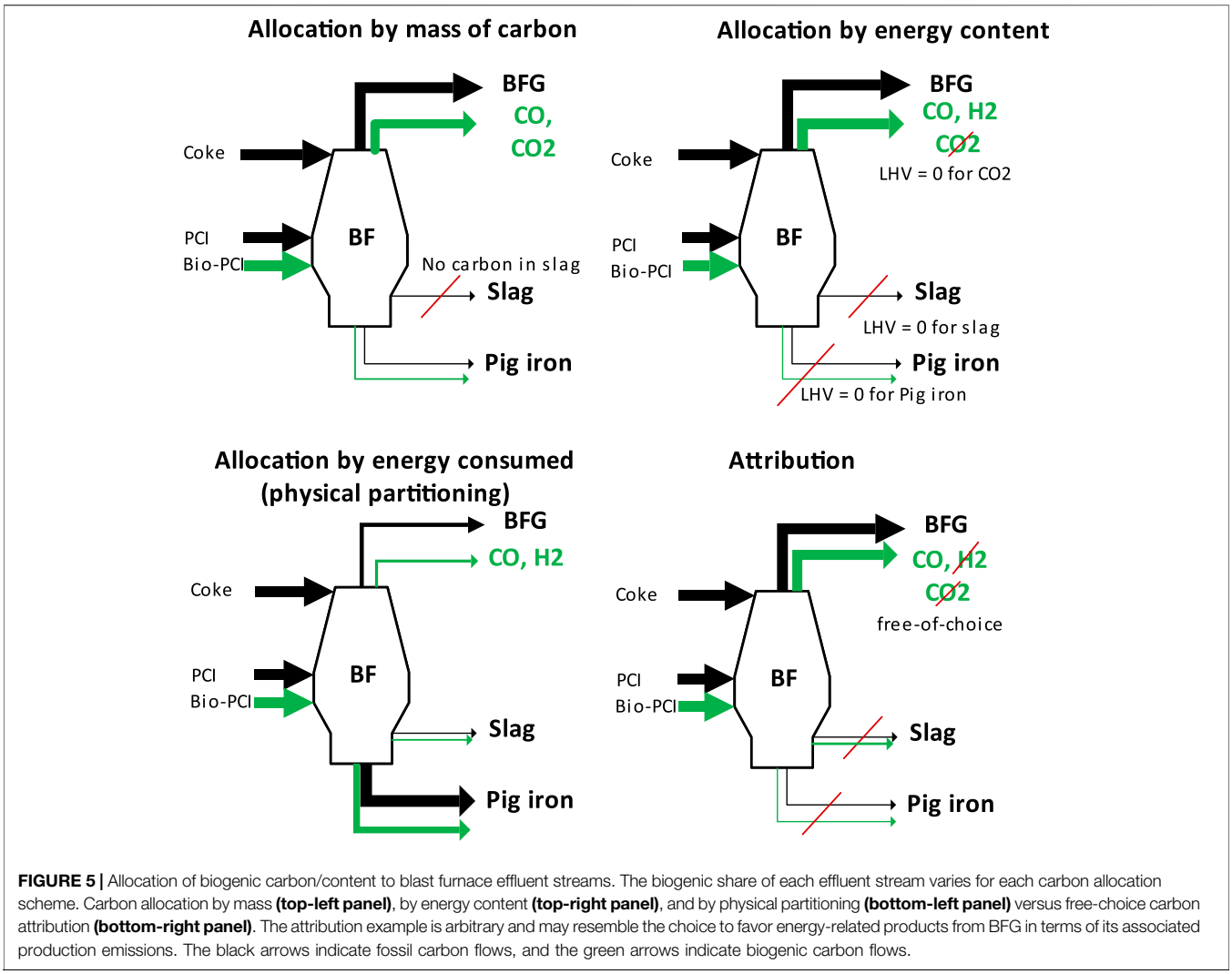

FIGURE 5 | Allocation of biogenic carbon/content to blast furnace effluent streams. The biogenic share of each effluent stream varies for each carbon allocation scheme. Carbon allocation by mass **(top-left panel)**, by energy content **(top-right panel)**, and by physical partitioning **(bottom-left panel)** versus free-choice carbon attribution **(bottom-right panel)**. The attribution example is arbitrary and may resemble the choice to favor energy-related products from BFG in terms of its associated production emissions. The black arrows indicate fossil carbon flows, and the green arrows indicate biogenic carbon flows.

33.91% is allocated to the BFG, which contains the remaining unconsumed energy (5,472 MJ/t HM); and 3.92% is allocated to the blast furnace slag (632 MJ/t HM).

- The fourth scheme involves attribution (bottom-right panel in **Figure 5**), which maximizes the allocation of biogenic carbon to CO in the BFG. Thus, no biogenic carbon is attributed to the slag, pig iron, or CO_2 in the BFG.

$$w_{\mathrm{bio,i,mass}} = f_{\mathrm{bio,BF,mass}} \cdot w_{\mathrm{C,i,total}} = \sum_{\text{species in i}} f_{\mathrm{bio,BF,mass}} \cdot w_{\mathrm{C,i,species}} \quad (3)$$

$$f_{\mathrm{bio,BF,mass}} = \frac{\dot{m}_{\mathrm{bio-PCI}} \cdot w_{\mathrm{C,bio-PCI}}}{\dot{m}_{\mathrm{bio-PCI}} \cdot w_{\mathrm{C,biochar}} + \dot{m}_{\mathrm{PCI}} \cdot w_{\mathrm{C,coal}} + \dot{m}_{\mathrm{coke}} \cdot w_{\mathrm{C,\ coke}}} \quad (4)$$

$$f_{\mathrm{bio,BF,LHV}} = \frac{\dot{m}_{\mathrm{bio-PCI}} \cdot LHV_{\mathrm{biocoal}}}{\dot{m}_{\mathrm{bio-PCI}} \cdot LHV_{\mathrm{biochar}} + \dot{m}_{\mathrm{PCI}} \cdot LHV_{\mathrm{coal}} + \dot{m}_{\mathrm{coke}} \cdot LHV_{\mathrm{coke}}} \quad (5)$$

$$w_{\mathrm{bio,i,LHV}} = \frac{f_{\mathrm{bio,BF,LHV}} \cdot \dot{m}_{\mathrm{BF,output}} \cdot \frac{\dot{m}_i \cdot LHV_i}{\sum_j \dot{m}_j \cdot LHV_j}}{\dot{m}_i} \quad (6)$$

Here, we investigate in greater detail the two schemes that represent the two extremes of the range of the above allocation schemes: 1) carbon allocation based on mass via a carbon mass balance and 2) an attribution scheme that favors energy-related products from BFG according to **Figure 5**. The carbon allocation by mass distributes biogenic carbon evenly according to the actual carbon flows in the steel mill. In this way, each stream that diverges to other purposes on the way from Bio-PCI to the ethanol product can be viewed as a "loss" of biogenic carbon to the atmosphere, thereby reducing the emission intensity of the steel, rather than raising the biogenic content of the ethanol. These diverging carbon flows are illustrated qualitatively in **Figure 6**. In contrast, the attribution scheme allows the following choices as to the

pathway from Bio-PCI to the ethanol and thus can maximize the biogenic content of the BFG for ethanol or electricity production:

- In the blast furnace, all biogenic carbon is attributed to CO in the BFG. To allow for comparison with the allocation by mass, the biogenic input to the blast furnace is determined by $f_{bio,BF,mass}$ according to **Eq. 3**.
- In the gasholder, all the Bio-CO is attributed to the BFG going to the syngas fermentation plant, such that none of it is attributed to the CHP plant or other steel units.
- In the syngas fermentation plant, all the Bio-CO is attributed to the carbon in the produced ethanol. The CO and H_2 that are not converted and remain in the spent gas (together with CO_2) are therefore fossil-derived. Note that due to conversion losses, any other allocation scheme would have allocated some biogenic CO/CO_2 to the spent gas.

In addition to the biogenic content, avoided CO_2 emissions due to CO_2 capture from the BFG are allocated, since the BFG is an effluent of the steel production process and a feed to the syngas fermentation, and is, thus, associated with the production of steel and ethanol (see also **Supplementary Material Section 1**). We propose that the allocation of avoided CO_2 $E_{CCS,avoided}$ to ethanol $E_{CCS,ethanol}$ and steel $E_{CCS,steel}$ be determined by the same set of allocation schemes as presented for the allocation of (biogenic) carbon. In this way, the selected allocation scheme governs the share of the CO_2-lean stream (effluent gas of the CCS plant) that each product or product system receives downstream of the CCS plant [see **Eq. 7**]. Thus, the CO_2 avoided from CCS $E_{CCS,avoided}$ is allocated to the products according to the ratio of the received CO_2-lean stream in terms of carbon mass content, energy content, or consumed energy or according to the attribution. The CO_2 avoided through CCS operation is calculated by **Eq. 8** and considers the emissions for powering the CCS plant (see *Allocation and Attribution Schemes in Co-Processing*), and for the transport and storage of the CO_2, which are deemed to be low and are not considered in this work. Furthermore, we assume that fossil CO_2 is prioritized for capture on a stream basis, which means that no biogenic carbon is allocated to the captured CO_2 unless all of the fossil CO_2 from a stream is captured. The biogenic share of CO_2 in a stream fed to a CCS plant needs to be higher than the rate of captured $r_{capture}$ and stored CO_2, according to **Eq. 9**. Since the aspect of negative emissions is not the focus of the present work, only fossil CO_2 is captured in the default settings (10% replacement of PCI with biomass, 90% CO_2 capture from BFG), unless stated otherwise.

$$\frac{\text{allocated } CO_2 \text{ lean BFG to syngas fermentation}}{\text{allocated } CO_2 \text{ lean BFG to steel units}} = \frac{E_{CCS,ethanol}}{E_{CCS,steel}} \tag{7}$$

$$E_{CCS,avoided} = E_{CCS,captured} - E_{CCS,heat+pow} - E_{CCS,transport+storage} \tag{8}$$

$$w_{CO2,bio,captured} = w_{CO2,bio,stream} - \left(1 - r_{capture}\right) \overset{!}{\geq} 0 \tag{9}$$

CO_2 Emission Intensities of Low-Carbon Products and Avoided CO_2 Emissions

The products considered in this work are steel, (bio)ethanol, and electricity. Other commodities typically produced in steel mills, such as benzoles, sulfur, argon, and crude tar, are not considered as they are not directly affected by either Bio-PCI or CCS operation. The blast furnace and BOF slags are considered waste products and, thus, have no CO_2 emission intensity. The following paragraphs describe the allocations of carbon and direct and indirect CO_2 emissions to each product—steel, electricity, and ethanol.

The direct emissions of the steel products are calculated according to **Eq. 10**. The introduction of biogenic carbon into the blast furnace leads to a reduction in the level of fossil emissions compared to the reference steel plant (2,094 $kgCO_2$/t HRC), corresponding to the levels of (biogenic and fossil) carbon converted to ethanol and (biogenic and fossil) carbon allocated to excess electricity. Furthermore, the biogenic carbon, which ends up in the steel product or is emitted as CO_2 via the steel mill units (i.e., biogenic carbon not allocated to the biofuel or electricity), is subtracted from the direct carbon emissions of the steel mill. The avoided CO_2 due to CCS that is allocated to the steel product [*cf.* **Eq. 7**] also reduces the direct emissions. New indirect emissions from imported electricity and other upstream/downstream emissions related to changes in fossil inputs are allocated to the mitigation technologies and not to the steel production (see last paragraph in this section). Changes to upstream (e.g., less PCI-coal) or downstream (in the steel product system) emissions due to the implementation of mitigation technologies are deemed to be negligible and are not considered.

$$e_{steel} = e_{REF} - \left(\left(f_{foss,EtOH} + f_{bio,EtOH}\right) \cdot m_{C,EtOH} - \left(f_{foss,pow} + f_{bio,pow}\right) \cdot m_{C,pow,export} - f_{bio} \cdot m_{C,steelunits}\right) \cdot \frac{44}{12} \cdot \frac{1}{m_{steel}} - \underbrace{e_{CCS,steel}}_{\frac{E_{CCS,steel}}{m_{steel}}} \left[\frac{\text{kgCO}_2}{\text{t HRC}}\right] \tag{10}$$

with the following definitions:

e_{steel} Direct emissions steel; equal to the steel product emissions in this work; in $kgCO_2$/t HRC.
e_{REF} Reference mill direct emissions; in $kgCO_2$/t HRC.
$(f_{foss,EtOH}+f_{bio,EtOH}) \cdot m_{C,EtOH}$ Biogenic and fossil carbon allocated to ethanol; in kg of C.
$(f_{foss,pow}+f_{bio,pow}) \cdot m_{C,pow,export}$ Biogenic and fossil carbon allocated to exported electricity; in kg of C.
$f_{bio} \cdot m_{C,steelunits}$ Biogenic carbon allocated to steel mill units; in kg of C.
$e_{CCS,steel}$ Avoided CO_2 emissions from CCS operation allocated to the steel product; in $kgCO_2$/t HRC.

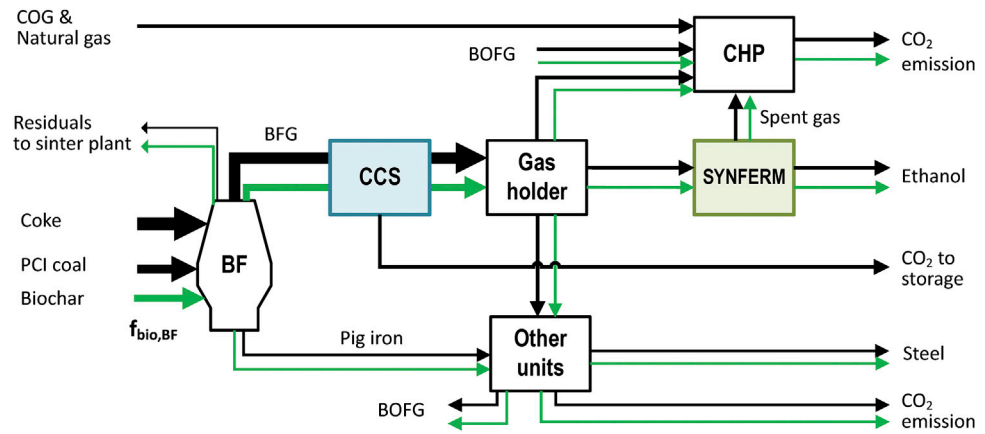

FIGURE 6 | Carbon flow pathways downstream of the blast furnace (CAS) when injecting biochar. The green arrows indicate the possible allocation/attribution of biogenic carbon to the respective process stream. The black arrows represent fossil carbon. Other units comprise steel mill units in the CAS, hot stoves, basic oxygen furnaces, gas flaring, ladle, and rolling and casting.

We base the allocation of emissions to exported electricity and heat produced from waste gases on the EU ETS guidance document (European Commission, 2019b) (see *Free Allowances for Electricity and Heat Produced from Steel Mill WasteGases*). The CO and H_2 in the BFG are oxidized in the CHP plant, and the resulting CO_2 emissions are allocated to the electricity. The CO_2 in the BFG is allocated to the waste gas producer, the blast furnace, and, thus, the steel product. These considerations yield an emission intensity of 546 gCO_2/kWh electricity for the reference steel mill (1,705 GWh/year). Since most of the electricity is consumed internally in the steel mill, only the exported excess electricity (157 GWh) leaving the steel mill carries this CO_2 burden. Respective EUAs have to be purchased from the market. Note that district heating supply is assumed to take place to non-ETS sectors, such as space heating for buildings, which means that free EUAs are received. Since they are not paid for, these emissions are not assigned an economic value. Therefore, we assume that they remain with the steel mill (steel product) and are not allocated to the heat supplied to a district heating system.

Regarding the ethanol emission intensity, we adopt the accounting methodology for transport biofuels from Annex V of RED II, though we simplify **Eqs. 1–11** by eliminating those terms that are not applicable to waste biomass (i.e., e_{ec}, e_l, and e_{sca}), since life cycle GHG emissions are not considered for waste up to the point of collection (Joint Research Centre, 2016; European Parliament and Council of the European Union, 2018a). The term e_{CCR} is omitted because no CO_2 is captured for the synthesis of other products or exported for utilization. The remaining terms in **Eq. 11** refer to the processing emissions $e_{p,SYN}$, transport and distribution emissions e_{td}, avoided emissions due to CCS allocated to ethanol $e_{CCS,EtOH}$, and emissions from the use of the fossil share of the ethanol $f_{foss,EtOH} \cdot eu$. Note that $e_{p,SYN}$ represents the processing of emissions from 1) fossil fuel combustion to cover the part of the heat demand of the syngas fermentation plant that exceeds the usable excess heat from the steel mill, 2) imported electricity to cover the electricity consumed by the syngas fermentation plant $P_{SYN,cons}$, and 3) imported electricity due to the diversion of BFG from the CHP to the syngas fermentation plant $P_{SYN,disp}$—the so-called counterfactual or displaced electricity demand. Diverting a share of the BFG from the power plant to produce a fuel instead will cause a shortfall in the electricity required for the steel mill, and this shortfall is assumed to be alleviated by imports from the grid (Joint Research Centre, 2016). The respective grid emissions are, therefore, allocated to the ethanol product. We assume that the loss of exported excess electricity in the reference steel mill is not included in this, since it is not the energy required to run the steel mill. Note that the spent gas leaving the syngas fermentation plant is directed back to the CHP plant; any CO in that stream is used for the electricity and heating purposes of both mitigation technologies, thereby reducing the amount of imported energy. CO_2 in the spent gas is assumed to originate from the blast furnace and is, therefore, allocated to the waste gas producer (steel mill). This simplified allocation is congruent to the EU ETS method for electricity and heat generation from waste gases.

$$e_{EtOH} = \underbrace{e_{p,SYN}}_{\frac{E_{p,SYN}}{m_{EtOH} \cdot LHV_{EtOH}}} + e_{td} - \underbrace{e_{CCS,EtOH}}_{\frac{E_{CCS,EtOH}}{m_{EtOH} \cdot LHV_{EtOH}}} + f_{foss,\,EtOH} \cdot e_u \left[\frac{gCO_2}{MJ}\right] \tag{11}$$

with the following definitions:

e_{EtOH} Emission intensity of the produced (bio)ethanol
$e_{p,SYN}$ Processing emissions from fossil fuel combustion for heating (if no excess heat is available), imported electricity for syngas fermentation operation, and displaced electricity (BFG diversion from CHP)
e_{td} Transport and distribution emissions for wood waste and the distribution of ethanol; 2.3 gCO_2 eq/MJ based on RED default values.

$e_{CCS,EtOH}$ Avoided CO_2 emissions from CCS operation allocated to the ethanol product.
$f_{foss,EtOH}$ Allocated fossil share in the produced ethanol
e_u Emissions from use of fuel; 71.54 gCO_2/MJ; 0 gCO_2/MJ for biogenic share.

The mitigation technologies require supplies of heat and electricity. We assume that heat is generated onsite in the existing CHP plant or in a CHP plant with similar performance profile, whereas electricity is bought from the grid when cogenerated electricity does not suffice to cover the demand. Modifying the CHP plant operation mode can maximize heat/steam production at a temperature of 130°C with electric and total efficiencies of 27.3% and 95.8%, respectively. The delivery of heat to district heating is maintained in all of the C1–C4 configurations. In case the switch in the CHP mode is insufficient, extra natural gas (NG) combustion is assumed and the respective direct emissions are allocated to the mitigation technologies corresponding to their heat demands, according to **Eq. 12**. In case power is imported, the emissions corresponding to the grid emission intensity are allocated to the mitigation technologies based on their ratios of power demand, according to **Eq. 13**. In case both CCS and syngas fermentation are implemented, the factors from **Eqs. 12**, **13** are used to calculate the emissions $E_{CCS,heat+pow}$ and $E_{SYN,heat+pow}$ in **Eqs. 14**, **15** for powering the CCS and syngas fermentation plant, respectively. To assess the sensitivity of heat integration, the fraction of the required heat that can be made available from excess heat via heat integration is defined in **Eq. 16** and varied between 0 and 1. The assumption of extra NG import is maintained when φ_{HEX} is <1.

$$f_{heat,CCS} = \frac{Q_{CCS}}{Q_{CCS} + Q_{SYN}};\ f_{heat,SYN} = 1 - f_{heat,CCS}\ [-] \tag{12}$$

$$f_{pow,CCS} = \frac{P_{CCS}}{P_{CCS} + P_{SYN,cons} + P_{SYN,disp}};\ f_{pow,syn} = 1 - f_{pow,CCS}\ [-] \tag{13}$$

$$E_{CCS,heat+pow} = Q_{foss,th} \cdot c_{foss} \cdot f_{heat,CCS} + P_{import} \cdot f_{pow,CCS} \cdot c_{pow,grid}\ [gCO_2] \tag{14}$$

$$E_{p,SYN} = Q_{foss,th} \cdot c_{foss} \cdot f_{heat,SYN} + P_{import} \cdot f_{pow,SYN} \cdot c_{pow,grid}\ [gCO_2] \tag{15}$$

$$\varphi_{HEX} = \frac{Q_{excess\ heat}}{Q_{CCS} + Q_{SYN}} = 1 - \frac{Q_{foss,th}}{Q_{CCS} + Q_{SYN}}\ [-] \tag{16}$$

where the following parameters are applied:

c_{foss} Emission intensity of NG combustion. A value of 65.9 gCO_2eq/MJ, including production and distribution, is used; EU mix (Guintoli et al., 2017).
$c_{pow,grid}$ Emission intensity of electricity imported from the grid. The default value of 295.6 gCO_2/kWh corresponds to the Year 2016 EU-28 average (European Environment Agency, 2018) Sensitivity analysis: 0–790 gCO_2/kWh, representing "extreme" cases of renewable electricity or coal condensation.
$f_{heat,CCS/SYN}$ Allocation factor for emissions related to the heat demand of the mitigation technologies.
$f_{pow,CCS/SYN}$ Allocation factor for emissions related to the power demand of the mitigation technologies.
$Q_{CCS/SYN}$ Heat demand of a mitigation technology
P_{CCS} Power demand of the CCS plant
$P_{SYN,cons}$ + $P_{SYN,disp}$ Power demand of the syngas fermentation plant due to consumption and displaced electricity demand (BFG diversion)
$Q_{foss,th}$ Thermal fuel input to the CHP plant from extra NG
P_{import} Imported power (total demand for steel, syngas fermentation, and CCS minus cogenerated electricity).
$Q_{excess\ heat}$ Heat demand of the mitigation technologies (combined) that can be covered through heat integration.

RESULTS

The first two Results sections present the carbon flows and product emissions intensities achievable with near-term mitigation technologies, that is, the replacement of 10% of the PCI with pyrolyzed biochar and corresponding ethanol production of 111.7 ktEtOH/year (27.9 kgEtOH/t HRC) or electricity generation of 157 GWh/year (39.3 kWh/t HRC) and 90% CO_2 capture from the BFG. The third section presents the results for long-term mitigation.

Effects of Carbon Allocation on the Flow Pathways of Biogenic Carbon

Figure 7 shows the flow of biogenic carbon for allocation by mass and attribution for a steel mill with ethanol production (C3) and for a steel mill with ethanol production and CCS (C4). Since the pulverized coal makes up around one-third of the fossil input to the blast furnace, the share of biogenic carbon is relatively small (3.2% of the total inlet) when replacing 10% of the PCI with biochar.

Without CCS, allocation by mass gives the same biogenic share in the ethanol as in the blast furnace input. The remaining share of biogenic carbon is either emitted as CO_2 (96.5%) in the steel mill units or contained in the final steel product (0.2%). For the attribution scheme, the total amount of injected biogenic carbon (14.6 kgC/t HRC) is attributed to the ethanol product—the unconverted feed to the syngas fermentation is counted as fossil-derived and emitted through the CHP plant.

With CCS, the biogenic share of the CO_2-lean BFG downstream of the capture unit is increased to 5.9% and 6.9% for mass-based allocation and attribution, respectively. This is because only fossil-derived CO_2 is assumed to be captured. The enhanced biogenic share of the CO_2-lean BFG leads to an increased share of biogenic carbon in the produced ethanol for the mass allocation scheme with CCS. For the attribution, the share of biogenic carbon attributed to the ethanol product is unaffected by CCS.

Emissions Intensities of the Cogenerated Products and Total Emissions Reductions

The overall emissions in TES (*cf.* **Figure 1**) are illustrated (diamond symbols) in **Figure 8**, together with the share of these emissions that each product system receives. The injection of biochar reduces the

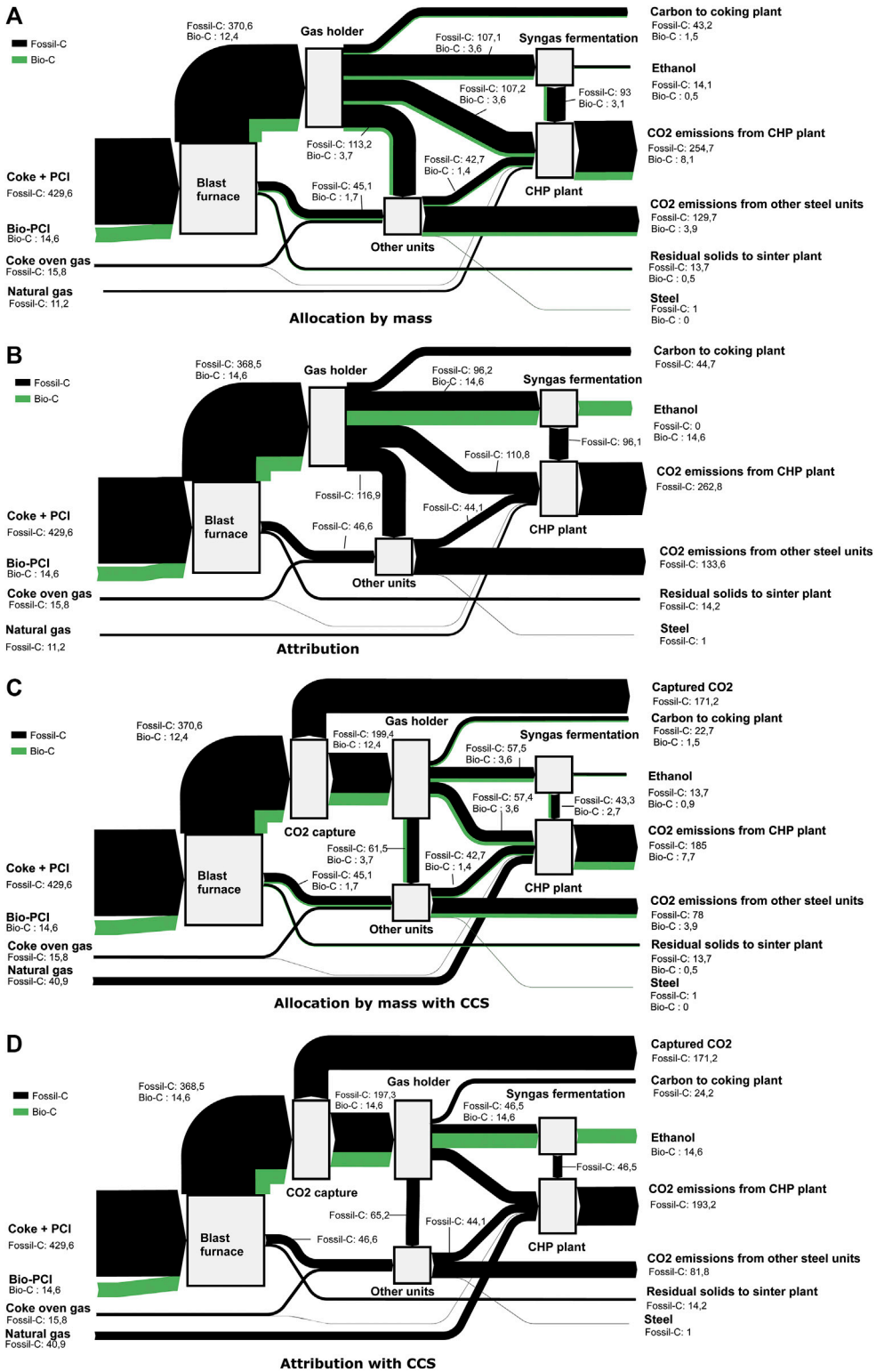

FIGURE 7 | Flow of biogenic carbon (green) throughout a mill with (A–D) ethanol production (C3) and (C, D) CCS (C4). The allocation between streams is given by (A, C) allocation by mass and (B, D) attribution. The green arrows are enhanced for visualization purposes (5:1) relative to the black arrows (fossil carbon). The values given are kg of carbon per ton HRC.

overall emissions by 2.5 and 3.5% in C2 and C3, respectively, when producing either electricity or ethanol. The application of CCS (C4) reduces emissions by 26.6%. The distribution of emissions varies as a function of the steel mill configuration and the carbon allocation scheme, although the steel product emissions clearly dominate due to the large differences in product volume. Note that the carbon allocation scheme does not affect the total emissions. The following three paragraphs consider each product system in detail.

The CO_2 emission intensities of the steel product when applying mitigation technologies [*cf.* **Eq. 10**] are shown in **Figure 9**. The emission intensity of steel produced in the reference mill (2,073 $kgCO_2$/t HRC) is reduced in all configurations, C2–C4, when biochar is introduced. Allocation by mass provides a large share of biogenic carbon to the steel product, *ca.* 50 $kgCO_2$/t HRC, which is more than the emission reduction achieved by cogenerating electricity in the reference case (C1). Attribution allocates all the biogenic carbon to ethanol and, thus, renders higher carbon emissions to the steel than allocation by mass. The cogeneration of ethanol (fossil + biogenic) has a similar effect on the steel-related emissions as the introduction of biochar (see C3 configuration with free attribution). The cogeneration of electricity (C2, mass allocation) is less-beneficial than cogeneration of ethanol with respect to the emissions from the steel product. As expected, CCS (C4) has the strongest impact on the emission intensity of steel, reducing it by 24%–26%. Note that allocation of the CO_2 emissions avoided (due to CCS) follows the allocation by mass principle also for the C4 configuration with free attribution. Thus, 93% of the avoided CO_2 emissions from CCS are allocated to steel.

The CO_2 emission intensities of the produced ethanol, as calculated from **Eq. 11**, are illustrated in **Figure 10**. The C1 and C2 configurations do not produce ethanol, and the emission intensity of the transport product system is the same as that of the fossil comparator, 94 gCO_{2eq}/MJ. In C3, the cogenerated ethanol has a higher emission intensity than the fossil comparator with mass-based allocation. Free attribution reduces the emission intensity, although the biofuel target is not met. Note that a large share of the ethanol emission intensity is related to the electricity demand caused by the diversion of BFG to the syngas fermentation plant (displaced electricity). If these emissions were allocated to the steel product instead, leading to an increase of 27 $kgCO_2$/t HRC; C3 with mass allocation would perform better than the fossil comparator, and C3 with free attribution would fulfill the biofuel criterion, that is, 65% emission savings compared to the fossil comparator.

Configuration C4, with syngas fermentation and CCS, requires the importation of NG to cover the heat demand ("$e_{P,SYN}$ heat consumed" in **Figure 10**). Since the heat is generated in the CHP plant, cogeneration of electricity increases, and this reduces the amount of emissions from the imported and displaced electricity. Despite this, the CO_2 avoided from CCS allocated to ethanol does not compensate for the fossil share of the ethanol when allocating based on mass. With free attribution, however, CCS may lead to negative emissions in the transport product system. The value of -7 gCO_{2eq}/MJ in **Figure 10** is based on a CO_2-avoided allocation of 93:7 between steel and ethanol (allocation by mass). The emission intensities would be +56 gCO_2eq/MJ and -624 gCO_{2eq}/MJ for the extreme (steel:ethanol) ratios of 100:0 and 0:100, respectively. This attribution of avoided emissions to a product beyond the zero-line (0 gCO_{2eq}/MJ) is unnecessary and should be avoided, unless the associated negative emissions can somehow be valorized by a robust, consumer-based, offsetting mechanism.

The absolute CO_2 emissions in the electricity grid system change when implementing mitigation technologies, as shown in **Figure 11**. For C1 and C2, electricity is exported, whereas for C3 and C4, electricity is imported. The indirect CO_2 emissions from the imported electricity are passed through to the cogenerated products (indicated by the bars cancelling out each other). The indirect emissions derived from the electricity required for CCS are considered in the CO_2 avoidance calculation. In C3 and C4, only the electricity previously exported from the steel mill (C1 and C2) must be generated elsewhere, causing emissions corresponding to the grid intensity (assuming that the existing capacities of power-generating facilities suffice). Since the default grid intensity (EU average of 295.6 gCO_2/kWh) is lower than the emissions intensities of the electricity in C1 and C2 (546 gCO_2/kWh and 384 gCO_2/kWh, respectively), C3 and C4 cause net lower emissions than C1 and C2. For grid intensities higher than the generated electricity's intensities in C1 and C2, the configurations C3 and C4 cause an increase in emissions in the electricity grid system.

Sensitivity of the Emission Intensity of Ethanol Toward the Emission Intensity of Electricity

Figure 12 shows the emission intensity of ethanol depending on grid intensities in the range of 0–788 gCO_2/kWh for configurations C3 (**Figure 12A**) and C4 (**Figure 12B**). The dashed lines indicate the ethanol intensity when displaced electricity is allocated to the steel product, rather than to ethanol. The emission intensity of ethanol in C3 is more sensitive to the grid intensity than C4. C3 has a lower intensity than the fossil comparator for grid intensities of <140 gCO_2/kWh and <580 gCO_2/kWh with mass allocation and free attribution, respectively. For attribution, the biofuel criterion is met for grid intensities of <180 gCO_2/kWh and <788 gCO_2/kWh, if the displaced electricity is allocated to steel. The C4 configuration performs better than the fossil comparator for all grid intensities. With the attribution of biogenic carbon, the biofuel criterion is met for all grid intensities. However, with mass allocation, the criterion cannot be reached even with carbon-free electricity due to the large fossil share in the ethanol and the heating of the syngas fermentation plant with NG. The C4 configuration with mass allocation could reach the biofuel criterion with low-carbon intensity heat, for example, excess heat or heating with zero-carbon electricity (electric boiler and heat pump).

Effect of Heat Integration on Product Emission Intensities

Figure 13 shows the CO_2 emission intensities of steel and ethanol as a function of the share of heat made available from heat integration, as defined by f_{HEX} in **Eq. 16** for the C3 and C4 configurations. Note that the filled symbols represent the default

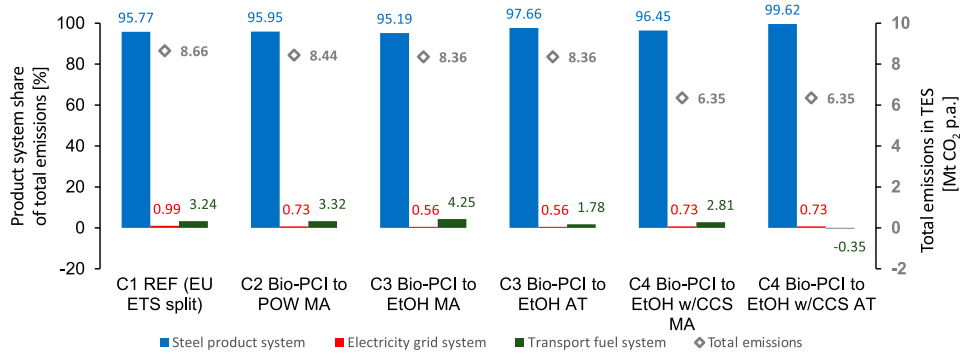

FIGURE 8 | Total emissions in TES and their distribution into the three product systems for the studied steel mill configurations C1–C4 depending on allocation by mass (MA) or attribution (AT). The grid intensity is 295.6 gCO_2/kWh (EU average). EtOH, ethanol production via fermentation of blast furnace gas; POW, electricity export; REF, reference mill with electricity export.

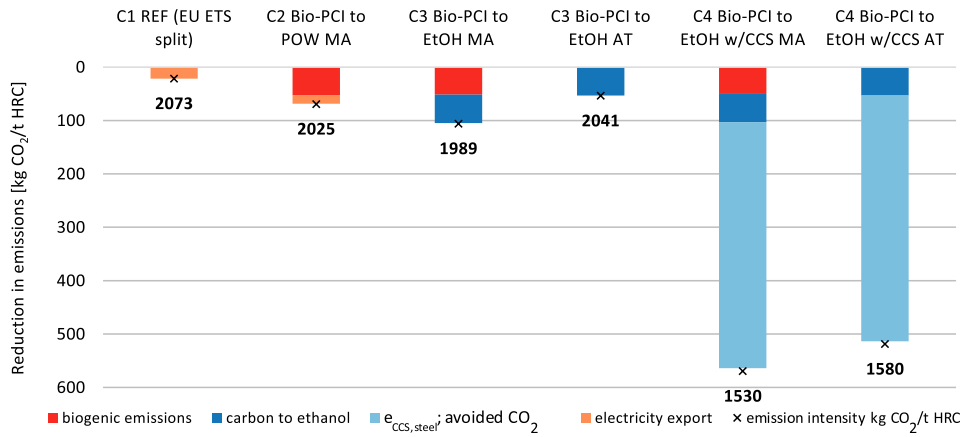

FIGURE 9 | Emissions compared to the reference mill and the resulting emission intensity (×) of the steel product, depending on the steel mill configuration and allocation scheme, that is, allocation by carbon mass balance (MA) and free attribution (AT), which maximizes the amount to biogenic carbon assigned to the ethanol production. The allocation of CO_2 avoided (CCS) is 93:7 (steel:ethanol) based on mass allocation. The grid intensity is 295.6 gCO_2/kWh (EU average).

value for f_{HEX} based on today's potential for extra hot-water delivery. For C3, there is enough excess heat available (320 GWh/year), while C4 can only cover 27.8% of the heat demand by maximizing heat generation (663 GWh/year). In general, the total emissions in the three product systems with increased heat integration are reduced relative to the reference system (8.65 $MtCO_2$ annually) and are within the ranges of 96.6%–97.4% and 68.8%–75.1% for C3 and C4, respectively. Since NG also generates electricity in the CHP plant, the level of electricity importation increases with increased heat integration. The CO_2 emission intensities of the products show different characteristics in C3 and C4 when varying the value of f_{HEX}:

- For the C3 configuration, the extra emissions at low levels of integration are allocated to the syngas fermentation plant [*cf.* **Eqs. 12–15**], since it causes the additional energy demand. This increases the emission intensity of ethanol when NG is required. The emission intensity of the steel product is unaffected.
- For the C4 configuration, the extra fossil-related emissions at low levels of integration are allocated to both the syngas fermentation plant and CCS plant. Since the demand for heat is dominated by the CCS plant ($f_{heat,CCS:fheat,SYN}$ = 87:13) and, conversely, the demand for electricity is dominated by the syngas fermentation plant ($f_{pow,CCS}$:$f_{pow,SYN}$ = 39:61), the processing emissions for ethanol production due to power importation dominate those due to heat supply. Relative to C3, this leads to a slight increase in the emission intensity of ethanol with heat integration. Since avoided CO_2 (CCS plant) is allocated to the steel product as well, the steel product intensity increases by up to 7% points with fossil fuel import.

Future Potential for Emission Reductions

To assess the future potential for emissions reductions, the extent of the mitigation is increased by setting the capture rate to 99%, the grid intensity to 0 gCO_2/kWh, and the replacement rate of PCI with biochar r_{bioPCI} to 100% (corresponds to 724,000 t/yr

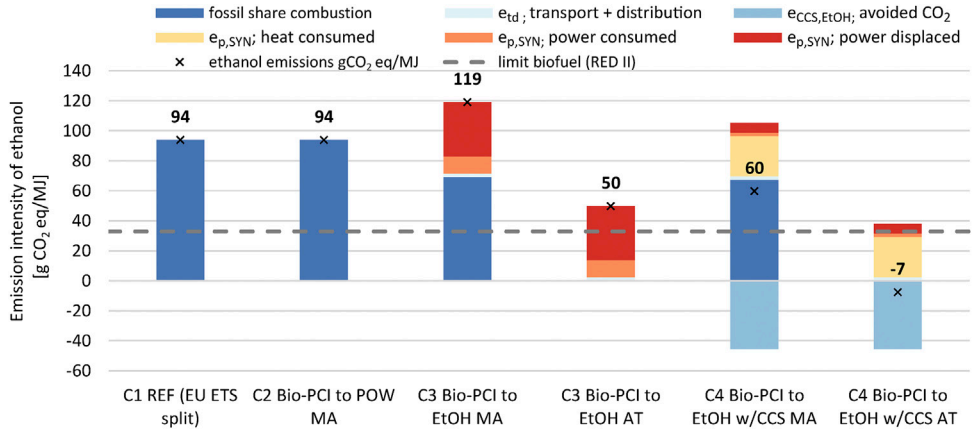

FIGURE 10 | Emissions intensities of the ethanol product depending on the steel mill configuration and allocation principles: allocation by carbon mass balance and free attribution maximizing the biogenic carbon to ethanol production. The allocation of CO_2 avoided (CCS) is 93:7 (steel:ethanol) based on mass allocation. The grid intensity is 295.6 gCO_2/kWh (EU average).

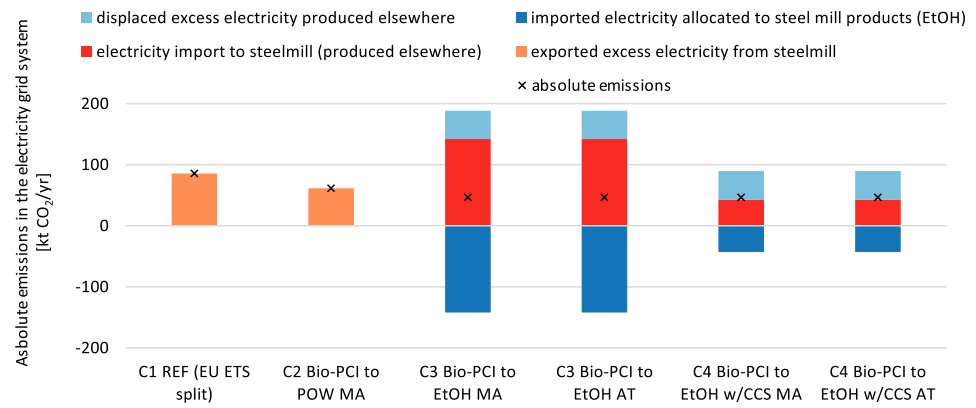

FIGURE 11 | Absolute emissions in the electricity grid system due to interaction with the steel mill (4 Mt HRC per year) depending on the steel mill configuration and allocation principles: allocation by carbon mass balance and free attribution maximizing the biogenic carbon to ethanol production. The allocation of CO_2 avoided (CCS) is 93:7 (steel:ethanol) based on mass allocation. The grid intensity is 295.6 gCO_2/kWh (EU average).

biochar). With a yield of 35 wt.% (Wang et al., 2015) for biochar production, this amount of biochar would require >2 million tons of wood waste. The maximum r_{bioPCI} leads to a share of 31.8% (by mass) of biogenic carbon in the input to the blast furnace. Ethanol production corresponding to the biogenic carbon input is not possible because the flow of BFG to the steel units would be insufficient. Therefore, only about 20% of the injected biogenic carbon may be converted to ethanol, yielding 226,000 tons of ethanol annually.

The impact of intensified mitigation on the total emissions and the product carbon and energy intensities is shown in **Figure 14**. The following observations can be made:

- The total emissions are reduced compared to the reference mill at the expense of extra energy consumption (**Figure 14A**). The largest total emission savings are achieved for C4 (47%), followed by C3 (24%) and C2 (21%), relative to the reference mill (C1); however, the emission reduction per invested extra energy is highest for C2 with approximately 10 tCO_2/MWh, followed by C3 and C4 with 1 tCO_2/MWh and 0.8 tCO_2/MWh, respectively. This is explained by the high energy demands for syngas fermentation and CCS in C3 and C4. Note that the extra energy demand in C2 (cogeneration of electricity) is related to the injection of biochar instead of fossil pulverized coal.
- The energy intensity of the steel product is highly dependent upon the use of the BFG (**Figure 14B**). The cogeneration of ethanol from the BFG (C3) leads to lower energy intensity than the reference mill and the cogeneration of electricity (C2). The energy demand of CCS (C4) increases the energy intensity of the steel product relative to the other configurations, although the lowest emission intensity of 1,080 $kgCO_2$/t HRC is achieved in C4.

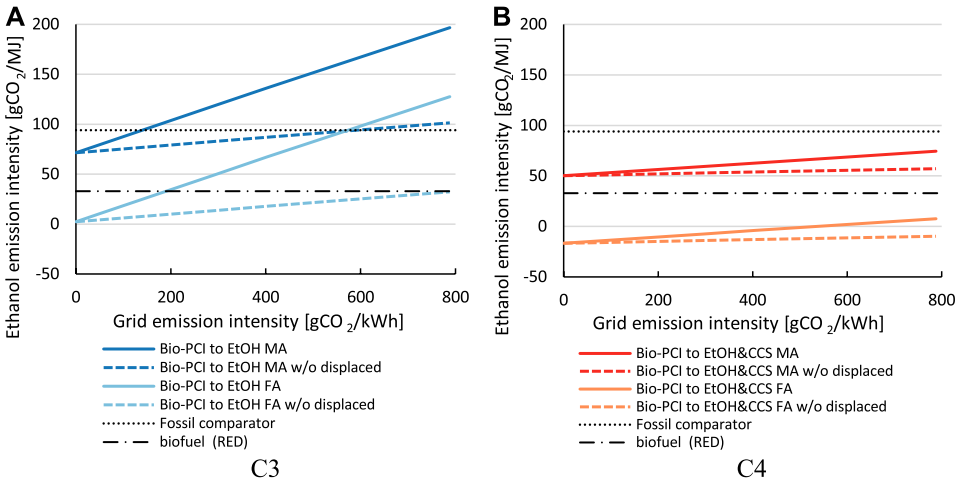

FIGURE 12 | CO_2 emission intensities of produced ethanol depending on the CO_2 emission intensity of imported electricity for Bio-PCI to ethanol configurations without CCS **(A)** and with CCS **(B)**. The dashed lines represent the emission intensity of ethanol if the displaced emissions from electricity import due to the diversion of BFG to the syngas fermentation are instead allocated to steel.

- The emission intensity of the produced ethanol increases with r_{bioPCI} increases in NG and electricity imports, which are caused by higher consumption of BFG to cogenerate ethanol. This increase in r_{bioPCI} process emissions is compensated for in C4 with allocation by mass, as increases in r_{bioPCI} and the capture rater $r_{capture}$ lead to an increased share of biogenic carbon in the ethanol, thereby lowering the overall emission intensity of ethanol with r_{bioPCI}. For C4 with attribution, the share of biogenic carbon in the ethanol is always 100%, such that an increase only increases the import of external energy, and thereby, increases the processing emissions. The energy intensity of produced ethanol, that is, the ratio of energy in the product to the energy demand (energy in the BFG feed + steam + factual power consumption), is 0.496 MJ/MJ. This value is the same for all replacement rates r_{bioPCI}, since the underlying, assumed specific energy demand and conversion rates are maintained (*cf.* **Figure 4** and Table S3).

DISCUSSION

Technical Challenges for Deep Emission Reduction and Thermodynamic Considerations for Off-Gas Conversion

Deep mitigation in steelmaking via biomass introduction is intrinsically linked to overcoming the challenges associated with implementing Bio-PCI. Biomass-upgrading processes are typically on a scale of 20–100 kt biomass (Koppejan et al., 2012; Ronsse, 2013; Suopajärvi et al., 2013) and would require upscaling or parallel trains to 2,000 kt to replace all the fossil PCI-coal at a single site. Furthermore, the sourcing of the type B wood waste at this scale exceeds the regional or even national potential availability (total wood waste in EU ~55 Mt, all types) (Borzecka, 2018), implying an increase in transborder wood waste flows (current total <2000 kt type B in EU) (Junginger et al., 2018) or the use of other sources of waste biomass. Even low-value wood waste might experience an increase in price with high-demand buyers entering the market. In addition, at higher shares of biomass (up to 100% PCI replacement), the requirements (e.g., related to the amounts of impurities) imposed on the injected biochar are likely to increase (depending on the upgrading technology) and require modifications to the blast furnace design (e.g., BFG recirculation).

The CCS technology faces fewer scale-up issues, since the absorption technology is already commercially operated at similar scales, for example, the Gorgon CCS project (Global CCS Institute, 2019), and is possible to operate at capture rates >99% (Feron et al., 2019), despite increases in energy and solvent consumption. However, implementation at smaller and more diluted sources/stacks will increase the mitigation cost considerably.

The synthesis of ethanol (or other chemicals) from the BFG is technically feasible, although the efficiencies of such syntheses may be improved. The economic feasibility will depend on the how the product is valued relative to other energy products. The typical conversion of steel mill gases into electricity occurs with 30%–42% efficiency and generates revenue from the sale of electricity not used in the steel mill. A shift to fuel synthesis may be thermodynamically favorable, owing to higher efficiencies, for example, 50% (MJ product/MJ syngas + heat + power) for ethanol (this work) and 50%–75% for methanol synthesis (Lundgren et al., 2013; Schittkowski et al., 2018). However, three important aspects must be considered when comparing these efficiencies: 1) the switch to fuel synthesis makes the mill a net importer of electricity; 2) cogeneration of heat (district heating or process heat) in a power plant can provide a total efficiency of >>90%; and 3) electricity has a

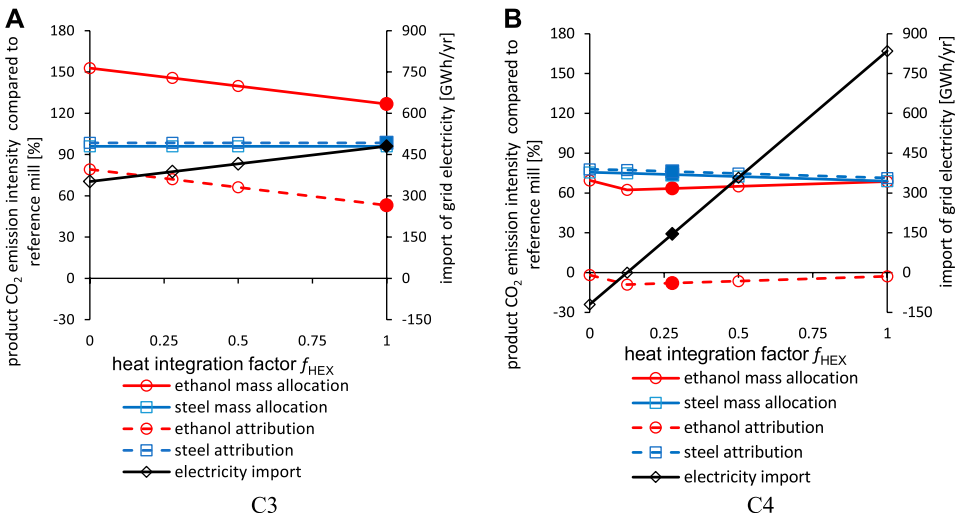

FIGURE 13 | CO_2 emission intensities of steel and ethanol depending on the extent of heat integration for a steel mill in Bio-PCI to ethanol configuration without CCS **(A)** and with CCS **(B)**. The filled symbols represent the default assumptions for heat integration with the reference steel mill CHP and a grid intensity of 295.6 gCO2/kWh (EU average).

higher efficiency and, thus, a greater mitigation effect when used for road-based passenger vehicles with electric drivelines (than internal combustion engines) in the form of synthesized chemicals or fuels for transport.

Governance of Carbon Allocation for Flexible Participation in Markets for Low-Carbon Products

As illustrated here, the scheme for the allocation of biogenic carbon and avoided CO_2 emissions influences the CO_2 emission intensities of cogenerated products. A key task for the regulatory bodies is to decide on the degree of flexibility that will be granted to producers in allocating biogenic shares or emission savings due to CCS to cogenerated products. A bullet point list of aspects to consider for policymakers is provided in **Supplementary Material Section 3**. Adhering to the currently applied voluntary allocation schemes (administrative schemes applying allocation by mass, energy content, or physical measurement) is understandable, since they achieve comparable results and reflect the current spirit of RED II (Schimmel et al., 2018) in the sense that the actual thermochemical processes are represented more or less accurately, especially in refineries. Concerning cogenerated ethanol from steel mill gases, the adherence to allocation by mass will most likely not facilitate the production of ethanol that meets the biofuel criterion (65% emission reduction relative to a fossil comparator), [*cf.* **Figures 10**, **12**]. This is because most of the lowered emissions are allocated to the steel product. In this case, the carbon mitigation is harder to monetize, since markets for low-carbon steel currently do not exist. In contrast, the attribution scheme will maximize the value of the carbon mitigation but will not represent the actual biogenic content of a product (if measured, so to speak).

Attribution and also "within-product" allocation (see *Allocation for Co-Processing of Biogenic and Fossil Feedstocks*), which is used to channel emission savings to the sale of climate-positive, consumer-demanded products that finance investments in CCS in the pulp industry via buyers' coalitions (Klement et al., 2020), could allow companies to adjust in a flexible manner, their mixes of low-carbon products sold to markets that currently value emissions and their mitigation differently. For example, emitting CO_2 from processes that are exposed to global competition is basically for free (EUAs at the EU level and nationally are often exempted from CO_2 taxation schemes), whereas locally or regionally used energy products are the targets of numerous funding schemes, for example, green electricity certificates (Sweden) and tax credits for blends of biofuel (US), or fines for below-standard blends of biofuels (Sweden). Thus, the flexibility conferred by free-choice attribution or within-product allocation may help emerging (sector-coupling) technologies to become implemented and help generate low-carbon products that fulfill the criteria for green public procurement and quotas on low-carbon materials (Agora Energiewende and Wuppertal Institut, 2019) or that could be sold with a small surcharge to the consumer, thereby offsetting the high investment costs of low-carbon processing (Rootzén and Johnsson, 2016).

Aside from economic motivation, support of this kind of attribution comes from the notion that the gasification of biomass could be executed in a designated stand-alone plant, which would generate ethanol with a 100% biogenic carbon content. The use of existing equipment, such as the blast furnace and heat integration using excess heat, allows for synergies, namely, lower emissions from producing steel and a fuel product with lower emissions than a comparable fossil fuel (*cf.* **Figures 9**, **10**). Furthermore, the flexibility conferred by attribution is likely more important to process industry that

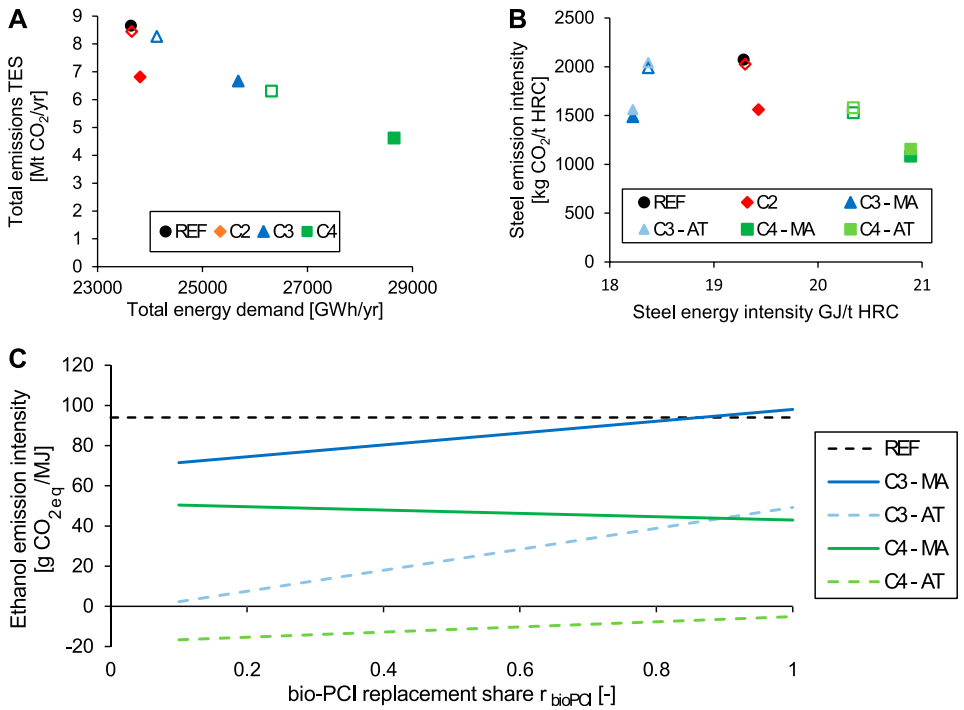

FIGURE 14 | Impacts of intensified mitigation technologies on the total emissions in TES for an integrated steel mill of 4 Mt HRC per year **(A)**, and the corresponding CO_2 emission intensities of steel **(B)** and ethanol **(C)**. The nonfilled symbols represent the default settings, that is, 90% CO_2 capture from BFG and 10% Bio-PCI; the filled symbols represent 99% CO_2 capture from BFG and 100% Bio-PCI. AT, attribution; C2, configuration with Bio-PCI and electricity export; C3, configuration with Bio-PCI and ethanol production; C4, configuration with ethanol production and CCS; MA, mass allocation; REF, reference (C1). The grid intensity is 0 gCO_2/kWh.

mainly produces nonfuel products at bulk scale and wants to incorporate biofuel schemes on a small scale, since just the difference in scale will lead to low biogenic shares in the produced fuel if the current voluntary schemes designed for refineries are applied. The major risk here is that attribution may be perceived as a stepladder for greenwashing, since products that are advertised as "green" may be linked to the continued consumption of fossil fuels. Decisions taken by the regulatory bodies regarding a set of valid allocation schemes are, therefore, ultimately political decisions, and they should reflect the value of the low-carbon products for society in mitigating CO_2 emissions.

CONCLUSIONS

To achieve drastic reductions in emissions from current production processes, a series of mitigation technologies implemented over time is needed. To motivate the implementation, funding schemes are needed in several sectors that create markets for low-carbon products. This work discusses the effects of carbon allocation on the emissions intensities of low-carbon products generated in facilities that co-process biogenic and fossil feedstocks using the example of an integrated steel mill (blast furnace route). The potential for CO_2 mitigation is investigated for biochar injection into the blast furnace (Bio-PCI), carbon capture and storage (CCS), and microbial fermentation of steel mill off-gases to produce ethanol. The emissions intensities of cogenerated low-carbon products are discussed for the allocation of biogenic inputs and avoided CO_2 emissions between the cogenerated steel, ethanol, and electricity. We present four allocation schemes, two of which are investigated in detail: *allocation by carbon mass*, representing the actual carbon flows, and a free-choice *attribution*, which maximizes the share of biogenic carbon in the ethanol (presently, the most-valued, low-carbon product).

Concerning the technical potential for emissions reductions in a reference integrated steel mill in Europe (4 Mt HRC and 8,377 $ktCO_2$ per year), we conclude the following:

- Replacement of 10% of fossil PCI with biochar, which is possible without affecting the blast furnace operation, would lead to emission reductions of 2.5–3.5% for any product (e.g., electricity or ethanol) made from the CO and H_2 in the BFG. The addition of CO_2 capture (90%) from the BFG with subsequent CO_2 storage would reduce emissions significantly (by 27% relative to the base case).
- Theoretical replacement of 100% of the fossil PCI with biochar and a 99% capture rate from the BFG would lead to ~21–24% and ~47% emissions reduction without and with CCS, respectively. Upscaling the biomass upgrading

Formulae

Symbols

e	Emission/amount of CO_2, specific per unit product [kg CO_{2eq}/t HRC, or g CO_{2eq}/MJ]
E	Emission/amount of CO_2, absolute on an annual basis kgCO_{2eq}/year
Q	Heat [MJ, MWh]
P	Power [MJ, MWh]
f	Allocation factor/allocated share of renewable/fossil content [-]
w	Concentration/fraction on mass basis [-]
ϕ_{subst}	Substitution ratio of pulverized coal to biochar [kg/kg]
r_{bioPCI}	Replacement rate of fossil PCI coal with biochar, as compared to the reference amount of PCI coal [kg/kg]
$r_{capture}$	Capture rate of CO_2 in the CCS plant; default value of 90%; [-]
φ_{HEX}	[-]
$m,\dot{m}$	Mass, mass flow
LHV	Lower heating value of a material/fuel/species [MJ/kg]
Indices	(Abbreviated ones only)
PC	Pulverized coal
bio	Biogenic content/carbon
Bio-PCI	Biochar injection
i,j	Stream, remaining streams
C	Carbon
mass	Allocation by carbon mass
LHV	Allocation by energy content on LHV basis
heat, pow	Related to heat, power supply/demand
foss	Fossil content/carbon
SYN	Related to syngas fermentation unit/plant
CCS	Related to CCS unit/plant
EtOH	Related to the ethanol product
steel	Related to the steel product
p	Related to processing to yield ethanol
td	Transport and distribution of feedstock/ethanol
u	Use of fuel (combustion)
th	Thermal
HEX	Heat integration/excess heat utilization
disp	Displaced; relates to displaced electricity due to BFG diversion from CHP plant
cons	Consumed; relates to consumed electricity

processes and sourcing are the most serious challenges, aside from blast furnace operation with large shares of biomass.
- Cogeneration of ethanol has a one order of magnitude lower CO_2 avoidance per extra energy demand (~1 tCO_2/MWh) than the cogeneration of electricity (~10 tCO_2/MWh).
- The emission intensity of cogenerated ethanol depends on the allocated biogenic share, heat integration potential, biomass replacement rate, and CO_2 intensity of the electricity imported.

Regarding the allocation schemes for co-processing, we conclude the following:

- The allocation scheme is important to the implementation of mitigation technologies, and the *mass allocation* and *attribution* schemes allocate the biogenic inputs to the products in diametrically opposite fashions.
- The *allocation by mass* will not yield an ethanol product from the BFG that is classified as bioethanol according to RED (65% reduction in emissions intensity of the transport fuel), even with the use of renewable electricity (0 gCO_2/kWh) and CCS. This is valid in the near-term and assumes the use of NG for heat supply. The *attribution* scheme, however, will fulfill the requirement even up to an electricity CO_2 intensity of 180 gCO_2/kWh (without CCS).
- The main product, steel, receives mostly biogenic carbon from the *allocation by mass*. However, its specific emission intensity is less severely affected by the allocation schemes due to the limited injection of biomass relative to the production volume — 4 Mt steel versus 0.1 Mt ethanol. Furthermore, indirect emissions from imported electricity are allocated to the ethanol in all the schemes.
- Regulations related to the co-processing of biogenic and fossil feedstocks for the allocation of biogenic input to products will become relevant to more industries as they extend their product portfolios and engage with other sectors.

DATA AVAILABILITY STATEMENT

All datasets presented in this study are included in the article/ **Supplementary Material**.

AUTHOR CONTRIBUTIONS

MB has contributed to conceptualization, literature research, methodology development, calculation, formal analysis, visualization, writing (original draft preparation and editing). RM has contributed to conceptualization, literature research, writing (original draft preparation, review and editing). FN has contributed to conceptualization, formal analysis, writing (review and editing), project administration. FJ has contributed to writing (review and editing), project administration, and funding acquisition. All authors have read and agreed to the published version of the manuscript.

FUNDING

This scientific publication is a result of the TORERO project. TORERO has received funding from the European Union's Horizon 2020 - Research and Innovation Framework Programme (H2020-EU.3.3.3. - Alternative fuels and mobile energy sources). Project ID: 745810.

ACKNOWLEDGMENTS

The authors thank Alberto Alamia, formerly Chalmers University, and Wim van der Stricht, ArcelorMittal, Belgium, Ghent, for discussions and inputs. The authors thank Vincent Collins for proofreading. This work is based entirely on literature research. No results/underlying assumptions reflect information from or intellectual property of the stakeholders and participants in the Torero and Steelanol projects. Process assumptions made here do not reflect processes licensed by project partners. The work does not claim to reflect up-to-date regulations/developments, and the statements concerning RED compliancy (biofuel criterion) are made regarding the chosen methodology and process assumptions.

SUPPLEMENTARY MATERIAL

The Supplementary Material for this article can be found online at: https://www.frontiersin.org/articles/10.3389/fceng.2020.596279/full#supplementary-material

REFERENCES

Agora Energiewende, and ; Wuppertal Institut (2019). Climate-neutral industry (executive summary): key technologies and policy options for steel, chemicals and cement. Berlin. Available at:https://www.agora-energiewende.de/fileadmin2/Projekte/2018/Dekarbonisierung_Industrie/168_A-EW_Climate-neutral-industry_EN_ExecSum_WEB.pdf.

Ali, H., Eldrup, N. H., Normann, F., Andersson, V., Skagestad, R., Mathisen, A., et al. (2018). Cost estimation of heat recovery networks for utilization of industrial excess heat for carbon dioxide absorption. *Int. J. Greenh. Gas Control* 74, 219–228. doi:10.1016/j.ijggc.2018.05.003

Arasto, A., Tsupari, E., Kärki, J., Pisilä, E., and Sorsamäki, L. (2013). Post-combustion capture of CO2 at an integrated steel mill–part I: technical concept analysis. *Int. J. Greenh. Gas Control* 16, 271–277. doi:10.1016/j.ijggc.2012.08.018

ArcelorMittal (2020). Climate Action in Europe-our carbon emissions reduction roadmap: 30% by 2030 and carbon neutral by 2050. Luxembourg. Available at: https://corporate-media.arcelormittal.com/media/b4wh4cd0/climate-action-in-europe.pdf.

Axelson, M., Robson, I., Wyns, T., and Khandekar, G. (2018). Breaking through-industrial low-CO2 technologies on the Horizon. Institute for European Studies, Vrije Universiteit Brussel. Available at:www.ies.be/Breaking-Through_Report_13072018.

Berghout, N., Meerman, H., van den Broek, M., and Faaij, A. (2019). Assessing deployment pathways for greenhouse gas emissions reductions in an industrial plant–a case study for a complex oil refinery. *Appl. Energy* 236, 354–378. doi:10.1016/j.apenergy.2018.11.074

Biermann, M., Ali, H., Sundqvist, M., Larsson, M., Normann, F., and Johnsson, F. (2019). Excess heat-driven carbon capture at an integrated steel mill–considerations for capture cost optimization. *Int. J. Greenh. Gas Control* 91, 102833. doi:10.1016/j.ijggc.2019.102833

Biermann, M., Normann, F., Johnsson, F., and Skagestad, R. (2018). Partial carbon capture by absorption cycle for reduced specific capture cost. *Ind. Eng. Chem. Res.* 57, acs.iecr.8b02074. doi:10.1021/acs.iecr.8b02074

Birat, J.-P. (2020). Society, materials, and the environment: the case of steel. *Metals (Basel).* 10, 331. doi:10.3390/met10030331

Borzecka, M. (2018). European wood waste statistics report for recipient and model regions. Available at:www.ies.be/Breaking-Through_Report_13072018.

Bui, M., Adjiman, C. S., Bardow, A., Anthony, E. J., Boston, A., Brown, S., et al. (2018). Carbon capture and storage (CCS): the way forward. *Energy Environ. Sci.* 11, 1062–1176. doi:10.1039/c7ee02342a

CORDIS (2017). Carbon4Pur-turning industrial waste gases (mixed CO/CO2 streams) into intermediates for polyurethane plastics for rigid foams/building insulation and coatings. Available at: https://cordis.europa.eu/project/id/768919 (Accessed July 1, 2020).

CORDIS (2020). DMX demonstration in Dunkirk. Available at: https://cordis.europa.eu/project/id/838031 (Accessed July 10, 2020).

CORDIS (2016). FReSMe-from residual steel gases to methanol. Available at: https://cordis.europa.eu/project/id/727504 (Accessed July 1, 2020).

Cormos, C.-C. (2016). Evaluation of reactive absorption and adsorption systems for post-combustion CO2 capture applied to iron and steel industry. *Appl. Therm. Eng.* 105, 56–64. doi:10.1016/j.applthermaleng.2016.05.149

Deng, H., Roussanaly, S., and Skaugen, G. (2019). Techno-economic analyses of CO2 liquefaction: impact of product pressure and impurities. *Int. J. Refrig.* 103, 301–315. doi:10.1016/j.ijrefrig.2019.04.011

Dreillard, M., Broutin, P., Briot, P., Huard, T., and Lettat, A. (2017). Application of the DMXTM CO2 capture process in steel industry. *Energy Procedia* 114, 2573–2589. doi:10.1016/j.egypro.2017.03.1415

ECN (2019). Process intensification: SEWGS case. Available at:https://www.ecn.nl/news/item/process-intensification-sewgs-case/ (Accessed April 19, 2019).

Energy Transition Commission (2018). Mission Possible: reaching net-zero carbon emissions from harder-to-abate sectors by mid-century. Available at: http://www.energy-transitions.org/sites/default/files/ETC_MissionPossible_FullReport.pdf.

European Commission (2015). Council Directive (EU) 2015/652 of 20 April 2015 laying down calculation methods and reporting requirements pursuant to Directive 98/70/EC of the European Parliament and of the Council relating to the quality of petrol and diesel fuels. 1–42. Available at:https://eur-lex.europa.eu/legal-content/EN/TXT/PDF/?uri=CELEX:32015L0652&from=EN.

European Commission (2019a). Guidance Document n°6 on the harmonized free allocation methodology for the EU-ETS post 2012-cross-Boundary Heat Flows. 1–47. Available at: https://ec.europa.eu/clima/sites/clima/files/ets/allowances/docs/gd6_cross_boundary_heat_flows_en.pdf Date of access: 2019-07-31.

European Commission (2019b). Guidance Document no 8 on the harmonised free allocation methodology for the EU ETS post 2020-waste gases and process emissions sub-installation. Available at:https://ec.europa.eu/clima/sites/clima/files/ets/allowances/docs/p4_gd8_waste_gases_process_emissions_en.pdf.

European Commission (2019c). The European green deal. Available at: https://eur-lex.europa.eu/legal-content/EN/TXT/?qid=1596443911913&uri=CELEX:52019DC0640#document2.

European Commission (2020). Voluntary schemes. Available at:https://ec.europa.eu/energy/topics/renewable-energy/biofuels/voluntary-schemes_en (Accessed July 8, 2020).

European Environment Agency (2018). Electricity generation-CO2 emission intensity European Union. Available at:https://www.eea.europa.eu/data-and-maps/daviz/sds/co2-emission-intensity-from-electricity-generation-2/@@view (Accessed August 3, 2020)

European Parliament and Council of the European Union (2018a). Directive (EU) 2018/2001 of the European Parliament and of the Council of 11 December 2018 on the promotion of the use of energy from renewable sources. Off. J. Eur. Union 2018. Available at:http://data.europa.eu/eli/dir/2018/2001/oj.

European Parliament and Council of the European Union (2018b). DIRECTIVE 98/70/EC OF THE EUROPEAN PARLIAMENT AND OF THE COUNCIL of 13 October 1998 relating to the quality of petrol and diesel fuels and amending Council Directive 93/12/EEC. Off. J. Eur. Union. Available at:https://ec.europa.eu/clima/policies/transport/fuel_en#tab-0-1.

Federal Ministry of Education and Research of Germany (2016). Carbon2Chem. Available at:https://www.fona.de/en/measures/funding-measures/carbon2chem-project.php (Accessed July 1, 2020).

Feron, P., Cousins, A., Jiang, K., Zhai, R., Shwe Hla, S., Thiruvenkatachari, R., et al. (2019). Towards zero emissions from fossil fuel power stations. *Int. J. Greenh. Gas Control* 87, 188–202. doi:10.1016/j.ijggc.2019.05.018

Gardarsdottir, S. O., De Lena, E., Romano, M., Roussanaly, S., Voldsund, M., Pérez-Calvo, J. F., et al. (2019). Comparison of technologies for CO2 capture from cement production—part 2: cost analysis. *Energies* 12, 542. doi:10.3390/en12030542

Gazzani, M., Romano, M. C., and Manzolini, G. (2015). CO2 capture in integrated steelworks by commercial-ready technologies and SEWGS process. *Int. J. Greenh. Gas Control* 41, 249–267. doi:10.1016/j.ijggc.2015.07.012

Global CCS Institute (2019). *The global status of CCS: 2019*.

Guintoli, J., Agostini, A., Edwards, R., and Marelli, L. (2017). Solid and gaseous bioenergy pathways: input values and GHG emissions. Calculated according to the methodology set in COM(2016) 767 (EUR 27215). 226. Available at:https://ec.europa.eu/energy/sites/ener/files/documents/Solid and gaseous bioenergy pathways.pdf.

Handler, R. M., Shonnard, D. R., Griffing, E. M., Lai, A., and Palou-Rivera, I. (2016). Life cycle assessments of ethanol production via gas fermentation: anticipated greenhouse gas emissions for cellulosic and waste gas feedstocks. *Ind. Eng. Chem. Res.* 55, 3253–3261. doi:10.1021/acs.iecr.5b03215

Hawighorst, P. (2019). Challenges for RED II sustainability certification from a certification scheme's point of view. Available at:http://www.etipbioenergy.eu/images/SPM9_Presentations/Day1/10_ETIP B SPM9_P. Hawighorst_Meo Carbon Solutions GmbH.pdf.

Ho, M. T., Bustamante, A., and Wiley, D. E. (2013). Comparison of CO2 capture economics for iron and steel mills. *Int. J. Greenh. Gas Control* 19, 145–159. doi:10.1016/j.ijggc.2013.08.003

IChemE Energy Centre (2018). *A chemical engineering perspective on the challenges and opportunities of delivering carbon capture and storage at commercial scale*.

IEA (2019). *Tracking transport 2019*. Paris.

IEAGHG (2013). 2013/04 Iron and Steel CCS study (Techno-economics integrated steel mill). Available at: https://www.google.com/search?q=2013%2F04+Iron+and+Steel+CCS+study+(Techno-economics+integrated+steel+mill)&rlz=1C1GCEU_en-GBIN857IN857&oq=2013%2F04+Iron+and+Steel+CCS+study+{Techno-economics+integrated+steel+mill)&aqs=chrome.69i57.1031j0j4&sourceid=chrome&ie=UTF-8

ISCC (2017). ISCC 203-01 guidance for the certification of Co-processing. 1–9. Available at: https://www.iscc-system.org/wp-content/uploads/2017/02/ISCC-Guidance-Document-203-01_Co-processing-requirements.pdf (Accessed 31 July, 2019).

ISO (2006). ISO 14044:2006(en) Environmental management—life cycle assessment—requirements and guidelines. Available at: https://www.iso.org/obp/ui/#iso:std:iso:14044:ed-1:v1:en (Accessed 31 July, 2019).

Joint Research Centre (2016). Data requirements and principles for calculating the life cycle GHG intensity of novel transport fuels and invitation to submit data. 2, 1–10.

Junginger, M., Järvinen, M., Olsson, O., Hennig, C., and Dadhich, P. (2018). Transboundary flows of woody biomass waste streams in Europe. Available at: http://task40.ieabioenergy.com/wp-content/uploads/2019/01/IEA-Bioenergy-2019.-Wood-waste-trade-study-FINAL.pdf.

Kirschen, M., Badr, K., and Pfeifer, H. (2011). Influence of direct reduced iron on the energy balance of the electric arc furnace in steel industry. *Energy* 36, 6146–6155. doi:10.1016/j.energy.2011.07.050

Klement, J., Rootzén, S., Normann, F., and Johnsson, F. (2020). Incentivising BECCS in the pulp and paper industry - a supply chain analysis. Submitted for Publication 32, 1–54.

Koppejan, J., Sokhansanj, S., Melin, S., and Madrali, S. (2012). Status overview of torrefaction technologies. *IEA Bioenergy Task* 32, 1–54.

Kuramochi, T., Ramírez, A., Turkenburg, W., and Faaij, A. (2012). Comparative assessment of CO2 capture technologies for carbon-intensive industrial processes. *Prog. Energy Combust. Sci.* 38, 87–112. doi:10.1016/j.pecs.2011.05.001

LanzaTech (2018). World's first commercial waste gas to ethanol plant starts up. Available at:https://www.lanzatech.com/2018/06/08/worlds-first-commercial-waste-gas-ethanol-plant-starts/. (Accessed July 1, 2020).

Liew, F., Martin, M. E., Tappel, R. C., and Heijstra, B. D. (2016). Gas fermentation—a flexible platform for commercial scale production of low-carbon-fuels and chemicals from waste and renewable feedstocks. *Front Microbiol.* 11, 694. doi:10.3389/fmicb.2016.00694

Lulekraft, A. B. (2018). LuleKraft-annual production. Available at:http://lulekraft.se/verksamheten/aarsproduktion.aspx (Accessed March 4, 2018).

Lundgren, J., Ekbom, T., Hulteberg, C., Larsson, M., Grip, C.-E., Nilsson, L., et al. (2013). Methanol production from steel-work off-gases and biomass based synthesis gas. *Appl. Energy* 112, 431–439. doi:10.1016/j.apenergy.2013.03.010

Müller, L. J., Kätelhön, A., Bringezu, S., McCoy, S., Suh, S., Edwards, R., et al. (2020). The carbon footprint of the carbon feedstock CO2. *Energy Environ. Sci.* 13, 2979–2992. doi:10.1039/D0EE01530J

Mandova, H., Patrizio, P., Leduc, S., Kjärstad, J., Wang, C., Wetterlund, E., et al. (2019). Achieving carbon-neutral iron and steelmaking in Europe through the deployment of bioenergy with carbon capture and storage. *J. Clean. Prod.* 218, 118–129. doi:10.1016/j.jclepro.2019.01.247

Martinez Castilla, G., Biermann, M., Montañés, R. M., Normann, F., and Johnsson, F. (2019). Integrating carbon capture into an industrial combined-heat-and-power plant: performance with hourly and seasonal load changes. *Int. J. Greenh. Gas Control* 82, 192–203. doi:10.1016/j.ijggc.2019.01.015

Masson-Delmotte, V., Zhai, P., Pörtner, H. O., Roberts, D., Skea, J., et al. (2018). "IPCC, 2018: summary for policymakers." in Global warming of 1.5°C: an IPCC Special Report on the impacts of global warming of 1.5°C above pre-industrial levels and related global greenhouse gas emission pathways, in the context of strengthening the global. Geneva, Switzerland, (World Meteorological Organization).

Mathieson, J. G., Rogers, H., Somerville, M. A., Jahanshahi, S., and Ridgeway, P. (2011). "Potential for the use of biomass in the iron and steel industry."in Chemeca 2011: Engineering a Better World, New South Wales, Australia, 18-21 September 2011, 1065–1076. Available at:http://search.informit.org/browsePublication;isbn=9780858259676;res=IELENG;subject=Zoology.

Meijer, K., Denys, M., Lasar, J., Birat, J.-P., Still, G., and Overmaat, B. (2009). ULCOS: ultra-low CO2 steelmaking. *Ironmak. Steelmak.* 36, 249–251. doi:10.1179/174328109X439298

Messagie, M., Boureima, F., Mertens, J., Sanfelix, J., Macharis, C., and Mierlo, J. (2013). The influence of allocation on the carbon footprint of electricity production from waste gas, a case study for blast furnace gas. *Energies* 6, 1217–1232. doi:10.3390/en6031217

Molitor, B., Richter, H., Martin, M. E., Jensen, R. O., Juminaga, A., Mihalcea, C., et al. (2016). Bioresource Technology Carbon recovery by fermentation of CO-rich off gases–turning steel mills into biorefineries. *Bioresour. Technol.* 215, 386–396. doi:10.1016/j.biortech.2016.03.094

Mousa, E., Wang, C., Riesbeck, J., and Larsson, M. (2016). Biomass applications in iron and steel industry: an overview of challenges and opportunities. *Renew. Sustain. Energy Rev.* 65, 1247–1266. doi:10.1016/j.rser.2016.07.061

Ng, K. W., Giroux, L., and MacPhee, T., and Todoschuk, T. (2010). "Direct injection of biofuel in blast furnace ironmaking."in Iron & steel technology conference; AISTech 2010, AISTECH -CONFERENCE PROCEEDINGS, Warrendale, PA (Association for Iron and Steel Technology). 643–652. Available at:https://www.tib.eu/de/suchen/id/BLCP%3ACN076471986 (Accessed 31 July, 2019).

Ou, X., Zhang, X., Zhang, Q., and Zhang, X. (2013). Life-cycle analysis of energy use and greenhouse gas emissions of gas-to-liquid fuel pathway from steel mill off-gas in China by the LanzaTech process. *Front. Energy* 7, 263–270. doi:10.1007/s11708-013-0263-9

Pardo-planas, O., Atiyeh, H. K., Phillips, J. R., Aichele, C. P., and Mohammad, S. (2017). Bioresource Technology Process simulation of ethanol production from biomass gasi fi cation and syngas fermentation. *Bioresour. Technol.* 245, 925–932. doi:10.1016/j.biortech.2017.08.193

Phillips, J. R., Huhnke, R. L., and Atiyeh, H. K. (2017). Syngas fermentation: a microbial conversion process of gaseous substrates to various products. *Fermentation* 3, 1–6. doi:10.3390/fermentation3020028

Piccolo, C. and Bezzo, F. (2009). A techno-economic comparison between two technologies for bioethanol production from lignocellulose. *Biomass and Bioenergy* 33, 478–491. doi:10.1016/j.biombioe.2008.08.008

Ramírez-Santos, Á. A., Castel, C., and Favre, E. (2018). A review of gas separation technologies within emission reduction programs in the iron and steel sector: current application and development perspectives. *Sep. Purif. Technol.* 194, 425–442. doi:10.1016/j.seppur.2017.11.063

Rao, A. B. and Rubin, E. S. (2006). Identifying cost-effective CO2 control levels for amine-based CO2 capture systems. *Ind. Eng. Chem. Res.* 45, 2421–2429. doi:10.1021/ie050603p

Robak, K. and Balcerek, M. (2018). Review of second generation bioethanol production from residual biomass. *Food Technol. Biotechnol.* 56, 174–187. doi:10.17113/ftb.56.02.18.542

Ronsse, F. (2013). "Commercial biochar production and its certification."in Interreg IVB Proj. Biochar Clim. Sav. soils, Groningen, Netherlands. Available at:http://archive.northsearegion.eu/files/repository/20140811101209_02_FrederikRonsse-Commercialbiocharproductionanditscertification.pdf (Accessed July 10, 2020).

Rootzén, J. and Johnsson, F. (2016). Paying the full price of steel–perspectives on the cost of reducing carbon dioxide emissions from the steel industry. *Energy Pol.* 98, 459–469. doi:10.1016/j.enpol.2016.09.021

Schimmel, M., Toop, G., Alberici, S., and Koper, M. (2018). Determining the renewability of co-processed fuels. 1–34. Available at:https://ec.europa.eu/energy/sites/ener/files/documents/co-processing_final_report_090418.pdf.

Schittkowski, J., Ruland, H., Laudenschleger, D., Girod, K., Kähler, K., Kaluza, S., et al. (2018). Methanol synthesis from steel mill exhaust gases: challenges for the industrial Cu/ZnO/Al2O3 catalyst. *Chemie Ing. Tech.* 90, 1419–1429. doi:10.1002/cite.201800017

Shankar Tumuluru, J., Sokhansanj, S., Hess, J. R., Wright, C. T., and Boardman, R. D. (2011). REVIEW: a review on biomass torrefaction process and product properties for energy applications. *Ind. Biotechnol.* 7, 384–401. doi:10.1089/ind.2011.7.384

SSAB (2019). SSAB to be first with fossil-free steel with HYBRIT technology. Available at:https://www.ssab.com/company/sustainability/sustainable-operations/hybrit (Accessed July 7, 2020).

Steelanol Consortium (2015). Steelanol - fueling a sustainable future. Available at: http://www.steelanol.eu/en (Accessed April 20, 2020).

Sundqvist, M., Biermann, M., Normann, F., Larsson, M., and Nilsson, L. (2018). Evaluation of low and high level integration options for carbon capture at an integrated iron and steel mill. *Int. J. Greenh. Gas Control* 77, 27–36. doi:10.1016/j.ijggc.2018.07.008

Suopajärvi, H., Kemppainen, A., Haapakangas, J., and Fabritius, T. (2017). Extensive review of the opportunities to use biomass-based fuels in iron and steelmaking processes. *J. Clean. Prod.* 148, 709–734. doi:10.1016/j.jclepro.2017.02.029

Suopajärvi, H., Pongrácz, E., and Fabritius, T. (2013). The potential of using biomass-based reducing agents in the blast furnace: a review of thermochemical conversion technologies and assessments related to sustainability. *Renew. Sustain. Energy Rev.* 25, 511–528. doi:10.1016/j.rser.2013.05.005

Suopajärvi, H., Umeki, K., Mousa, E., Hedayati, A., Romar, H., Kemppainen, A., et al. (2018). Use of biomass in integrated steelmaking–status quo, future needs and comparison to other low-CO2 steel production technologies. *Appl. Energy* 213, 384–407. doi:10.1016/j.apenergy.2018.01.060

Tanzer, S. E., Blok, K., and Ramírez, A. (2020). Can bioenergy with carbon capture and storage result in carbon negative steel? *Int. J. Greenh. Gas Control* 100, 103104. doi:10.1016/j.ijggc.2020.103104

Toktarova, A., Karlsson, I., Rootzén, J., Göransson, L., Odenberger, M., and Johnsson, F. (2020). Pathways for low-carbon transition of the steel industry—a Swedish case study. *Energies* 13, 3840. doi:10.3390/en13153840

Torero Consortium (2017). Torero project - fueling a sustainable future. Available at:http://www.torero.eu/ (Accessed April 20, 2020).

Tsupari, E., Kärki, J., Arasto, A., and Pisilä, E. (2013). Post-combustion capture of CO2 at an integrated steel mill–part II: economic feasibility. *Int. J. Greenh. Gas Control* 16, 278–286. doi:10.1016/j.ijggc.2012.08.017

van Dyk, S., Su, J., Mcmillan, J. D., and Saddler, J. (2019). Potential synergies of drop-in biofuel production with further co-processing at oil refineries. *Biofuels Bioprod. Biorefining* 13, 760–775. doi:10.1002/bbb.1974

Vogl, V., Åhman, M., and Nilsson, L. J. (2018). Assessment of hydrogen direct reduction for fossil-free steelmaking. *J. Clean. Prod.* 203, 736–745. doi:10.1016/j.jclepro.2018.08.279

Vogl, V. and Åhman, M. (2019). "What is green steel?-towards a strategic decision tool for decarbonising EU steel." in METEC-ESTAD conference, Düsseldorf, June 24–28, 2019. Available at:https://lup.lub.lu.se/search/publication/89d45b6d-b432-49ac-864f-33f93be3290b.

Voldsund, M., Gardarsdottir, S., De Lena, E., Pérez-Calvo, J.-F., Jamali, A., Berstad, D., et al. (2019). Comparison of technologies for CO2 capture from cement production—part 1: technical evaluation. *Energies* 12, 559. doi:10.3390/en12030559

Wang, C., Mellin, P., Lövgren, J., Nilsson, L., Yang, W., Salman, H., et al. (2015). Biomass as blast furnace injectant – considering availability, pretreatment and deployment in the Swedish steel industry. *Energy Convers. Manag.* 102, 217–226. doi:10.1016/j.enconman.2015.04.013

Wiklund, C. M., Helle, M., Kohl, T., Järvinen, M., and Saxén, H. (2017). Feasibility study of woody-biomass use in a steel plant through process integration. *J. Clean. Prod.* 142, 4127–4141. doi:10.1016/j.jclepro.2016.09.210

World Bioenergy Association (2019). *Global bioenergy statistics 2019*. Available at:https://worldbioenergy.org/uploads/191129 WBA GBS 2019_HQ.pdf.

World Steel Association (2014). *A methodology to determine the LCI of steel industry co-products*. 1–38. Available at:https://www.worldsteel.org/steel-by-topic/life-cycle-thinking/methodology-for-slag-LCI-calculation-.html.

Conflict of Interest: The authors declare that the research was conducted in the absence of any commercial or financial relationships that could be construed as a potential conflict of interest.

GLOSSARY

BFG Blast furnace gas

COG Coke oven gas

BOF Basic oxygen furnace

BOFG Basic oxygen furnace gas

CHP Combined heat and power

EtOH Ethanol

HRC Hot-rolled coil (final steel product)Hot metal (intermediate product of the blast furnace)Bio-PCI

PCI Pulverized coal injection (common fossil blast furnace injectant)

CCS, CCU, CCUS Carbon capture, utilization and/or storage

CAS Carbon allocation system (system defined in this work)

TES Total emissions system (system defined in this work)

MEA Monoethanolamine (solvent for CO2 absorption)

TRL Technology readiness level

EUA EU Allowance

EU ETS credit corresponding to one ton CO2eq.

FT Fischer-Tropsch

RED II Renewable Energy Directive (EU Directive 2018/2001)

FQD Fuel Quality Directive (EU Directive 98/70/EC)

LHV Lower heating value

GHG Greenhouse gas

ETS Emission trading system

C1–C4 Cases/Configurations of the studied integrated steel mill

frontiers in Chemical Engineering

ORIGINAL RESEARCH
published: 22 December 2020
doi: 10.3389/fceng.2020.594884

The Techno-Economic Benefit of Sorption Enhancement: Evaluation of Sorption-Enhanced Dimethyl Ether Synthesis for CO_2 Utilization

*Galina Skorikova[1], Marija Saric[1], Soraya Nicole Sluijter[1], Jasper van Kampen[1], Carlos Sánchez-Martínez[2] and Jurriaan Boon[1]**

[1]Sustainable Technologies for Industrial Processes, Energy Transition, TNO, Petten, Netherlands, [2]Sustainable Process & Energy Systems, Energy Transition, TNO, Delft, Netherlands

OPEN ACCESS

Edited by:
Simon Roussanaly,
SINTEF Energy Research, Norway

Reviewed by:
Juan Gabriel Segovia Hernandez,
University of Guanajuato, Mexico
Qingchun Yang,
Hefei University of Technology, China

***Correspondence:**
Jurriaan Boon
jurriaan.boon@tno.nl

Specialty section:
This article was submitted to Separation Processes, a section of the journal Frontiers in Chemical Engineering

Received: 14 August 2020
Accepted: 20 October 2020
Published: 22 December 2020

Citation:
Skorikova G, Saric M, Sluijter SN, van Kampen J, Sánchez-Martínez C and Boon J (2020) The Techno-Economic Benefit of Sorption Enhancement: Evaluation of Sorption-Enhanced Dimethyl Ether Synthesis for CO_2 Utilization. Front. Chem. Eng. 2:594884. doi: 10.3389/fceng.2020.594884

Dimethyl ether (DME) is an important platform chemical and fuel that can be synthesized from CO_2 and H_2 directly. In particular, sorption-enhanced DME synthesis (SEDMES) is a novel process that uses the *in situ* removal of H_2O with an adsorbent to ensure high conversion efficiency in a single unit operation. The *in situ* removal of steam has been shown to enhance catalyst lifetime and boost process efficiency. In addition, the hydrogen may be supplied through water electrolysis using renewable energy, making it a promising example of the (indirect) power-to-X technology. Recently, major advances have been made in SEDMES, both experimentally and in terms of modeling and cycle design. The current work presents a techno-economic evaluation of SEDMES using H_2 produced by a PEM electrolyzer. A conceptual process design has been made for the conversion of CO_2 and green H_2 to DME, including the purification section to meet ISO fuel standards. By means of a previously developed dynamic cycle model for the SEDMES reactors, a DME yield per pass of 72.4 % and a carbon selectivity of 84.7% were achieved for the studied process design after optimization of the recycle streams. The production costs for DME by the power-to-X technology SEDMES process at 23 kt/year scale are determined at ~€1.3 per kg. These costs are higher than the current market price but lower than the cost of conventional DME synthesis from CO_2. Factors with the highest impact on the business cases are the electricity and CO_2 cost price as well as the CAPEX of the electrolyzer, which is considered an important component for technology development. Furthermore, as the H_2 cost constitutes the largest part of the DME production cost, SEDMES is demonstrated to be a powerful technology for efficient conversion of green H_2 into DME.

Keywords: sorption-enhanced reaction, dimethyl ether, electrolysis, power-to-X, electrification, industry, techno-economic analysis

INTRODUCTION

In the energy transition, industry plays an essential role. Industry accounted for 37% (156 EJ) of the total global energy use in 2017, of which around 70% originates from fossil fuels (IEA, 2019). These are used as a fuel and feedstock, leading to concomitant emissions of carbon dioxide. Conversely, according to the United Nations' 2030 Agenda for Sustainable Development (UNFPA, 2020), industry needs to become sustainable, with increased resource-use efficiency and greater adoption of clean and environmentally sound technologies and industrial processes. Indeed, with increasing shares of renewables in electricity generation portfolios, the electrification of industrial processes contributes to the uptake of renewable energy in industry (IEA, 2019). In addition, through the development and implementation of circular practices including the chemical recycling of carbon dioxide, industry will become an essential element of the carbon-neutral economy (Centi and Perathoner, 2009; Olah et al., 2009; Ordomsky et al., 2017; SPIRE, 2020). The conversion of carbon dioxide into fuels and feedstock using electricity can thus contribute to a sustainable society (Artz et al., 2018; Detz et al., 2018; Kätelhön et al., 2019).

The conversion of carbon dioxide with electricity can be accomplished through the so-called power-to-X (PtX) technologies (Rego de Vasconcelos and Lavoie, 2019; Sánchez et al., 2019). Such PtX technologies comprise the direct electrochemical conversion of carbon dioxide to chemicals, as well as indirect conversion of carbon dioxide via thermochemical conversion routes, using hydrogen produced by electrolysis. Both approaches are currently under development in a multinational consortium in the European Interreg project Electrons to High-Value Chemical Products (E2C, 2020). As shown in **Figure 1**, the current work focuses on the indirect conversion of carbon dioxide with hydrogen to dimethyl ether (DME), a promising fuel and platform chemical (Semelsberger et al., 2006; Olah et al., 2009; Matzen and Demirel, 2016; Bongartz et al., 2018).

Although several routes exist and are currently in operation for the industrial synthesis of DME (Müller and Hübsch, 2000; Azizi et al., 2014), separation-enhanced synthesis routes have shown to offer major advantages in the conversion of carbon dioxide to chemicals (van Kampen et al., 2019). In fact, sorption-enhanced DME synthesis (SEDMES) has proven to yield a very high single-pass carbon selectivity to DME (Iliuta et al., 2011; van Kampen et al., 2020a; van Kampen et al., 2020b; van Kampen et al., 2020c). In this novel technology, steam is adsorbed *in situ* to overcome the thermodynamic limits of the reactions involved, resulting in the high single-pass DME yield. Previous research has focused on process development, including reactor engineering (Guffanti et al., 2020) and catalytic aspects (Boon et al., 2019; Liuzzi et al., 2020). A techno-economic assessment (TEA) of the SEDMES technology has not yet been published, although the production of DME from CO_2 and water using renewable energy has been studied in terms of economics (Martín, 2016) and life cycle analysis (LCA) (Matzen and Demirel, 2016).

The Interreg E2C project has the objective to combine hydrogen from electrolysis with an advanced SEDMES technology leading to a versatile and powerful route from carbon dioxide to high-value chemical products. This includes the construction of a containerized and highly flexible pilot demonstrator, and the development of the business case.

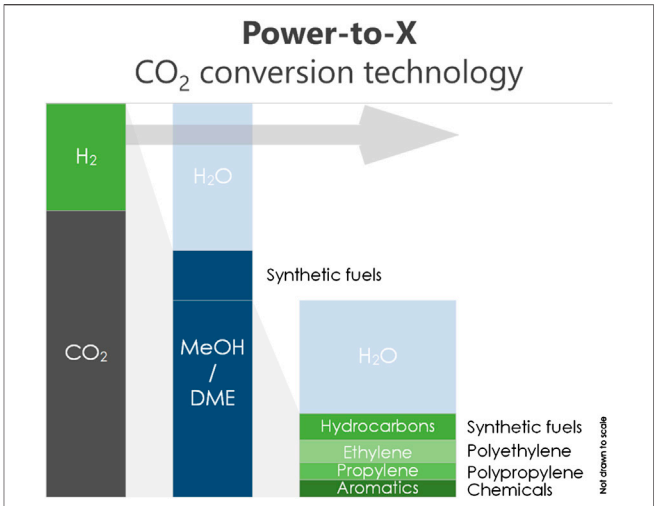

FIGURE 1 | Fuels and chemicals from carbon dioxide via methanol/dimethyl ether.

This article presents the techno-economic assessment of DME synthesis from carbon dioxide using the SEDMES technology in the two sea areas, meaning the coastal regions along the Southern North Sea and the Channel area in England, France, the Netherlands, and Belgium. First, a flow sheet is developed for the process to produce DME starting from electricity and carbon dioxide, including downstream processing (DSP) (**Figure 2**). Specific attention will be paid to the SEDMES unit, presenting the first full design for the conversion of carbon dioxide and hydrogen to DME. Finally, the TEA is presented, with the goal to assess the cost of producing DME via the PtX SEDMES process and to identify the most important cost drivers and corresponding R&D priorities. Sensitivity analyses on these factors are discussed. While a comparative assessment to conventional DME synthesis is outside the scope of the current work, the economic potential of sorption-enhanced synthesis will be highlighted by comparison to DME synthesis from electricity and carbon dioxide via the conventional reactor technology.

METHODOLOGY

Process Description

The studied process of DME production from captured CO_2 and H_2 formed in the electrolyzer powered by renewable energy is depicted schematically in **Figure 2**. The process consists of three main parts: i) a proton exchange membrane (PEM) water electrolyzer, ii) the SEDMES unit, and iii) distillation train for DME purification. A wind farm in the two sea areas would be a suitable energy source for the PEM, but this is out of the scope of this assessment. The flow sheet was designed using Aspen Plus software version 10 (**Figure 3**) (Aspen Plus). The Peng–Robinson

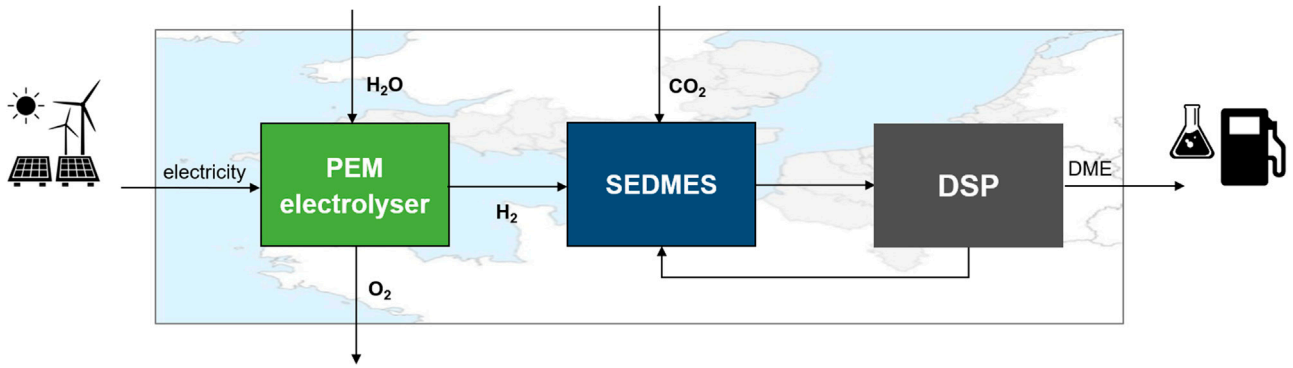

FIGURE 2 | Overview of the envisioned PtX process to convert CO_2 to dimethyl ether and scope of the techno-economic assessment.

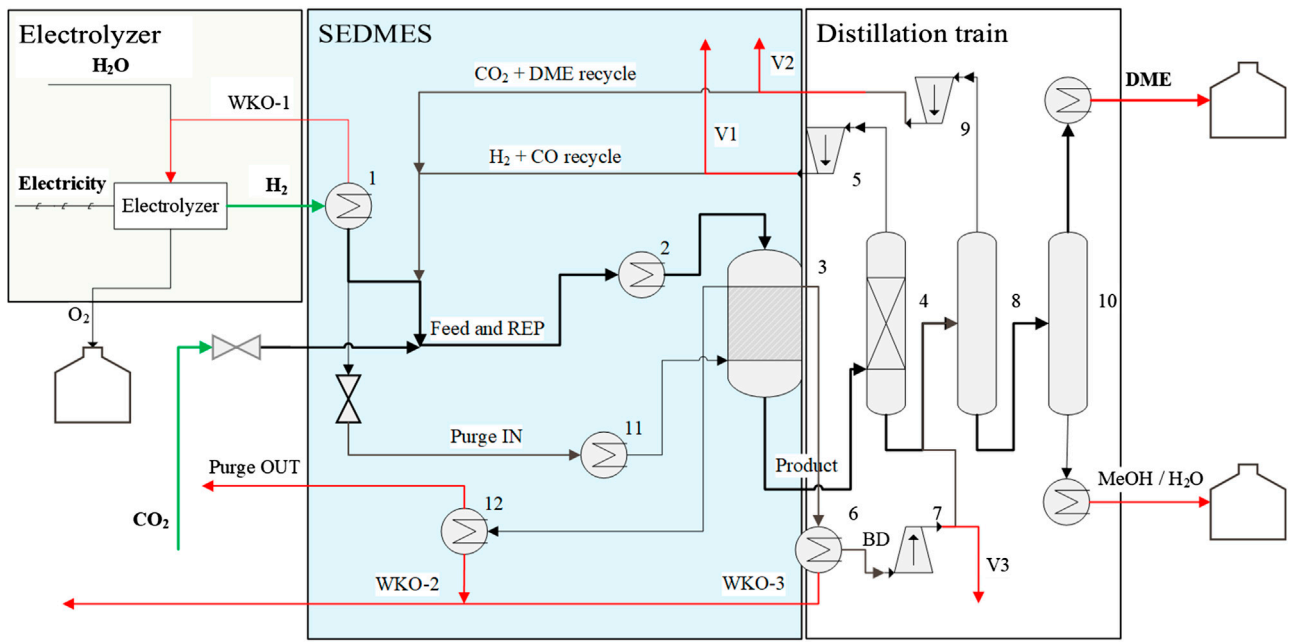

FIGURE 3 | Flow sheet of the power-to-X technology sorption-enhanced dimethyl ether synthesis process, including the following main equipment: 1: heat exchanger for H_2 dehumidification (cooling); 2: heat exchanger for the feed to reach operating temperature; 3: sorption-enhanced dimethyl ether synthesis columns; 4: flash drum to remove noncondensables; 5: blower for recycling of noncondensables; 6: heat exchanger to dehumidify blowdown stream; 7: compressor for blowdown; 8: distillation column for CO_2 separation (DSP-1); 9: compressor for recycling of CO_2; 10: distillation column for DME/MeOH + H_2O separation (DSP-2); 11: heat exchanger for purge dehumidification (cooling); 12: heat exchanger for purge stream (heating).

equation of state was selected as a property method and validated using data on experimental results from the integrated NIST library (Jonasson et al., 1995). For this techno-economical evaluation, the electrolyzer was considered as a "black box" without studies of its process parameters.

Electrolyzer

The electrolyzer supplied with electricity from renewable sources splits water into hydrogen and oxygen streams. While hydrogen is used as a feedstock for further DME production, oxygen acts as a side product, which can be sold after purification. For the hydrogen production from electricity, a PEM electrolyzer is selected. PEM electrolysis is an upcoming technology that is currently entering the market with systems at limited scales (Hydrogenics, 2020; Hydron, 2020; ITM, 2020; Nel Hydrogen, 2020). Due to their advantages in terms of high-pressure operation, high efficiencies and hydrogen purity, it is expected that PEM will become the preferred choice over the currently industrially used alkaline electrolyzers, provided that the costs will be reduced (Shiva Kumar and Himabindu, 2019). The electricity input for the PEM electrolyzer is set to 40 MW because it is minimal commercially available size would allow for plant-scale operation.

TABLE 1 | ISO 16861:2015 standard for DME as a fuel (ISO, 2020).

Characteristic	Category			
	Unit	Limit	DME at the gate of the manufacture	DME specifications for end-users
Purity	mass%.	minimum	99.5	98.5
Methanol	mass%.	maximum	0.050	0.050
Water	mass%.	maximum	0.030	0.030
Hydrocarbons (up to C_4)	mass%.	maximum	0.050	0.050
Carbon dioxide (CO_2)	mass%.	maximum	0.100	0.100
Carbon monoxide (CO)	mass%.	maximum	0.010	0.010
Methyl formate	mass%.	maximum	0.050	0.050
Ethyl methyl ether	mass%.	maximum	0.200	0.200
Residue after evaporation	mass%.	maximum	0.007	0.007
Total sulfur	mass%.	maximum	3.0	3.0

Saturated hydrogen comes out of the electrolyzer at 80°C and 30 bara containing 1.5 wt% of water. It is therefore cooled to 28.2°C in order to reduce the water level to nearly 0 wt%. In the calculation, it was assumed that cooling water is available at temperature of 18.2°C, with a temperature difference in the gas/liquid heat exchanger of 10°C (Anantharaman et al., 2018). Operating pressure of the SEDMES unit is selected to be determined by the electrolyzer so that H_2 would not need to be additionally pressurized, which contributes to the savings on a compressor installation and operation.

Sorption-Enhanced Dimethyl Ether Synthesis Unit

The feedstock for the DME production is captured CO_2 supplied from a pipeline with a pipeline pressure of 80 bara. After CO_2 is expanded to 30 bara, it is mixed with H_2 in stoichiometric ratio and preheated to the SEDMES operating pressure which is selected to be 250°C. The feed thereafter goes through the SEDMES reactor section (three-column cycle design), which is described in the next subchapter, to be converted into DME. The SEDMES product is cooled and sent to a distillation train to achieve ISO standard purity of DME product. The purge stream is dried and reused in a recycle purge loop, and no gas losses were considered.

Distillation Train

The goal of the SEDMES separation train is to obtain DME with the desired specifications, denoted in **Table 1**. First, the SEDMES product is cooled and sent to a flash drum to separate the noncondensables such as unconverted H_2 and the CO by-product. Depending on the temperature in the separator, some fractions of CO_2 and DME are removed as gas fractions. Therefore, sensitivity studies on the optimal temperature in the flash column were performed. The column is operated at the pressure of the SEDMES product stream, which is considered to be 29 bara. Therefore, a compact compressor is needed to recycle the noncondensables back to the SEDMES reactor. Second, a first distillation column (DSP-1) is used for the separation of CO_2 and DME, which is expected to be the most energy-intensive process due to similar characteristics of the compounds. Removed CO_2 with some fraction of DME is compressed and recycled back to the SEDMES reactor to eliminate losses of the feed or the product. Finally, DME is separated from methanol and water fraction in the second distillation column (DSP-2) until the desired purity is achieved, cooled down, and stored in a tank ready for transportation.

TABLE 2 | Parameters used in the SEDMES modeling (MATLAB).

Model parameter of a single tubular reactor	Value
Height (m)	7.500
Inner diameter (m)	0.037
Reactor volume (m^3)	0.008
Bed voidage	0.372
Catalyst/adsorbent loading (kg)	6.044
Catalyst fraction	0.200
Process parameters	**Value**
Operating pressure (bara)	30
Wall temperature (°C)	250
Cycle time (min)	36–72
GHSV of the feed ($m^3_{feed}\ hr^{-1}\ m^{-3}_{reactor}$)	160–325
GHSV of the purge ($m^3_{purge}\ hr^{-1}\ m^{-3}_{reactor}$)	380–600

Sorption-Enhanced Dimethyl Ether Synthesis Modeling

SEDMES is a reactive adsorption process in which steam is removed in situ by a sorbent. As a typical pressure swing adsorption (PSA) system, it is operated cyclic between reactive adsorption and sorbent regeneration. The studied case consists of four consecutive steps presented in **Figure 4**: adsorption (ADS): the feed is converted into DME on the catalyst, while steam is removed by a zeolite adsorbent; blowdown (BD): countercurrent depressurization of the system in order to desorb water; purge (PURGE): countercurrent flow of dry hydrogen to remove water from the column; repressurization (REP): cocurrent pressurization of the column with the feed stream. In order to maintain a continuous process, one column needs to be in adsorption mode, while another one undergoes regeneration. Therefore, a minimum of two columns is required for an

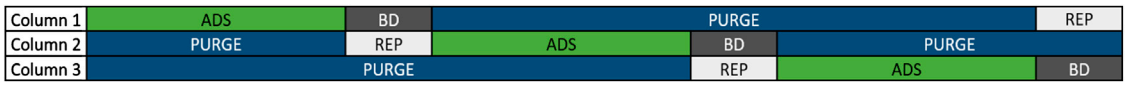

FIGURE 4 | Three-column cycle design for the four-step SEDMES process with (ADS) adsorption step, (BD) blowdown step, (PURGE) purge step, (REP) repressurization step.

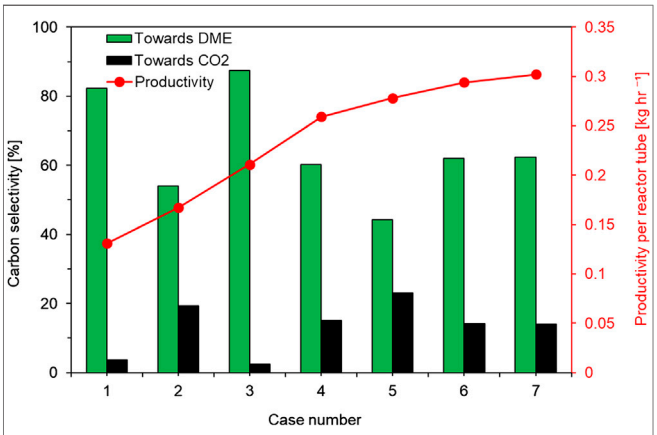

FIGURE 5 | Results of the dynamic cycle modeling showing the trade-off between carbon selectivity and productivity for the chosen three columns SEDMES cycle design.

efficient process. However, the duration of the regeneration has a critical effect on the process performance since a longer PURGE step provides drier conditions. In order to design the PURGE step to be longer than ADS, a minimum of three columns are required. Therefore, for the first TEA, a three-column cycle design is considered (**Figure 4**).

In order to design a cycle, the boundary conditions have to be set. Since adsorption and repressurization are performed with the same feed, it is important from a technical point of view to maintain a continuous feed flow. Additionally, it is beneficial to keep the REP step as short as possible to maintain production close to continuous. Such important parameters as cycle time and gas hourly space velocities (GHSV) of the feed and purge streams were tuned to achieve high DME yield at high production rate. A previously developed, verified and validated (van Kampen et al., 2020a; van Kampen et al., 2020c) one-dimensional dynamic reactor model (MATLAB) (van Kampen et al., 2020b) is used to study the SEDMES cycle. Several resulting output flows are subsequently studied in the overall process with downstream processing and recycle loops using Aspen Plus software.

The process performance was evaluated using carbon selectivity toward DME, carbon selectivity toward CO_2, and the productivity as key parameters. The carbon selectivities were calculated as molar concentration–based selectivity for each of the carbon containing species, $y(x)$:

$$C - DME = \frac{2y(DME)}{y(\mathrm{CO}) + y(\mathrm{CO_2}) + 2y(DME) + y(\mathrm{MeOH})} \quad (1)$$

$$C - \mathrm{CO_2} = \frac{y(\mathrm{CO_2})}{y(\mathrm{CO}) + y(\mathrm{CO_2}) + 2y(DME) + y(\mathrm{MeOH})} \quad (2)$$

Productivity P presented in **Figure 5** (kg/hr) is defined as the mass of DME m collected during the adsorption step over the duration of this step τ per 1 reactor tube:

$$P - DME\ (\mathrm{kg/hr}) = \frac{m(DME)}{\tau(ADS)} \quad (3)$$

Downstream Processing Modeling

The first step of the DSP is a flash drum, which was optimized with respect to the fraction of CO_2 slip to the liquid product (<6% mol.) in order to reduce the condenser duty from the next purification step. The pressure was maintained the same as the outlet stream of the reactor to reduce the electrical duty required for recompression of the recycle stream.

The liquid product of the flash drum is sent to the first distillation column. In this column, the separation of DME and CO_2 takes place which is recognized as the most energy-intensive process in the DSP block. The resulting bottom product (DME) contains a level of methanol exceeding the limit of the ISO standard, and therefore, a second distillation column is required to separate the small fraction of methanol. For optimization of the distillation columns, the shortcut method (DSTWU) was used by which, a specified reflux ratio and the minimal number of stages were calculated. These results were then used as the input for simulation of RadFrac columns. The distillate/feed (D/F) ratio was varied in order to meet the following product specifications: 1^{st} *column*: CO_2 < 0.1% wt; 2^{nd} *column*: methanol <0.05% wt.

The cold gas efficiency is a measure of the feedstock conversion into a product, accounting for the energy preserved in the gas phase. Here, the low heating value (LHV) of the components was used for the calculations. Since the LHV of CO_2 is zero, CGE reflects the H_2 conversion into DME product:

$$CGE\ (\%) = \frac{LHV_{DME,out}}{LHV_{H2,in}} \times 100 \quad (4)$$

Economic Evaluation

Economic evaluation of the DME production cost was performed using relevant starting points listed in **Table 3**: Summary of the assumed key economic parameter indicators and assumptions for the PtX SEDMES process base case. For the CAPEX evaluation of the flash and distillation columns as well as tubular reactors of the SEDMES unit, Aspen APEA vr 10 software was used. The reactor

was considered as a shell-and-tube heat exchanger, in order to enable heat management (Guffanti, 2020). Heuristics for design of the flash and distillation columns were used (ISO, 2020). The equipment costs were determined by the column diameters which are calculated for the given liquid (flash) and vapor (distillation column) flows. The height of the distillation columns was determined by the amount of stages and a typical height equivalent to a theoretical plate (HETP) for the packed bed columns. For the flash columns, a liquid residence time of 5 min was assumed. The costs for compressors were evaluated using data on electrical duty based on Aspen Plus simulations and Matche website (Matche, 2020). Installation factors for the compressors were taken from the literature (Humphreys & English, 1993). Finally, a sensitivity study on the prices of the main cost contributors on the DME production was performed. However, after the first cost estimated, the utilities and CAPEX contribution of the downstream processing to the total PtX SEDMES process were found to have a low impact on the DME production cost. Therefore, further optimizations of the DSP unit were left out of the scope of this study.

The installation cost for the PEM electrolyzer is assumed to be 950 €/kW (**Table 3**) (IRENA, 2018), which is on the low side of reported ranges in the literature (Schmidt et al., 2017). The electrolyzer is assumed to use 49 kWh per 1 kg of H_2 (efficiency of 68% LHV) (Martín, 2016). The cost of CO_2 varies significantly depending on the capture technology and source used (Armstrong et al., 2019; Della Vigna et al., 2019). We assumed a relatively optimistic CO_2 price of 70 €/t CO_2 based on the estimated average CO_2 abatement costs of current technologies for the industry and power sector (Della Vigna et al., 2019), and study a range from 50 to 250 € per ton in our sensitivity analysis. Similarly, energy prices are dependent on many factors in the (future) energy market, and the impact on the PtX SEDMES process for a broad range of energy prices is studied. For the base case, we adopt a value of 50 €/MWh based on the Dutch Climate and Energy Outlook 2019 (Schoots & Hammingh, 2019).

DME production costs were calculated using following equation:

$$DME\ costs\left(\frac{€}{kg}\right) = \frac{Annualized\ CAPEX + OPEX}{DME\ production} \tag{5}$$

Annualized CAPEX is calculated using following equation, where n is the lifetime plant and i is the interest rate:

$$Annualized\ CAPEX\ (€/\text{year}) = \frac{i}{1-(1+i)^{-n}} \tag{6}$$

When performing the sensitivity analysis, one of the studied parameters is the total annual production of DME using the PtX SEDMES process. The annual capacity influences the annualized CAPEX per ton DME, coming from the economy of the scale effect: for higher throughput, the capital expenses become smaller per kilogram product.

TABLE 3 | Summary of the assumed key economic parameter indicators and assumptions for the power-to-X technology SEDMES process base case.

Lifetime plant (years)	20
System lifetime of electrolyzer (years) (IRENA, 2018)	20
Lifetime of electrolyzer stack (h) (IRENA, 2018)	60,000
Catalyst lifetime (years)	5
Operating hours/year (h)	8,000
Assumed nr operators/shift	1
Number of shifts	3
Salary operator (€/year)	60,000
Electricity costs (€/MWh)	50
CO_2 price (€/t)	70
Gas costs (€/GJ)	6
Cooling tower water ($/GJ) (Turton et al., 2003)	0.354
Chilling water 5–15°C ($/GJ) (Turton et al., 2003)	4.43
Catalyst cost (€/kg) (Alfa Aesar, 2020)	124.4
Adsorbent cost (€/t)	63
Electrolyzer cost (€/kW) (Schmidt et al., 2017; IRENA, 2018)	950
OPEX for electrolyzer (% of CAPEX) (IRENA, 2018)	2%
CAPEX stack replacement (€/kW) (IRENA, 2018)	420
Interest rate	8%
Dollar to euro (2020)	1.18
Contigency (% installed CAPEX + general utilities) (AACE, 1991)	15%
General facilities (installed CAPEX) (AACE, 1991)	10%
Indirect costs (installed CAPEX) (AACE, 1991)	15%
Pre-paid roallites (installed CAPEX) (AACE, 1991)	0.50%
Start-up costs (total plant costs) (AACE, 1991)	2%
Working capital (total capital requirements) (AACE, 1991)	15%
Spare parts (total plant costs) (AACE, 1991)	0.50%
Scale-up factor CAPEX PEM (—) (Smolinka, 2015)	0.83
Max capacity PEM for scale-up factor (MWel) (Reutemann & Kieczka, 2000)	100
Scale-up factor CAPEX SEDMES (—)	0.59
Max capacity SEDMES for scale-up factor (kt DME/year)	47
Scale-up factor distillation train and vessel (—) (NREL, 2006)	0.62
Scale-up factor compressor (centrifugal) (—)	0.62

TABLE 4 | Parameters used for tuning of the SEDMES cycle parameters.

Case number	Cycle time (min)	Feed GHSV ($m^3_{feed}\ h^{-1}\ m^{-3}_{reactor}$)	Purge GHSV ($m^3_{purge}\ h^{-1}\ m^{-3}_{reactor}$)
1	36	160	380
2	36	240	600
3	48	160	380
4	36	240	380
5	36	325	380
6	48	240	380
7	72	240	380

The estimation of the CAPEX for the SEDMES unit, the PEM electrolyzer, and the distillation columns depending on the annual production is done as follows, where C_{New} is the capacity (in $(kt/annum)$ or (MW_{el})) at which the CAPEX will be estimated, and C_{Ref} (in $(kt/annum)$ or (MW_{el})) is the capacity at which the reference CAPEX, $CAPEX\,(C_{Ref})$, is based on:

$$CAPEX\,(€) = CAPEX\big(C_{Ref}\big)\cdot\left(\frac{C_{New}}{C_{Ref}}\right)^{\gamma} \tag{7}$$

It must be noted that when the new capacity C_{New} exceeds the max capacity (listed in **Table 3** for SEDMES, PEM, and distillation column), then the CAPEX value, $CAPEX\,(C_{New})\,(€/tDME)$, must

TABLE 5 | Conditions and compositions of the inlet and outlet streams simulated using the dynamic cycle model for a single 0.008 m (Olah et al., 2009) reactor tube.

Inlet streams				Outlet streams			
Process step	**ADS**	**PURGE**	**REP**	**Process step**	**ADS**	**PURGE**	**BD**
Duration (min)	12	28	4	Duration (min)	12	28	4
Temperature (°C)	250	250	250	Temperature (°C)	255	246	256
Pressure (bara)	30	1.2	1.2	Pressure (bara)	30	1.2	1.2
Flow rate (kg/h)	0.72	0.27	0.73	Flow rate (kg/h)	0.26	0.43	0.95
Total mass (kg)	0.18	0.16	0.06	Total mass (kg)	0.06	0.25	0.08
Composition (%mol.)				Composition (%mol.)			
H_2	75.03	99.99	75.03	H_2	36.99	93.72	63.02
DME	0.00	0.00	0.00	DME	48.84	0.00	8.15
CO	0.00	0.00	0.00	CO	10.25	0.01	7.30
CO_2	24.97	0.00	24.97	CO_2	2.77	0.05	16.07
MeOH	0.00	0.00	0.00	MeOH	0.94	0.00	1.00
H_2O	0.00	0.01	0.00	H_2O	0.21	6.23	4.45

be taken at the upper bound capacity, that is, above the referred maximum capacity, there is no more economy of the scale effect that can lower down the CAPEX.

RESULTS AND DISCUSSION

Sorption-Enhanced Dimethyl Ether Synthesis Modeling

For the first PtX SEDMES production cost estimate, a simple tuning of the SEDMES cycle design parameters was performed, varying the cycle times and flows (**Table 4**). The results in terms of productivity and carbon selectivity toward DME of this dynamic cycle modeling are given in **Figure 5**. As is typical for sorption-enhanced processes, there is a trade-off between carbon selectivity and productivity observed for the SEDMES process. The potential benefit of high carbon selectivity toward DME (C-DME) > 80% and low carbon selectivity toward CO_2 (C-CO_2) < 5% includes reduced duties for the distillation train, lower volume of recycles, and thus potentially higher resource efficiency. As case #3 exhibits the highest C-DME (84.7%) among the studied cases and a reasonably high productivity (higher than the case #1), this case was selected for further simulations and techno-economical evaluations, which are discussed below.

The conditions and compositions of the inlet and outlet streams for the selected case are listed in **Table 5**. The yield per pass for SEDMES under these conditions is 65%, which is 57% points more than the conversion without sorption enhancement (maximum 8% for conventional DME synthesis). The BD stream for this case is considerably large (10 vs 7.5 $kg/m^3_{reactor}$ during adsorption mode) and contains valuable components (8.2 mol% DME product and 79.1 mol% unconverted feed). It is thus essential to further process and recycle the BD product. There are two options for this: 1) recycling the BD product directly to the feed stream or 2) sending the BD product to the distillation train. Since the BD stream is one-third of the feed (30 $kg/m^3_{reactor}$), consisting of 8.2 mol% of DME, it will keep on changing the feed composition due to accumulation of DME if option 1 is adopted. We anticipate that this will increase C-DME, while decreasing the conversion per pass. Sending the BD product to the distillation train allows collecting additional DME as a product and, therefore, removing undesired product recycling. Therefore, the BD stream will be sent to the DSP as well (option 2).

The data on the inlet and outlet streams generated by means of the dynamic cycle model (MATLAB) were used as an input for the flow sheet simulations in the Aspen Plus environment to provide the new feed composition after purification and recycling. This new feed composition was used in the cycle model to simulate the process after the iteration, and new mass flows were generated that are listed in **Table 6**. It can be observed that the feed composition after the chosen recycling routes does not noticeably deviate from the original feed composition, and it introduces 1.43 mol% DME. Therefore, for the first DME production, cost evaluation for one iteration of recycling seems to be sufficient. The yield per pass with the recycle increased to 72.4%. After performing all the recycling processes, it was calculated that 5966 reactor tubes of 0.008 m^3 per reactor column are required to process the fixed H_2 feed.

Economic Evaluation

The first techno-economical evaluation of PtX DME production from CO_2 and green H_2 by means of the SEDMES technology was performed, and the main cost contributors are listed in **Table 7**. The total investment cost for envisioned plant is 48 M€. The contribution of the operational costs (OPEX) exceeds the capital cost (CAPEX) contribution 2.75 times. The OPEX mainly comprises electricity (72%) and CO_2 cost (14%). Since the electricity usage is mainly related to H_2 production (99.2%) in the PEM electrolyzer, it is evident that the cost of H_2 is the cost-driving factor for the DME production in the studied scenario with a hydrogen production cost of ~€3.8 per kg of H_2. Therefore, it is important to design a process with maximum H_2 conversion into DME. This is also supported by the impact of electrolyzer cost on the total installation cost, where hydrogen production makes up 78% of the installation cost contribution.

In order to reach this high H_2 conversion, all hydrogen losses, mostly in the vent streams, should be minimized. This can be achieved by reducing the size of recycle streams which is strongly related to the DME yield per pass. As discussed

TABLE 6 | Mass flows and composition of the input and output streams for the power-to-X technology SEDMES process simulated using ASPEN.

	Inlet streams			Outlet streams							
	H_2	CO_2	Purge IN	DME	MeOH/ H_2O	WKO-1	WKO-2	WKO-3	V1	V2	Purge OUT
Mass flows (kg/h)	920.8	5899.5	2519.9	2929.5	102.0	108.0	141.8	3183.8	21.5	38.7	2814.9
H_2	810.5	0.0	2519.9	0.0	0.0	0.0	0.0	0.0	1.0	1.9	2534.3
DME	0.0	0.0	0.0	2925.2	2.5	0.0	0.0	0.0	1.2	11.8	0.0
CO	0.0	0.0	0.0	0.0	0.0	0.0	0.0	0.0	3.4	18.9	14.6
CO_2	0.0	5899.5	0.0	2.6	0.0	0.0	0.0	0.0	15.9	6.1	65.2
MeOH	0.0	0.0	0.0	1.4	94.8	0.0	0.0	0.0	0.0	0.0	0.7
H_2O	110.3	0.0	0.0	0.2	4.7	108.0	141.8	3183.8	0.0	0.0	200.0

earlier, the single-pass DME yield for the SEDMES process under these conditions is over 72%, while for the conventional indirect DME production process, the yield would only be 19% at more severe conditions (100 bara standard operation) (Martin Mendez, 2016). The high single-pass conversion and high selectivity to DME make SEDMES technology more efficient in converting the valuable H_2 and reducing its loss, which is crucial due to the major impact of the hydrogen production on the total cost. Moreover, during the SEDMES process, high amounts of steam are produced, which can be purified and reused to produce H_2 in the PEM electrolyzer.

The cold gas efficiency (CGE) reflects the conversion of H_2 to DME based on their lower heating value (LHV). For the overall SEDMES process (after purification), the CGE is already 90%, while the theoretical maximum for the conversion of CO_2 and H_2 to DME is 92%. The losses consist of MeOH by-product formation (1.98%) and losses in recycle vents (up to 0.02%). Hence, the CGE could be optimized further by minimizing by-product formation and/or recycling. Noteworthy, the overall efficiency of 90% exceeds the theoretical maximum CGE of 88% for the conversion of CO_2 and H_2 to methanol, indicating that PtX SEDMES is inherently more efficient.

The results indicate that the installation cost for the SEDMES unit is 19% of the total installation cost (6.3% per reactor column); thus, further studies on the effect of the number of SEDMES reactor columns on the production cost would be of interest. More SEDMES reactor columns would allow different cycle designs, including pressure equalization, to improve the carbon selectivity toward DME, DME yield, and/or production rate, whereas two columns would potentially allow to reduce installation costs.

For the studied case, a DME production rate of 23 kt/year is achieved, which corresponds to a production cost of 1.30 €/kg_{DME} (**Figure 6**). Currently, the DME market price is around €0.56 per kg of DME (Hepburn et al., 2019), and the production cost of PtX DME thus exceeds the market price of fossil-based DME. However, the costs lie well below those found as the average cost of producing DME from CO_2 according to Hepburn et al. (2019) (2.74 $/kg). Furthermore, the reported production cost is in the same range as evaluated by Martin for conventional DME synthesis combined with water electrolysis (1.43 €/kg), although his assessment has the benefit of scale (197 versus 23 kt/year) and includes revenues of O_2 sales (Martín, 2016). This similar cost could be expected, whereas it is shown that the hydrogen production is the major determining factor. However, besides the technical benefits of the SEDMES technology, the results for relatively small-scale DME production reported here also indicate that the SEDMES technology is not more expensive than the conventional technology and even has the potential of reducing the cost over the conventional route.

The results of the sensitivity analysis on the cost contributors to PtX SEDMES process are depicted in **Figure 7**. The central value of around 1,300 €/t_{DME} represents our base case. The DME production costs are notably dominated by the PEM electrolyzer at a given efficiency, and the electricity cost has the largest impact on the fuel production costs. Therefore, improving the electrolyzer efficiency is one possibility to achieve a lower DME production cost. By increasing the efficiency to 75% the cost drops to below 1,200 €/t_{DME}. Another promising development to cut CAPEX costs of the electrolyzer is replacement of the PEM electrolyzer with its less expensive anion exchange membrane (AEM) alternative (Vincent and Bessarabov, 2018). However, this should not come with a high loss in efficiency. In the E2C project, AEM electrolyzers with non-noble metal catalysts are already being developed to reduce the electrolyzer costs (Loh et al., 2020; Ullah et al., 2020).

The sensitivity analysis indicates that the reduction in the electricity price has the highest potential to bring down the production cost. Regions with high wind and solar availability, such as coastal areas, will probably have high supplies of renewable electricity in the future, leading to significantly reduced price and, even to grid balancing problems. If the PtX SEDMES process is compatible with the intermittency of energy, this provides the process with the opportunity to use the power excess for the production of DME. Therefore, the compatibility of the PtX SEDMES process with intermittent electricity is an interesting research direction, which will be investigated in the E2C project.

Like other processes, the costs of PtX technologies are known to be reduced by economies of scale (Schmidt et al., 2017). Therefore, production scale of DME with the PtX SEDMES process was also investigated in the sensitivity analysis. As can be discerned from **Figure 7**, the increase from 23 to 200 kt DME/year (production scale from Martín (2016)) brings the DME cost below 1,300 €/t DME, outperforming the conventional DME synthesis route even

TABLE 7 | Breakdown of the costs contributors of the power-to-X technology DME production using SEDMES in euro per ton of DME.

Cost contributor (€/t DME)			
Annualized CAPEX		**OPEX**	
Annualized installed equipment costs	240.8	Electricity	689.5
Electrolyzer	190.2	CO_2	134.8
SEDMES reactors	45.3	Stack replacement	71.8
Distillation train	5.3	Catalyst and adsorbent	0.2
Other costs (e.g., contingency and start-up costs)	107.2	Other costs (e.g., utilities and labor costs)	56.0
Total annualized CAPEX	348.0	Total OPEX	952.3
DME production costs (€/t DME)			1300.2

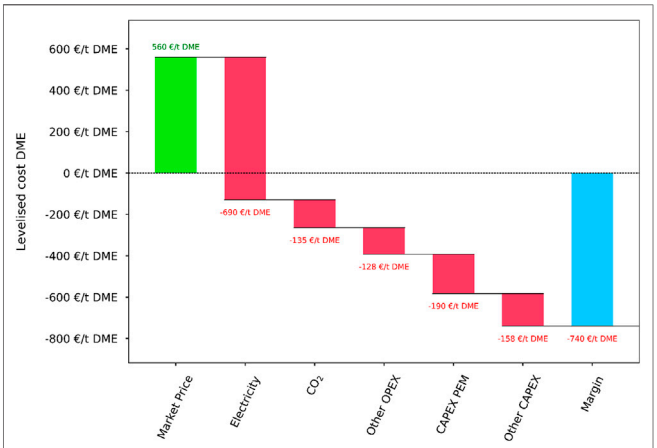

FIGURE 6 | Waterfall chart showing the main cost contributions to the production cost for a ton of DME using the power-to-X technology SEDMES process.

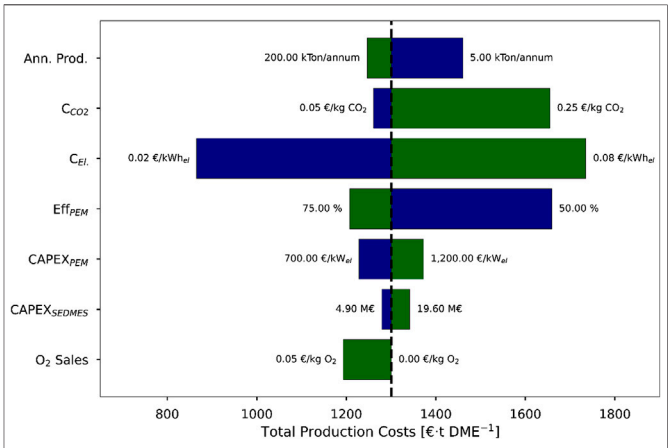

FIGURE 7 | Sensitivity analysis on the main cost contributing factors to the power-to-X technology SEDMES process. H_2 is produced by PEM electrolysis and reacts with captured CO_2 to produce DME. Ann Prod, annual production scale; C_{CO2}, carbon dioxide cost; C_{El}, electricity cost; Eff_{PEM}, efficiency of the PEM electrolyzer; $CAPEX_{PEM}$, capital costs electrolyzer; $CAPEX_{SEDMES}$, capital costs SEDMES unit. Blue and green bar indicate lower and higher values compared to the base case, respectively.

further (Martín, 2016). Additionally, the SEDMES PtX technology allows DME production at very small scale envisioned for the decentralized PtX technology. An annual production of 5 kt/year only increases CAPEX by ca. 150 €/t DME. This is an additional advantage of a sorption-enhanced technology over the conventional DME production, which is unattractive for small-scale production (Detz et al., 2018).

The costs of the PtX SEDMES process are also sensitive to the cost of CO_2. The CO_2 price constitutes 14% of total OPEX and 10% of the total production cost. The break-even cost for CO_2, which is required to make the process economically viable, is −0.31 €/kg_{CO2}, meaning that incentives for CO_2 utilization and/or costs for emission should amount to this value. Although it is foreseen that policy changes in CO_2 emission will have a high impact on the price formation, 310 €/t_{CO2} is significantly more than any suggested carbon dioxide tax so far (Hepburn et al., 2019).

The impact of the CAPEX of the SEDMES unit was also investigated. As can be seen from **Figure 7**, reducing the capital costs of this installation has a limited effect on the DME production price. Another option to make the PtX SEDMES process more attractive is to sell the produced oxygen (credit 0.05 €/kg) from the PEM electrolyzer as a product. As can be seen from **Figure 7**, this would lower the DME production price with around 10 cents.

CONCLUSION

In this article, the techno-economic assessment of the PtX SEDMES process, producing fuel-grade DME from carbon dioxide and green H_2, is presented. By means of a previously developed dynamic cycle model for the SEDMES reactors, a DME yield per pass of 72.4% and a carbon selectivity toward DME of 84.7% were achieved for the studied process design after optimization of the recycles streams. The production cost for DME was found to be ~€1.3 per kg for a relatively small-scale production plant of 23 kt/year. Although the production cost is higher than the current market price for fossil-based DME, the results are more promising than other studies on DME production from CO_2 by conventional DME synthesis processes. The environmental impact of the proposed PtX SEDMES process should be analyzed in the follow-up work.

The main cost contributing factors within the PtX process are related to the H_2 production by the PEM electrolyzer. The

energy costs have the largest impact on the production price followed by the CAPEX of the PEM electrolyzer. The sensitivity analysis indicates that also the CO_2 price has an impact on the production cost. A break-even cost, which is required to make the process economically viable, for this feedstock is −310 €/t_{CO2}. Since the main cost drivers of the PtX SEDMES process are related to the PEM electrolyzer, research directions should be geared toward reducing electrolyzer costs by enhancing efficiencies and the use of less expensive materials. Moreover, SEDMES is demonstrated to be a powerful technology for efficient conversion of green H_2 into DME, which is an essential benefit due to the determining role of the hydrogen cost in the total production cost.

DATA AVAILABILITY STATEMENT

The raw data supporting the conclusions of this article will be made available by the authors, without undue reservation.

AUTHOR CONTRIBUTIONS

JK developed the computational (MATLAB) model and GS performed the modelling. GS and MS developed the flowsheet in Aspen and gathered the data with input from CM and SS. GS performed the calculations, while CM performed the sensitivity study. All authors provided critical feedback and helped shape the research and analysis. GS and SS wrote the manuscript in consultation with JK and JB. JB conceived the original idea for the study and supervised the project together with SS.

FUNDING

This project has received funding from the Interreg 2 Seas programme 2014–2020 co-funded by the European Regional Development Fund under subsidy contract no 2S03–019 E2C. Additional funding has been received by Smartport, Provincie Zuid-Holland, Provincie Noord-Holland, and the Dutch Ministry for Economic Affairs and Climate Policy.

ACKNOWLEDGMENTS

We acknowledge Florian Estreguil from CPE Lyon and TNO, Katy Armstrong and Peter Sanderson from the university of Exeter and Jan Wilco Dijkstra and Yvonne van Delft from TNO, for fruitful discussions that helped improving the quality of this manuscript.

REFERENCES

AACE (1991). *Conducting technical and economic evaluations: as applied for the process and utility industries*. Morgantown, WV: AACE International Recommended Practice

Alfa Aesar (2020). Available at: https://www.alfa.com/en/catalog/045776/

Anantharaman, R., Bolland, O., Booth, N., Van Dorst, E., Sanchez Fernandez, E., Franco, F., et al. (2018). D2.4.3. European best practice guidelines for assessment of CO_2 capture technologies (Version 8/3/2011). Available at: https://doi.org/10.5281/zenodo.1312801

Armstrong, K., Sanderson, P., and Styring, P. (2019). "Promising CO_2 point sources for utilisation," in *Carbon dioxide utilization fundamentals*. M. N. Styring (Editor) (De Gruyter), 47–62. doi:10.1515/9783110563191-004

Artz, J., Müller, T. E., Thenert, K., Kleinekorte, J., Meys, R., Sternberg, A., et al. (2018). Sustainable conversion of carbon dioxide: an integrated review of catalysis and life cycle assessment. *Chem. Rev.* 118 (2), 434–504. doi:10.1021/acs.chemrev.7b00435.

Aspen Plus (2020). Available at: https://www.aspentech.com/en/products/engineering/aspen-plus

Azizi, Z., Rezaeimanesh, M., Tohidian, T., and Rahimpour, M. R. (2014). Dimethyl ether: a review of technologies and production challenges. *Chem. Eng. Process: Process Intensification*. 82, 150–172. doi:10.1016/j.cep.2014.06.007.

Bongartz, D., Doré, L., Eichler, K., Grube, T., Heuser, B., Hombach, L. E., et al. (2018). Comparison of light-duty transportation fuels produced from renewable hydrogen and green carbon dioxide. *Appl. Energy.* 231, 757–767. doi:10.1016/j.apenergy.2018.09.106

Boon, J., van Kampen, J., Hoogendoorn, R., Tanase, S., van Berkel, F. P. F., and van Sint Annaland, M. (2019). Reversible deactivation of γ-alumina by steam in the gas-phase dehydration of methanol to dimethyl ether. *Catal. Commun.* 119, 22–27. doi:10.1016/j.catcom.2018.10.008

Centi, G., and Perathoner, S. (2009). Opportunities and prospects in the chemical recycling of carbon dioxide to fuels. *Catal. Today.* 148 (3–4), 191–205. doi:10.1016/j.cattod.2009.07.075

Della Vigna, M., Stavrinou, Z., Bhandari, N., Mehta, N., and Singer, B. (2019). *Carbonomics: the future of energy in the age of climate change.*

Detz, R. J., Reek, J. N. H., and van der Zwaan, B. C. C. (2018). The future of solar fuels: when could they become competitive? *Energy Environ. Sci.* 11 (7), 1653–1669. doi:10.1039/c8ee00111a

E2C (2020). Electrons to high-value chemical products - E2C. Available at: https://www.voltachem.com/e2c

Guffanti, S., Giorgio Visconti, C., van Kampen, J., Boon, J., and Groppi, G. (2020). Reactor modelling and design for sorption enhanced dimethyl ether synthesis. *Chem. Eng. J.* 2020, 126573. doi:10.1016/j.cej.2020.126573

Hepburn, C., Adlen, E., Beddington, J., Carter, E. A., Fuss, S., Mac Dowell, N., et al. (2019). The technological and economic prospects for CO_2 utilization and removal. *Nature.* 575 (7781), 87–97. doi:10.1038/s41586-019-1681-6

Humphreys, K., and English, L. M. (1993). *Project and cost engineers' handbook*, 3rd Edition. New York: CRC Press

Hydrogenics (2020). Available at: http://www.hydrogenics.com/wp-content/uploads/Renewable-Hydrogen-Brochure.pdf

Hydron (2020). Available at: https://hydron-energy.com/products/

IEA (2019). Tracking Industry 2019. Available at: https://www.iea.org/reports/tracking-industry-2019.

Iliuta, I., Iliuta, M. C., and Larachi, F. (2011). Sorption-enhanced dimethyl ether synthesis-multiscale reactor modeling. *Chem. Eng. Sci.* 66 (10), 2241–2251. doi:10.1016/j.ces.2011.02.047

IRENA (2018). *Hydrogen from renewable power- technology Outlook for the energy transition*. IRENA

ISO (2020). ISO standard. Available at: https://www.iso.org/standard/57835.html

ITM (2020). Available at: https://www.itm-power.com/products

Jonasson, A., Persson, O., and Fredenslund, A. (1995). High pressure solubility of carbon dioxide and carbon monoxide in dimethyl ether. *J. Chem. Eng. Data.* 40 (1), 296–300. doi:10.1021/je00017a066

Kätelhön, A., Meys, R., Deutz, S., Suh, S., and Bardow, A. (2019). Climate change mitigation potential of carbon capture and utilization in the chemical industry. *Proc. Natl. Acad. Sci. U.S.A.* 116 (23), 11187–11194. doi:10.1073/pnas.1821029116

Liuzzi, D., Peinado, C., Peña, M. A., van Kampen, J., Boon, J., and Rojas, S. (2020). Increasing dimethyl ether production from biomass-derived syngas via sorption enhanced dimethyl ether synthesis. *Sustain. Energy Fuels.* 4 (11), 5674–5681. doi:10.1039/d0se01172j

Loh, A., Li, X., Taiwo, O. O., Tariq, F., Brandon, N. P., Wang, P., et al. (2020). Development of Ni–Fe based ternary metal hydroxides as highly efficient oxygen evolution catalysts in AEM water electrolysis for hydrogen production. *Int. J. Hydrogen Energy*. 45(46), 24232–24247. doi:10.1016/j.ijhydene.2020.06.253

Martín, M. (2016). Optimal year-round production of DME from CO_2 and water using renewable energy. *J. CO2 Util.* 13, 105–113. doi:10.1016/j.jcou.2016.01.003

Martin Mendez, L. (2016). *Process design and control of dimethyl ether synthesis*. Madrid: Polytechnic University of Madrid

Matche (2020). Available at: http://www.matche.com/equipcost/Default.html

Matzen, M., and Demirel, Y. (2016). Methanol and dimethyl ether from renewable hydrogen and carbon dioxide: alternative fuels production and life-cycle assessment. *J. Clean. Prod.* 139, 1068–1077. doi:10.1016/j.jclepro.2016.08.163

Müller, M., and Hübsch, U. (2000). "Dimethyl ether," in *Ullmann's encyclopedia of industrial chemistry*. Weinheim (Germany): Wiley-VCH Verlag GmbH & Co. KGaA. doi:10.1002/14356007.a08_541

Nel Hydrogen (2020). Available at: https://nelhydrogen.com/water-electrolysers-hydrogen-generators/

NREL (2006). *Equipment design and cost estimation for small modular biomass systems, synthesis gas cleanup, and oxygen separation equipment; task 2: gas cleanup design and cost estimates—black liquor gasification*. Golden, CO: National Renewable Energy Laboratory. doi:10.2172/882504

Olah, G. A., Goeppert, A., and Prakash, G. K. S. (2009). Chemical recycling of carbon dioxide to methanol and dimethyl ether: from greenhouse gas to renewable, environmentally carbon neutral fuels and synthetic hydrocarbons. *J. Org. Chem.* 74 (2), 487–498. doi:10.1021/jo801260f

Ordomsky, V. V., Dros, A.-B., Schwiedernoch, R., and Khodakov, A. Y. (2017). "Challenges and role of catalysis in CO_2 conversion to chemicals and fuels," in *Nanotechnology in catalysis*. Weinheim (Germany): Wiley-VCH Verlag GmbH & Co. KGaA. 803–850. doi:10.1002/9783527699827.ch30

Rego de Vasconcelos, B., and Lavoie, J.-M. (2019). Recent advances in power-to-X technology for the production of fuels and chemicals. *Front. Chem.* 7. doi:10.3389/fchem.2019.00392

Reutemann, W., and Kieczka, H. (2000). "Formic acid," in *Ullmann's encyclopedia of industrial chemistry*. Weinheim (Germany): Wiley-VCH Verlag GmbH & Co. KGaA. doi:10.1002/14356007.a12_013

Sánchez, O. G., Birdja, Y. Y., Bulut, M., Vaes, J., Breugelmans, T., and Pant, D. (2019). Recent advances in industrial CO2 electroreduction. *Curr. Opin. Green Sustain. Chem.* 16, 47–56. doi:10.1016/j.cogsc.2019.01.005

Schmidt, O., Gambhir, A., Staffell, I., Hawkes, A., Nelson, J., and Few, S. (2017). Future cost and performance of water electrolysis: an expert elicitation study. *Int. J. Hydrogen Energy.* 42 (52), 30470–30492. doi:10.1016/j.ijhydene.2017.10.045

Schoots, K., and Hammingh, P. (2019). *Climate and energy outlook 2019. (Netherlands).*

Semelsberger, T. A., Borup, R. L., and Greene, H. L. (2006). Dimethyl ether (DME) as an alternative fuel. *J. Power Sources.* 156 (2), 497–511. doi:10.1016/j.jpowsour.2005.05.082

Shiva Kumar, S., and Himabindu, V. (2019). Hydrogen production by PEM water electrolysis - a review. *Mater. Sci. Energy Technol.* 2 (3), 442–454. doi:10.1016/j.mset.2019.03.002

Smolinka, T. (2015). *Cost break down and analysis of PEM electrolysis systems for different industrial and power to gas applications.*

SPIRE (2020). SPIRE 2050 vision towards the next generation of European process industries. Available at: https://www.spire2030.eu/sites/default/files/users/user85/Vision_Document_V5_Pages_Online_0.pdf

Turton, R., Bailie, R. C., Whiting, W. B., and Shaeiwitz, J. A. (2003). *Analysis, synthesis, and design of chemical processes*. 7th Edition. Upper Saddle River: Prentice Hall

Ullah, H., Loh, A., Trudgeon, D. P., and Li, X. (2020). Density functional theory study of NiFeCo trinary oxy-hydroxides for an efficient and stable oxygen evolution reaction catalyst. *ACS Omega.* 2020, 0c02679. doi:10.1021/acsomega.0c02679

UNFPA (2020). Transforming our world: the 2030 Agenda for sustainable development. Available at: https://sustainabledevelopment.un.org/post2015/transformingourworld

van Kampen, J., Boon, J., van Berkel, F., Vente, J., and van Sint Annaland, M. (2019). Steam separation enhanced reactions: review and outlook. *Chem. Eng. J.* 374, 1286–1303. doi:10.1016/j.cej.2019.06.031

van Kampen, J., Boon, J., Vente, J., and van Sint Annaland, M. (2020a). Sorption enhanced dimethyl ether synthesis for high efficiency carbon conversion: modelling and cycle design. *J. CO2 Util.* 37, 295–308. doi:10.1016/j.jcou.2019.12.021

van Kampen, J., Boon, J., Vente, J., and van Sint Annaland, M. (2020b). Sorption enhanced dimethyl ether synthesis under industrially relevant conditions: experimental validation of pressure swing regeneration. *Energy Environ. Sci.*

van Kampen, J., Booneveld, S., Boon, J., Vente, J., and van Sint Annaland, M. (2020c). Experimental validation of pressure swing regeneration for faster cycling in sorption enhanced dimethyl ether synthesis. *Chem. Commun.* doi:10.1039/d0cc06093c

Vincent, I., and Bessarabov, D. Low cost hydrogen production by anion exchange membrane electrolysis: a review. *Renew. Sustain. Energy Rev.* (2018). 81, 1690–1704. doi:10.1016/j.rser.2017.05.258

Conflict of Interest: The authors declare that the research was conducted in the absence of any commercial or financial relationships that could be construed as a potential conflict of interest.

frontiers in Chemical Engineering

ORIGINAL RESEARCH
published: 11 January 2021
doi: 10.3389/fceng.2020.596417

Techno-Economic Analyses of the $CaO/CaCO_3$ Post-Combustion CO_2 Capture From NGCC Power Plants

Chao Fu, Simon Roussanaly, Kristin Jordal and Rahul Anantharaman*

SINTEF Energy Research, Trondheim, Norway

Calcium looping is a post-combustion technology that enables CO_2 capture from the flue gases of industrial processes. While considerable studies have been performed at various levels from fundamental reaction kinetics to the overall plant efficiency, research work on techno-economic analyses of the calcium looping processes is quite limited, particularly for the Natural Gas Combined Cycle (NGCC). Earlier work has shown that theoretically, a high thermal efficiency can be obtained when integrating calcium looping in the NGCC using advanced process configurations and a synthetic CaO sorbent. This paper presents an investigation of calcium looping capture for the NGCC through a techno-economic study. One simple and one advanced calcium looping processes for CO_2 capture from NGCC are evaluated. Detailed sizing of non-conventional equipment such as the carbonator/calciner and the solid-solid heat exchanger are performed for cost analyses. The study shows that the CO_2 avoided cost is 86–95 €/tCO_2, avoided, which is considerably more expensive than the reference amine (MEA) capture system (49 €/tCO_2, avoided). The calcium looping processes considered have thus been found not to be competitive with the reference MEA process for CO_2 capture from NGCC with the inputs assumed in this work. Significant improvements would be required, for example, in terms of equipment capital cost, plant efficiency and sorbent annual cost in order to be make the calcium looping technology more attractive for capturing CO_2 from NGCC plants.

Keywords: calcium looping, CO_2 capture, sizing, techno-economic analysis, natural gas combined cycles

OPEN ACCESS

Edited by:
Gyorgy Szekely,
King Abdullah University of Science and Technology, Saudi Arabia

Reviewed by:
Mani Sarathy,
KAUST, Clean Combustion Research Center, Thuwal, Saudi Arabia
Edward Anthony,
University of Ottawa, Canada

****Correspondence:***
Chao Fu
chao.fu@sintef.no

Specialty section:
This article was submitted to Separation Processes, a section of the journal Frontiers in Chemical Engineering

Received: *19 August 2020*
Accepted: *01 December 2020*
Published: *11 January 2021*

Citation:
Fu C, Roussanaly S, Jordal K and Anantharaman R (2021) Techno-Economic Analyses of the $CaO/CaCO_3$ Post-Combustion CO_2 Capture From NGCC Power Plants. Front. Chem. Eng. 2:596417. doi: 10.3389/fceng.2020.596417

INTRODUCTION

Carbon Capture and Storage (CCS) is an economically competitive technology for CO_2 mitigations in the 450 Scenario (IEA, 2015). The power sector is expected to be responsible for around 60% of the cumulative investment in CCS to 2040. Among various CO_2 capture technologies, post-combustion capture using amine-based solvents is the most mature technology and is currently being demonstrated at large scale at different sites according to the Global CCS Institute (2016). However, other post-combustion technologies such as membranes, low-temperature, adsorption and absorption using more advanced solvents (Figueroa et al., 2008), have also been being investigated to further reduce the cost of CO_2 capture to an acceptable level. $CaO/CaCO_3$ looping or calcium looping (CaL) has been regarded as a promising alternative that is expected to achieve lower capture cost (Hanak et al., 2015) and avoid the emissions of potentially toxic chemical residues (Berstad et al., 2012). Increasing studies have been performed on CaL at different levels including experiments on reaction kinetics and sorbent performance enhancement (Grasa et al., 2008; Fang et al., 2009; Rodríguez et al., 2010; Martínez et al., 2012), reactors (carbonator/

calciner) modeling (Alonso et al., 2009; Romano, 2012; Ylätalo et al., 2012; Martínez et al., 2013), pilot facilities test (Arias et al., 2013; Kremer et al., 2013; Dieter et al., 2014) and process simulation and system energy performance evaluation (Yang et al., 2010; Martínez et al., 2011; Berstad et al., 2012; Berstad et al., 2014; Ylätalo et al., 2014). More details can be referred to the comprehensive reviews (Hanak et al., 2015; Martínez et al., 2016; Perejón et al., 2016).

Due to large CO_2 emissions from coal-fired power plants, most of CaL studies have focused on coal based power generation. Only a few studies (Berstad et al., 2012; Berstad et al., 2014; Cormos, 2015) have been performed for natural gas combined cycles (NGCC) which have lower CO_2 concentration in the exhaust (~4 vol% according to (Anantharaman et al., 2011)). The carbonation reaction is operated around 600 °C (Hanak et al., 2015). This temperature is close to the exhaust flue gas temperature of gas turbines. From a thermodynamic point of view, the CaL system therewith appears to have a possibility for efficient integration into the NGCC. Simulation studies (Berstad et al., 2012) on the entire NGCC with CO_2 capture found that a basic CaL process using natural limestone sorbent resulted in a larger energy penalty than CO_2 capture with amine solvents such as MEA (monoethanolamine). However, a subsequent study (Berstad et al., 2014) concluded that there is a large efficiency improvement potential for the CaL process. For example, the energy penalty can be considerably reduced when hot flue gas recycling and a solid-solid heat exchange are used, and also when operating parameters (calcination temperature, make-up ratio, solids circulation rate, etc.) are improved. As a result, compared to the MEA CO_2 capture process, the thermal efficiency penalty (lower heating value-LHV basis) is reduced by 0.5–3.6% points (depending on the sorbents used).

As calcium looping is at a low level of maturity, a rather limited number of techno-economic studies has been performed and most of them have been focused on coal-fired power plants. Ylätalo et al. (2014) presented a conceptual design of a Cal system for a 250 MW_{th} coal fired power plant. The sizing of reactors was based on flue gas flow rates, particle size and other proper assumptions. On the basis of the Kunii-Levenspiel models for circulating fluidized beds (Kunii and Levenspiel, 2000), Romano (2012) proposed a carbonator model that can be used for preliminary sizing calculation of carbonators. This model includes the carbonation reaction kinetics and solid vertical distributions in the reactor. Only limited techno-economic studies on CaL-based CO_2 capture from NGCC plants have been published. Cormos (2015) presented a comparative study on the entire NGCC power plant with CO_2 capture using CaL adsorption and MDEA (methyl-diethanol-amine) absorption. Similar to the study by Berstad et al. (2012) the CaL process was found to have a larger energy penalty (3.4% points in overall thermal efficiency) than the MDEA process. However, due to lower capital cost, this study evaluated the CO_2 avoided cost of the CaL process to be 34 €/t (only half of the cost for the MDEA process). Eran et al. (2016) evaluated techno-economic performance for NGCC with CaL CO_2 capture. It is concluded that the energy penalty related to CO_2 capture can be considerably reduced when one additional heat recovery steam generator is introduced before the capture plant. The CO_2 avoided cost was reported to be 29.3 €/t. Meanwhile, Hu and Ahn (2017) estimated CO_2 avoided cost of a CaL process from NGCC at 72 and 68 €/t for respectively a case without and with exhaust gas recirculation. In these studies, limited information on the cost methodology was presented and the costing of the major equipment cost such as carbonator and calciner was not included in detail. Michalski et al. (2019) evaluated the techno-economic performance of coal-fired power plants with CaL CO_2 capture using a bottom-up approach. The costing data of the CaL system is based on empirical correlations. De Lena et al. (2019) presented a techno-economic study for a cement production process with CaL CO_2 capture. Again, empirical correlations for the costing of CaL systems have been assumed and used in the cost analysis. These empirical correlations have been used in another techno-economic study of coal-fired power plants where the CaL system has been proposed to capture CO_2 and SO_2 simultaneously (Coppola and Scala, 2020).

Against this background, the purpose of the present paper is to investigate the sizes and costs of a NGCC with integrated Ca-looping capture, and evaluate if this technology can compete with the reference CO_2 capture with MEA from a cost point of view. Investigations are done for two cases previously assessed: case 1A in reference (Berstad et al., 2012), which has an net electric efficiency of 45.6%, and case 3A in reference (Berstad et al., 2014), which has a net electric efficiency of 52.3%. Case 1A is selected for this study since it is the simplest of all cases, i.e. could have a potential for low investment cost. Case 3A is selected for the opposite reason: its complex process configuration is likely to yield a high investment cost, but this could potentially be offset by the significantly higher process efficiency. In comparison, the reference NGCC with MEA capture has a net electric efficiency of 49.5% (case 0B in both papers (Berstad et al., 2012; Berstad et al., 2014)). Detailed equipment sizing calculations are performed and used as the basis of the cost estimation for both the CaL cases and the reference MEA plant. Finally, sensitivity analyses are performed to understand the uncertainties of the results and the impact of material performances is also discussed.

PROCESS DESCRIPTION

Conceptual designs of NGCC plants with CaL capture and detailed process parameters were presented in previous studies (Berstad et al., 2014; Berstad et al., 2012). The designs are used as the basis of this sizing and cost study. The process flow diagram of overall NGCC with CaL CO_2 capture system is presented in **Figure 1**. The exhaust flue gas from the gas turbines enters the CaL unit where CO_2 is captured. The lean CO_2 flue gas from the top of the carbonator is vented into the atmosphere after heat recovery by the primary heat recovery steam generator (HRSG) system. The secondary HRSG system is used to recover the carbonation heat as well as the heat of the CO_2 captured. The primary consideration of installing the secondary HRSG is to have a higher level of flexibility, particularly for the case when the CO_2 capture unit is shut down (Berstad et al., 2012). The CO_2 is

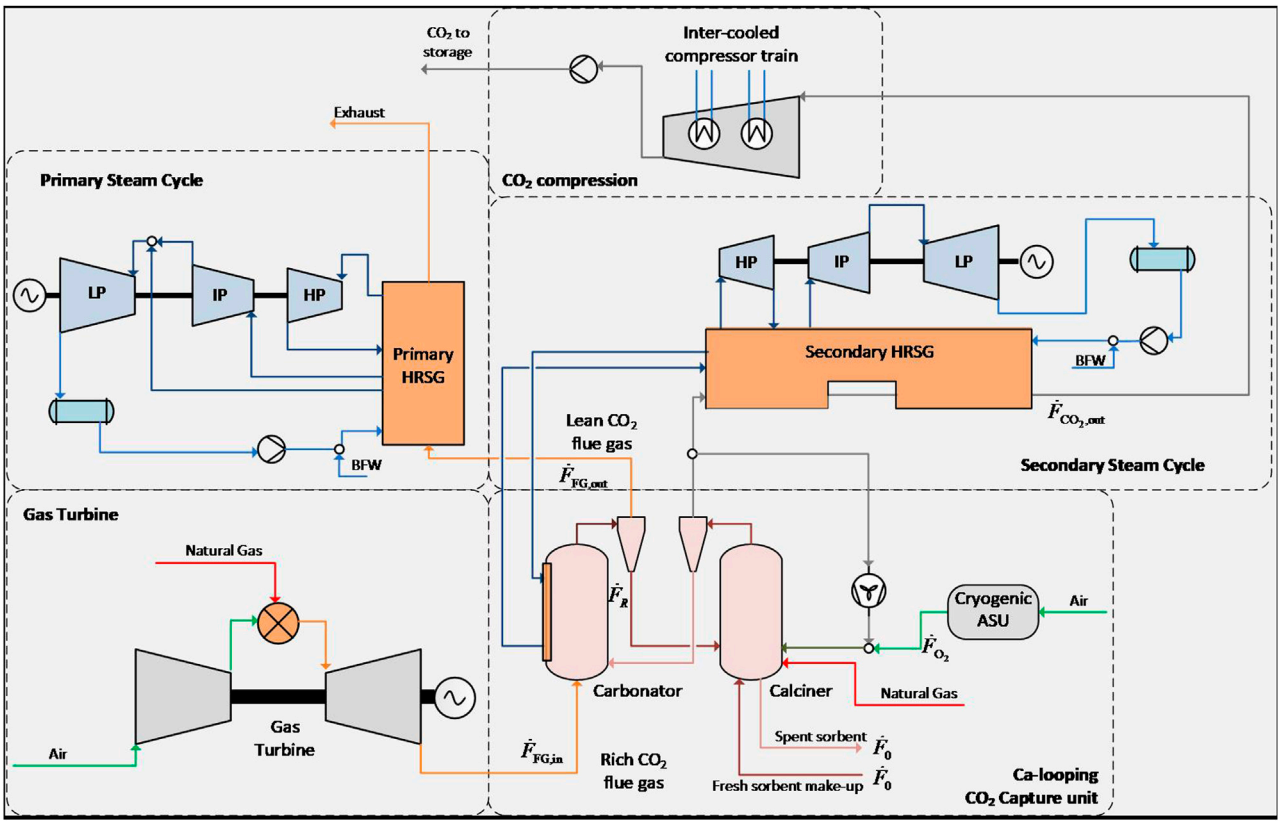

FIGURE 1 | Process flow diagram of the overall NGCC plant with hot CO_2 recycle for CaL capture (revised from Berstad et al. (2014)).

ready for transportation after being compressed by a 4-stage compression process and then pumped to transport pressure (150 bar).

A more detailed description of the CaL CO_2 capture unit is presented as following. The rich CO_2 flue gas enters the carbonator where carbonation reactions take place. CO_2 and CaO are converted into $CaCO_3$. The CO_2 lean flue gas passes through the carbonator cyclone where the carbonated particles are removed from the flue gas. The particles are sent to the calciner for regeneration (calcination). $CaCO_3$ is decomposed into CO_2 and CaO. The regenerated particles are removed from the CO_2 stream by the calciner cyclone and sent back to the carbonator. The CO_2 is sent for conditioning (compression and purification) after heat recovery. Heat is consumed in the calciner for calcination reactions and the heating of the feed streams (carbonated particles, fuels and the oxidant gases). In order to avoid dilute the CO_2 stream, oxy-combustion of natural gas is used for heat supply to the calciner. A cryogenic air separation unit (ASU) is used for the O_2 supply. A portion of the CO_2 captured is recycled to the burner for temperature control. Note that the CO_2 can be recycled either before or after partial heat recovery by the second HRSG. The former case (hot CO_2 recycle) reduces the fuel supply to the calciner. However, it should be noted that the hot CO_2 recycle is a considerable challenge in practice. Due to the degradation of sorbent particles, some solids are purged and substituted with fresh $CaCO_3$ as make-up. A solid-solid heat exchanger has been used between the carbonated particles and regenerated particles for heat recovery in case 3A while not used in case 1A.

The key operating parameters and plant performance for the four cases are shown in **Table 1**. There are several differences between Cases 1A and 3A: 1) the sorbents are calcite and synthetic CaO respectively, 2) the calciner temperatures are 1,223.2 and 1,173.2 K respectively (see **Table 2**) 3) the solid-solid heat exchanger is not used in case 1A and is used in case 3A; 4) the recycled flue gas (CO_2 captured) is cooled against the secondary HRSG system in case 1A before recycling and is not cooled in case 3A. Due to the secondary steam cycle, the NGCC with CaL capture generates more power than the NGCC without CO_2 capture or with MEA capture, although they use the same gas turbine. The net power output is 547.0 MWe for case 1Aand 466.3 MWe for case 3A. Note that the gas turbine power is lower in the CaL capture cases (1A and 3A) since the exhaust pressure at the turbine outlet is assumed to be higher to properly account for the pressure losses in the CaL system. A pressure drop of 2 kPa was assumed in reference (Berstad et al., 2012) based on the results of a test rig of chemical looping combustion (CLC) at SINTEF Energy Research. The pressure drop calculation has not been included in details in this study. The pressure drop can be estimated using the solid inventory (unit area) multiplying by the gravity acceleration constant. According to the modeling results as shown in **Table 2**, a pressure drop of 20 kPa is assumed in this

TABLE 1 | Key parameters for the NGCC plants (Berstad et al., 2012; Berstad et al., 2014).

Cases	0A	0B	1A	3A
Description	NGCC without CO_2 capture	MEA capture	CaL capture using calcite	CaL capture using synthetic CaO
Thermal energy input (LHV) [MW]	716.3	716.3	1,228	916.1
Net power output [MW]	416.4	354.3	547.0	466.3
Net thermal efficiency [%]	58.1	49.5	44.5	50.9
Gas turbine [MW]	272.9	272.9	249.2	249.2
Primary steam cycle gross power [MW]	145.9	105.6	143.6	143.6
Primary steam cycle auxiliaries [MW]	1.7	1.7	1.6	1.6
Secondary steam cycle gross power [MW]	—	—	222.4	120.4
Secondary steam cycle auxiliaries [MW]	—	—	3.0	1.6
Exhaust gas fans [MW]	—	7.3	0.3	1.0
Auxiliaries for heat rejection [MW]	0.7	0.5	2.0	1.0
Recirculation pumps [MW]	—	2.3	—	—
CO_2 compressors [MW]	—	12.4	30.8	31.1
Cryogenic air separation unit [MW]	—	—	30.5	10.6
Turbine exhaust flow [kmol/s]	23.4	23.4	23.4	23.4
CO_2 molar fraction in flue gas	0.04	0.04	0.04	0.04
Overall CO_2 capture rate	—	90.5	92.4	92.2
CO_2 molar fraction in the CO_2 captured	—	99.9	94.8	96.6

TABLE 2 | Main design parameters for the carbonators and calciners.

Cases	1A	3A	Data source
Carbonator			
Number of units	2	2	Result
Diameter, D (m)	14.47	14.47	Result
Height, H (m)	45	45	Result
Operating temperature, T (K)	873	873	Assumption
Mean superficial velocity, u_0 (m/s)	5	5	Assumption
Residual conversion capacity, X_r	0.075	0.38	Assumption
Deactivation constant, k	0.39	0.66	Assumption
Ratio of the flowrates of fresh solid makeup and CO_2 in the flue gas, $\dot{F}_0/\dot{F}_{CO_2}$	0.126	0.05	Result
Ratio of the flowrates of circulated solids and CO_2 in the flue gas, $\dot{F}_R/\dot{F}_{CO_2}$	4.281	2.08	Result
Solid inventory, W_s (kg)	285,000	300,000	Result
Average carbonation degree, X_{ave}	0.2113	0.4361	Result
Maximum average carbonation degree, $X_{max,ave}$	0.2379	0.4659	Result
Average carbonation level, $f_{carb} = X_{ave}/X_{max,ave}$	0.8881	0.9361	Result
CO_2 Capture rate	0.8997	0.9008	Result
Calciner			
Number of units	1	1	Result
Diameter, D (m)	9.47	6.67	Result
Height, H (m)	28.42	20.01	Result
Operating temperature, T (K)	1,223	1,173	Assumption
Mean superficial velocity, u_0 (m/s)	10	10	Assumption

study. The turbine power as well as the primary gross steam cycle power are correspondingly updated. Also note that a removal efficiency of 90% is specified for the CO_2 in the exhaust flue gas of the NGCC. However, a total capture rate of higher than 90% is achieved in the CaL capture cases since the CO_2 is captured from the following three carbon sources: 1) the exhaust flue gas of the NGCC, 2) the fresh sorbent make-up, and 3) the oxy-combustion of fuels (natural gas) for heat supply to the calciner. Since the impurities in the CO_2 captured are mainly introduced due to the oxy-combustion of fuels, the CO_2 mole fraction in the CO_2 captured are different in the two CaL capture cases due to different consumptions of fuels.

SIZING STUDY

While most equipment of the CaL process can be sized using standard engineering approaches (cyclones, conveyor systems for solid particles, blower for the recycled flue gas and the air separation units, etc.), the sizing of the carbonator, calciner and solid-solid heat-exchanger is more challenging. Indeed, since CaL systems have never been implemented in industry, the sizing of non-standard equipment for industrial scale CaL systems is not straight forward. However, model based studies can still provide useful guidelines for preliminary sizing estimations.

Carbonator and Calciner Sizing

The carbonator model developed by Romano (2012) is here used for the sizing of carbonators in this work. This model is based on the Kunii-Levenspiel theory for circulating fluidized beds (Kunii and Levenspiel, 2000). Both reaction kinetics and solid flow distribution are considered in the model. The reactor has been divided into a bottom dense zone and an upper lean zone. The models are solved based on the carbon balance: the carbon removed from the gas phase equals to the carbon absorbed by the solid particles in the reactor. More details are referred to the work by Romano (2012) The assigned values for all the parameters are presented in Romano (2012) and are used in this study. The models are implemented with the numerical computation tool GNU Octave 4.0.0. (Eaton et al., 2015). The cross-section area and height of the carbonators can be determined using the model. Note that the carbonation reaction is exothermic and heat needs to be removed for steam generation as shown in **Figure 1**. It is assumed that 50% of the internal surface area (considering the installation) is covered by tubes for transferring the heat of carbonation reaction to the steam cycle. The number of units is specified as the minimum while the area is sufficient for heat transfer.

The sizing of the calciners is performed in a similar way. The calcination reaction is adiabatic and heat transfer area is not a concern for the calciners. The main design parameters of the carbonators and calciners in Cases 1A and 3A are presented in **Table 2**. Note that due to insufficient public sources for the design of carbonator/calciner particularly with large sizes, the two reactors (carbonator and calciner) are assumed to be circular types for the conceptual evaluation in this study. Similar assumptions have been used in other modeling studies (Romano, 2012; Ylätalo et al., 2014). The volumetric gas flow and thus the sizes of the calciner are smaller in case 3A for the following two reasons: 1) The amount of flue gas recycled is much smaller in case 3A due to the hot flue gas recycling, and 2) The operating temperature of the calciner is lower based on different assumptions.

Sizing of the Solid-Solid Heat Exchanger

According to Berstad et al. (2014), the energy penalty related to CO_2 capture can be considerably reduced by using a solid-solid heat exchanger between the carbonated solids and the calcinated solids. The inclusion of the solid-solid heat exchanger in case 3A plays a significant part in the increase in efficiency of case 3A over case 1A. However, industrial applications of solid-solid heat exchangers are not common. Very little experience is available about the design of this type of heat exchangers. Vorrias et al. (2013) presented a configuration of concentric L-valves for the solid-solid heat exchange in the CaL process. The configuration is somewhat similar to the traditional shell-tube heat exchangers. Although the feasibilities of implementing this type of heat exchangers need further investigations, the L-valve exchanger is used for a conceptual design in this work for simplification. Calcination reaction may take place for some carbonated particles, however, the reaction is expected to have negligible influences on the overall energy balance. The calcination reaction is thus neglected in the heat exchanger. The minimum temperature difference for heat transfer is assumed to be 50 °C. The heat transfer coefficient on one side of the heat exchanger is assumed to be 400 $W/(m^2 \cdot K)$ according to a similar study on the heat transfer performance of solids in tubes (Flamant et al., 2013). The heat conduction between the particles on the same side of the heat exchanger is assumed to be fast due to good mixing of the solid particles with very small sizes. As a result, the heat transfer area for the solid-solid heat exchanger is calculated to be 2,818 m^2 in case 3A.

COST ANALYSIS

In order to fully assess the potential of CaL, the costs of both CaL processes with their corresponding power plant are assessed and compared with the costs of a NGCC without capture and with MEA-based capture previously assessed by the European Benchmarking Task Force (EBTF) (Anantharaman et al., 2011).

Costing Methodology

A factored method is here used in order to assess the capital plant of the NGCC without and with CO_2 capture (Roussanaly et al., 2013). Here the direct costs of the NGCC plant with and without MEA-based capture are scaled from Anantharaman et al. (2011). The direct costs of other processes are estimated, in Euro, with Aspen Process Economic AspenTech (2010) based on the equipment design. However, due to their specificity, the direct cost of the carbonator, calciner and solid-solid heat exchanger are assessed using the cost model proposed by the CEMCAP project (Cinti et al., 2018; Gardarsdottir et al., 2019; Voldsund et al., 2019) for these equipment. The investment cost of the NGCC plant with CO_2 capture units is then calculated by multiplying the direct investment cost of equipment in the appropriate material by an indirect cost factor of 1.31 (Anantharaman et al., 2011).

The annual fixed operating costs are scaled based on the estimated labor cost and an annual maintenance and insurance cost equivalent to 4.5% of total direct costs. Meanwhile the annual variable operating costs are assessed based on the estimated utilities and material consumptions with the unit cost presented in **Table 3**. As the synthetic sorbent used in case 3A corresponds to a hypothetical material, its cost is, as a first approximation, assumed to be equal to that of conventional calcium oxide. However, the impact between sorbent performances and maximum acceptable sorbent cost will be explored in (Sorbent Performance).

The levelized cost of Electricity (LCOE) and CO_2 avoided cost (CAC) as defined in reference (Roussanaly, 2019) are assessed and used as key performance indicators (KPIs) to compare the four cases. Both KPIs are calculated assuming a real discount rate of 8%, 7,400 annual operating hours and an economic lifetime of 25 years (Anantharaman et al., 2011). In addition, investment costs consider that construction is shared over a 3-years construction period (Anantharaman et al., 2011).

Cost Results

The results for the levelized cost of electricity (LCOE) and CO_2 avoided cost (CAC) for the four cases considered are presented in

TABLE 3 | Utilities cost.

Utilities	Reference costs	Cost units
Natural gas Anantharaman et al. (2011)	6	€/GJ
Sorbent (CaO) Anantharaman et al. (2011)	40	€/t
Make-up water Cormos, 2015	0.35	€/m^3
Process water Anantharaman et al. (2011)	6	€/m^3

TABLE 4 | Breakdown of CAPEX (M€) by section for the calcium looping configuration 1A and 3A.

	1A	3A
NGCC plant	514	487
Carbonators	196	196
Calciner	12	12
Air separation unit	107	107
Auxiliary units for the calcium looping	6	20
Secondary HRSG and gas turbine	115	76
Initial sorbent batch	2	2
CO_2 compression unit	41	41
Sum	993	940

Figure 2, while further details on the direct cost breakdown of the calcium looping cases is provided in **Figure 3**. The breakdown of CAPEX for the calcium looping configurations (1A and 3A) by section are presented in **Table 4**. The LCOEs of both the 1A and 3A concepts are respectively 86 and 83 €/MWh, while their corresponding CACs are equal to 95 and 86 €/$t_{CO2,avoided}$. The calcium looping 1A and 3A processes are therefore respectively 21 and 17% more expensive than for the NGCC plant with MEA-based CO_2 capture (71 €/MWh). As a consequence, the CAC in the cases 1A and 3A is significantly higher than for the MEA based capture (respectively 94 and 74% more expensive). These numbers clearly show that the CaL cases with the investigated process configurations are not economically competitive.

To understand strong increases, it is important to look at the LCOE and CAC cost breakdowns. The CAC of the 1A process shows that the strongest contributor to the cost increase of the process is the loss in net electric efficiency of the plant (−3.9%-points compared to MEA), as well as the increased CO_2 capture investment cost due to the complex process and large equipment (carbonator, calciners, ASU, etc). However, in the case 3A the cost increase is due to different factors. Indeed, while the high plant efficiency (+2.8 pt compared to MEA) limits the contribution of fuel to the CAC, the CO_2 capture investment costs increases significantly, especially due to the large solid-solid heat exchanger. In both the 1A and 3A cases, the costs associated with sorbent make-up also play a significant role in the increase compared to the MEA-based case. Finally, it is worth noting that the CO_2 avoided costs obtained here seems to be slightly higher than the one from Hu and Ahn (2017) (72 €/t). The difference between both studies may be explained by variation in energy penalty, sorbent make-up rate, gas cost, system boundaries considered in both studies.

It is worth noting that the plant net power output and the amount of CO_2 captured varies between the three CO_2 capture cases. Indeed, in the CaL processes, more power is produced by the oxy-combustion of natural gas in the calciner that generates more CO_2 which must be captured in the process.

Finally, it should be noted that the CO_2 purity after capture varies between the different cases. For the MEA capture process, the CO_2 purity exceeds 99.9%, whereas it is 94.8% and 96.6% in cases 1A and 3A CaL processes. Although this is not included here, this may result in higher cost of transport or in additional purification steps for the CaL processes (Skaugen et al., 2016; Deng et al., 2019).

In order to understand how the LCOE and CAC for the CaL capture processes may be reduced in order to compete with MEA-based CO_2 capture, sensitivity analyses are carried out on 10 key parameters and are presented in **Figures 4**, **5** (Van Der Spek et al., 2020). The parameter range variation considered are ±50%, except for the project duration which varies between 10 and 40 years, and the plant utilization rate which varies between 65 and 90%, and the plant thermal efficiency with the CaL process which varies by ± 5 pts. Indeed, a 5% pt increase in CO_2 efficiency for case 3A is not thermodynamically possible, this would mean that the efficiency penalty for CO_2 capture and compression would be 0.8% (which is lower than the thermodynamic minimum energy penalty). But this variation is included in order to provide an impression of whether the chasing further process improvements for the complex case 3A by adding further process components is relevant to investigate.

As expected from the large gaps in LCOEs and CACs, significant efforts would be required for the CaL process to become cost-competitive with MEA-based capture. The results show that improvement of a single parameter is far from enough to reach competitiveness of the CaL processes. Strong simultaneous improvements of the CO_2 capture investment cost, the plant efficiency with CaL processes, and the annual sorbent cost would be required together in order to reach competitiveness in term of both LCOE and CAC. Furthermore, taking into account that the integration of CaL into the NGCC plant in practice would mean adding the carbonator between the gas turbine exhaust and the heat recovery steam generator, while the process integration for amine capture with the NGCC is much simpler, CaL capture from NGCC, with the investigated process configurations does not appear very attractive.

Although sensitivity on the power plant costs and project valuation (discount rate, project duration and utilization rate) for the NGCC with the two CaL processes are not compared with the NGCC plant without or with MEA-based capture, it is worth noting that they follow the same trends (Anantharaman et al., 2011).

Sorbent Performance

As shown by the sensitivity analyses, exploring more advanced sorbent is a critically parameter to reduce the cost of the CaL processes. Thus, the impact of two critical sorbent characteristics are considered: 1) the potential gain in overall plant efficiency, and 2) the annual make-up rate. The impact on these two parameters on the advanced sorbent cost, which results in the same electricity cost as in the base 1A and 3A. This advanced

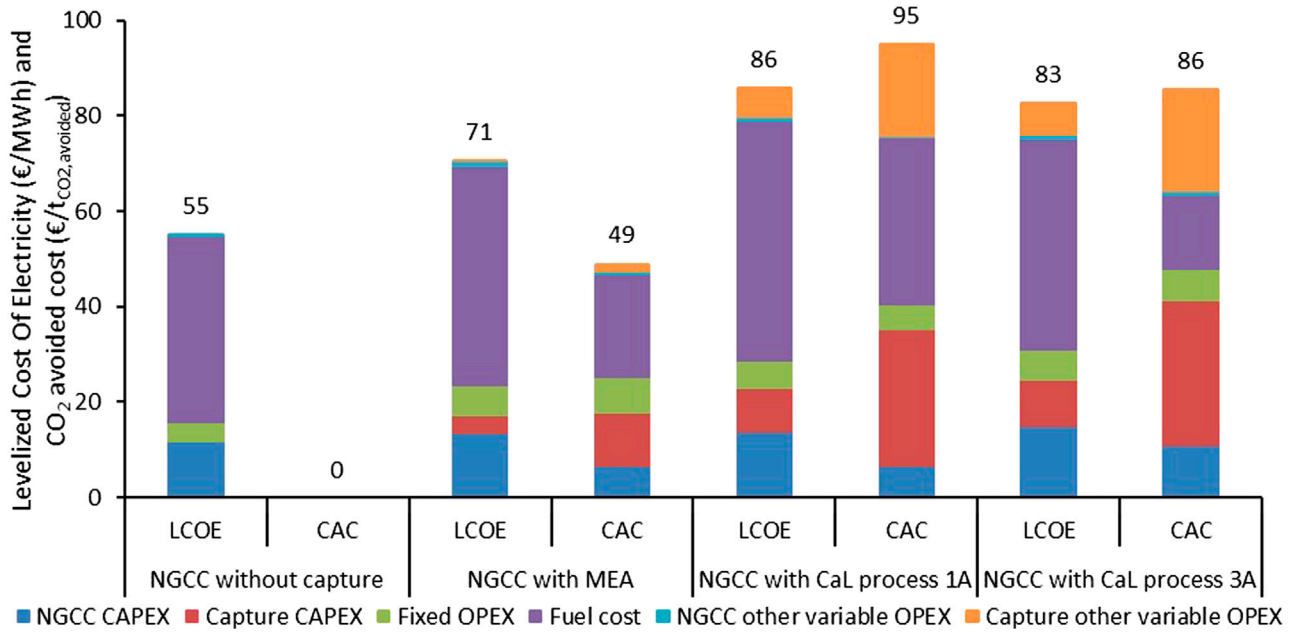

FIGURE 2 | Levelized cost of electricity and CO_2 avoided cost for the four NGCC cases considered.

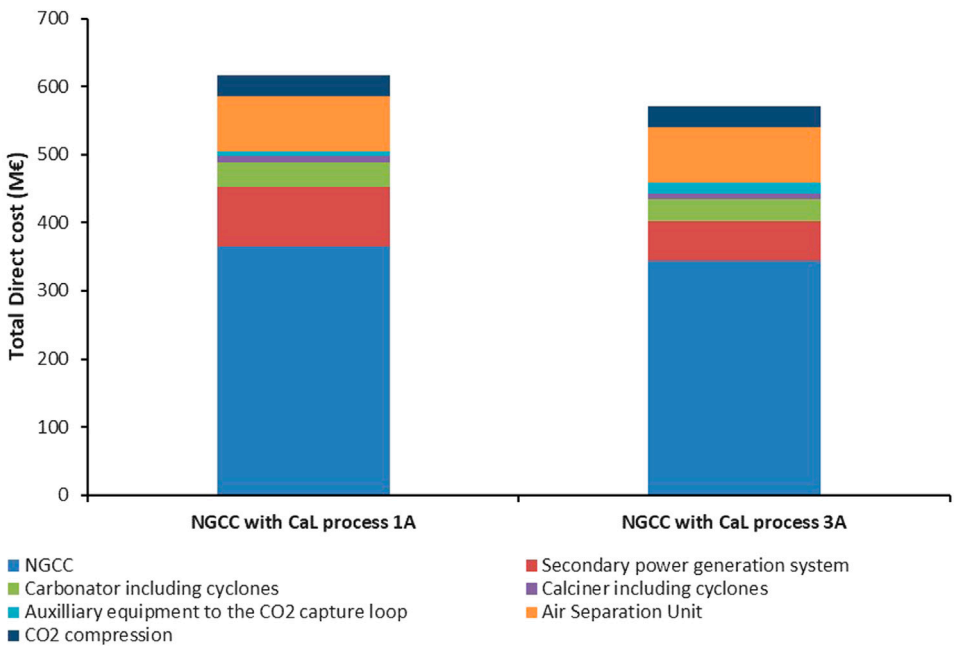

FIGURE 3 | Breakdown of the total direct costs of the NGCC with calcium looping processes 1A and 3A.

sorbent cost, plotted in **Figure 6**, represent the maximum advanced sorbent cost acceptable in order to make a CaL process cheaper than in the base cases.

The evaluation illustrates that advanced sorbent which could increase the plant efficiency and reduce sorbent make-up have a significant value. Indeed, the maximum advanced sorbent cost increases by a factor up to 200 for the ranges considered. The strongest impacts appear to be due to the reduction in the sorbent make-up rate, which emphasizes the potential of stable sorbent for the CaL

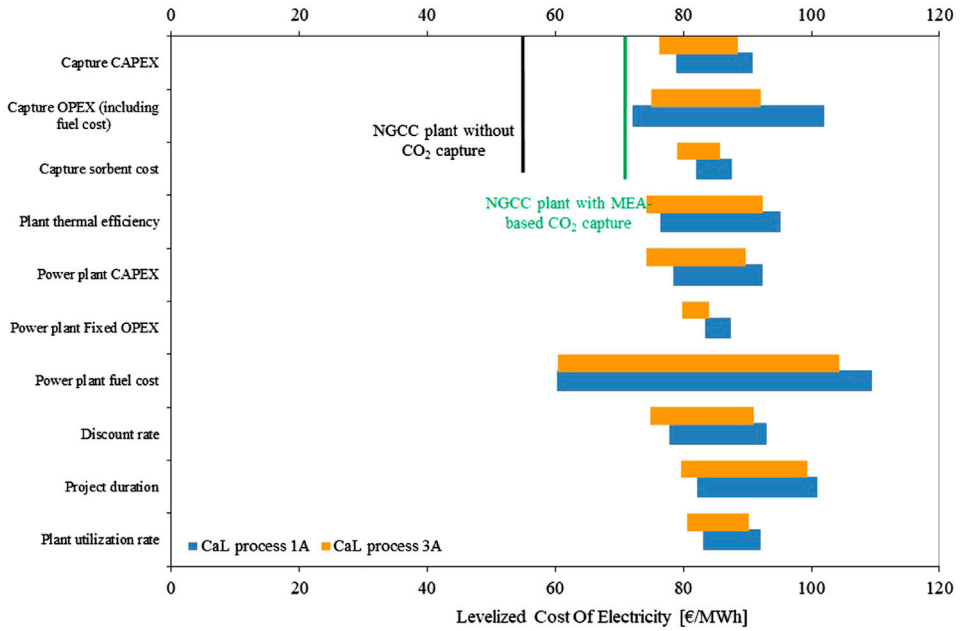

FIGURE 4 | Sensitivity analyses on the LCOEs of the NGCC with the 1A and 3A CaL processes.

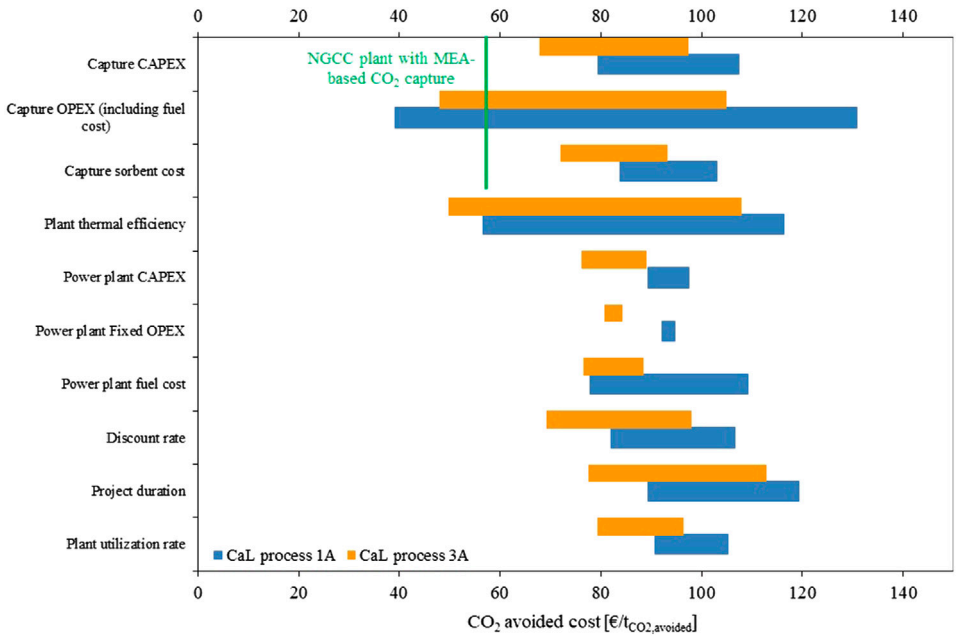

FIGURE 5 | Sensitivity analyses on the CACs of the NGCC with the 1A and 3A CaL processes.

processes, while improvements in the energy performance also play an important role. Although these evaluations assumed that the remaining part of the CaL process remains identical to the base cases, the evaluation presented in **Figure 6** could be used to perform a material screening and identify advanced sorbent which could result in improved performance for the CaL processes.

CONCLUSION

The paper has presented a techno-economic study on two CaL processes for CO_2 capture from a NGCC. The sizing of non-conventional equipment such as the carbonator, calciner and the solid-solid heat exchanger has been introduced in details. The modeling and sizing results have been used as the basis for

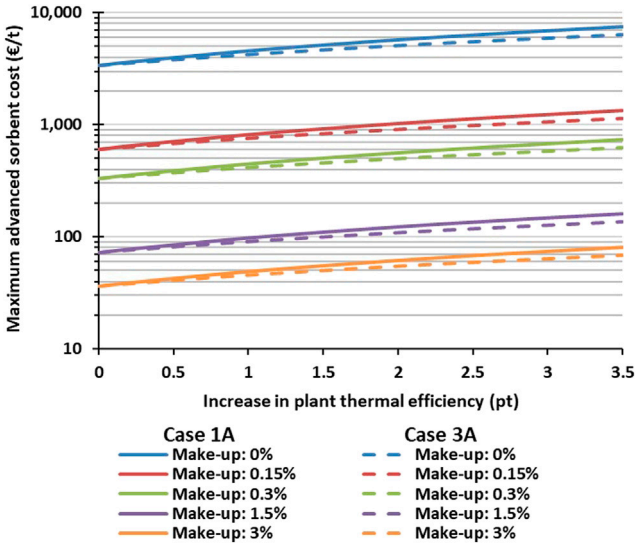

FIGURE 6 | The maximum unitary cost of a sorbent to compete with the CaL processes in this study.

cost analyses for the non-conventional equipment. A reference MEA capture process and a NGCC without CO_2 capture have been included for the comparison basis. While the cost of NGCCs is performed using a scaling approach, the direct cost of other processes are estimated with Aspen Process Economic Analyzer. The key finding from the cost analyses is that the CaL system presented in this study does not appear to be cost competitive with the MEA capture process. The CO_2 avoided cost is 95 and 86 €/$t_{CO2,avoided}$ for the two CaL cases respectively. The values are considerably higher than the cost of MEA capture, which is 49 €/$t_{CO2,avoided}$. The largest contribution to the CO_2 avoided cost is the capture CAPEX. The combination of the primary and secondary steam cycles into one could possibly reduce the NGCC CAPEX. Nevertheless, the hot gas recycling, the solid-solid heat exchanger, and the integration of the carbonator process between the gas turbine exhaust and the heat recovery steam generator remain practical challenges.

DATA AVAILABILITY STATEMENT

The original contributions presented in the study are included in the article/Supplementary Material, further inquiries can be directed to the corresponding author.

AUTHOR CONTRIBUTIONS

FC and SR wrote the first version of the manuscript. RA and KJ contributed to conceptualization, analysis and review.

FUNDING

This publication has been produced with support from the BIGCCS Center, performed under the Norwegian research program Centers for Environment-friendly Energy Research (FME). The authors acknowledge the following partners for their contributions: Gassco, Shell, Statoil, TOTAL, Engie and the Research Council of Norway (193816/S60). This publication has been produced with support from the NCCS Center, performed under the Norwegian research program Centers for Environment-friendly Energy Research (FME). The authors acknowledge the following partners for their contributions: Aker Solutions, Ansaldo Energia, CoorsTek Membrane Sciences, EMGS, Equinor, Gassco, Krohne, Larvik Shipping, Lundin, Norcem, Norwegian Oil and Gas, Quad Geometrics, Total, Vår Energi, and the Research Council of Norway (257579/E20).

ACKNOWLEDGMENTS

The authors acknowledge Karl Lindqvist at SINTEF Energy Research for his preliminary sizing work about the cyclones and calciners in the CaL system.

REFERENCES

Alonso, M., Rodríguez, N., Grasa, G., and Abanades, J. C. (2009). Modelling of a fluidized bed carbonator reactor to capture CO_2 from a combustion flue gas. *Chem. Eng. Sci.* 64, 883–891. doi:10.1016/j.ces.2008.10.044

Anantharaman, R., Bolland, O., Booth, N., Van Dorst, E., Ekstrom, C., Sanchez Fernandez, E., et al. (2011). European best practice guidelines for assessment of CO2 capture technologies. in *Public deliverable D1*. (London, United Kingdom: Alstom), 4.

Arias, B., Diego, M. E., Abanades, J. C., Lorenzo, M., Diaz, L., Martínez, D., et al. (2013). Demonstration of steady state CO_2 capture in a 1.7 MWth calcium looping pilot. *Int. J. Greenh. Gas Control.* 18, 237–245. doi:10.1016/j.ijggc.2013.07.014

AspenTech (2010). *Aspen icarus reference guide*. Burlington, MA: AspenTech.

Berstad, D., Anantharaman, R., Blom, R., Jordal, K., and Arstad, B. (2014). NGCC post-combustion CO_2 capture with Ca/carbonate looping: efficiency dependency on sorbent properties, capture unit performance and process configuration. *Int. J. Greenh. Gas Control.* 24, 43–53. doi:10.1016/j.ijggc.2014.02.015

Berstad, D., Anantharaman, R., and Jordal, K. (2012). Post-combustion CO_2 capture from a natural gas combined cycle by CaO/$CaCO_3$ looping. *Int. J. Greenh. Gas Control.* 11, 25–33. doi:10.1016/j.ijggc.2012.07.021

Cinti, G., Anantharaman, R., De Lena, E., Fu, C., Gardarsdottir, S. O., Hoppe, H., et al. (2018). CEMCAP, D4.4 Cost of critical components in CO_2 capture processes. Available at: https://www.sintef.no/globalassets/project/cemcap/2018-11-14-deliverables/d4.4-cost-of-critical-components-in-co2-capture-processes.pdf. (Accessed November 12, 2020)

Coppola, A., and Scala, F. (2020). A preliminary techno-economic analysis on the calcium looping process with simultaneous capture of CO_2 and SO_2 from a coal-based combustion power plant. *Energies* 13, 2176. doi:10.3390/en13092176

Cormos, C.-C. (2015). Assessment of chemical absorption/adsorption for post-combustion CO_2 capture from Natural Gas Combined Cycle (NGCC) power plants. *Appl. Therm. Eng.* 82, 120–128. doi:10.1016/j.applthermaleng.2015.02.054

De Lena, E., Spinelli, M., Gatti, M., Scaccabarozzi, R., Campanari, S., Consonni, S., et al. (2019). Techno-economic analysis of calcium looping processes for low CO_2 emission cement plants. *Int. J. Greenh. Gas Control.* 82, 244–260. doi:10.1016/j.ijggc.2019.01.005

Deng, H., Roussanaly, S., and Skaugen, G. (2019). Techno-economic analyses of CO_2 liquefaction: impact of product pressure and impurities. *Int. J. Refrig.* 103, 301–315. doi:10.1016/j.ijrefrig.2019.04.011

Dieter, H., Bidwe, A. R., Varela-Duelli, G., Charitos, A., Hawthorne, C., and Scheffknecht, G. (2014). Development of the calcium looping CO_2 capture technology from lab to pilot scale at IFK. *Fuel.*, 127, 23–37. doi:10.1016/j.fuel.2014.01.063

Eaton, J. W., Bateman, D., Hauberg, S., and Wehbring, R. (2015). GNU Octave version 4.0.0 manual: a high-level interactive language for numerical computations. Available at: https://www.gnu.org/software/octave/doc/interpreter/. (Accessed November 12, 2020)

Eran, M., Hanak, D., Mir, J., Anthony, E. J., and Manovic, V. (2016). Process modelling and techno-economic analysis of natural gas combined cycle integrated with calcium looping. *Therm. Sci.* 20, S59–S67. doi:10.2298/TSC1151001209E

Fang, F., Li, Z.-S., and Cai, N.-S. (2009). Experiment and modeling of CO_2 capture from flue gases at high temperature in a fluidized bed reactor with Ca-based sorbents. *Energy & Fuels* 23, 207–216. doi:10.1021/ef800474n

Figueroa, J. D., Fout, T., Plasynski, S., Mcilvried, H., and Srivastava, R. D. (2008). Advances in CO_2 capture technology-the U.S. Department of energy's carbon sequestration program. *Int. J. Greenh. Gas Control.* 2, 9–20. doi:10.1016/S1750-5836(07)00094-1

Flamant, G., Gauthier, D., Benoit, H., Sans, J.-L., Garcia, R., Boissière, B., et al. (2013). Dense suspension of solid particles as a new heat transfer fluid for concentrated solar thermal plants: on-sun proof of concept. *Chem. Eng. Sci.* 102, 567–576. doi:10.1016/j.ces.2013.08.051

Gardarsdottir, S. O., De Lena, E., Romano, M., Roussanaly, S., Voldsund, M., Pérez-Calvo, J.-F., et al. (2019). Comparison of technologies for CO_2 capture from cement production—Part 2: cost analysis. *Energies* 12, 542. doi:10.3390/en12030542

Global CCS Institute (2016). Global status of CCS: 2016 summary report, Availabale at: https://www.globalccsinstitute.com/archive/hub/publications/201158/global-status-ccs-2016-summary-report.pdf. (Accessed November 12, 2020)

Grasa, G., Abanades, J., Alonso, M., and Gonzalez, B. (2008). Reactivity of highly cycled particles of CaO in a carbonation/calcination loop. *Chem. Eng. J.* 137, 561–567. doi:10.1016/j.cej.2007.05.017

Hanak, D. P., Anthony, E. J., and Manovic, V. (2015). A review of developments in pilot-plant testing and modelling of calcium looping process for CO_2 capture from power generation systems. *Energy Environ. Sci.* 8, 2199–2249. doi:10.1039/C5EE01228G

Hu, Y., and Ahn, H. (2017). Techno-economic analysis of a natural gas combined cycle power plant integrated with a Ca-looping process for post-combustion capture. *Energy Procedia* 105, 4555–4560. doi:10.1016/j.egypro.2017.03.978

IEA (2015). *World energy outlook special report: energy and climate change*. Paris, France: IEA.

Kremer, J., Galloy, A., Ströhle, J., and Epple, B. (2013). Continuous CO_2 capture in a 1-MW th carbonate looping pilot plant. *Chem. Eng. Technol.* 36, 1518–1524. doi:10.1002/ceat.201300084

Kunii, D., and Levenspiel, O. (2000). The K-L reactor model for circulating fluidized beds. *Chem. Eng. Sci.* 55, 4563–4570. doi:10.1016/S0009-2509(00)00073-7

Martínez, I., Grasa, G., Murillo, R., Arias, B., and Abanades, J. C. (2012). Kinetics of calcination of partially carbonated particles in a Ca-looping system for CO_2 capture. *Energy & Fuels* 26, 1432–1440. doi:10.1021/ef201525k

Martínez, I., Grasa, G., Murillo, R., Arias, B., and Abanades, J. C. (2013). Modelling the continuous calcination of $CaCO_3$ in a Ca-looping system. *Chem. Eng. J.* 215-216, 174–181. doi:10.1016/j.cej.2012.09.134

Martínez, I., Grasa, G., Parkkinen, J., Tynjälä, T., Hyppänen, T., Murillo, R., et al. (2016). Review and research needs of Ca-Looping systems modelling for post-combustion CO_2 capture applications. *Int. J. Greenh. Gas Control.* 50, 271–304. doi:10.1016/j.ijggc.2016.04.002

Martínez, I., Murillo, R., Grasa, G., and Carlos Abanades, J. (2011). Integration of a Ca looping system for CO_2 capture in existing power plants. *AIChE J.* 57, 2599–2607. doi:10.1016/j.egypro.2011.02.043

Michalski, S., Hanak, D. P., and Manovic, V. (2019). Techno-economic feasibility assessment of calcium looping combustion using commercial technology appraisal tools. *J. Clean. Prod.* 219, 540–551. doi:10.1016/j.jclepro.2019.02.049

Perejón, A., Romeo, L. M., Lara, Y., Lisbona, P., Martínez, A., and Valverde, J. M. (2016). The Calcium-Looping technology for CO_2 capture: on the important roles of energy integration and sorbent behavior. *Appl. Energy* 162, 787–807. doi:10.1016/j.apenergy.2015.10.121

Rodríguez, N., Alonso, M., and Abanades, J. C. (2010). Average activity of CaO particles in a calcium looping system. *Chem. Eng. J.* 156, 388–394. doi:10.1016/j.cej.2009.10.055

Romano, M. C. (2012). Modeling the carbonator of a Ca-looping process for CO_2 capture from power plant flue gas. *Chem. Eng. Sci.* 69, 257–269. doi:10.1016/j.ces.2011.10.041

Roussanaly, S., Brunsvold, A. L., Hognes, E. S., Jakobsen, J. P., and Zhang, X. (2013). Integrated techno-economic and environmental assessment of an amine-based capture. *Energy Procedia* 37, 2453–2461. doi:10.1016/j.egypro.2013.06.126

Roussanaly, S. (2019). Calculating CO_2 avoidance costs of carbon capture and storage from industry. *Carbon Manag.* 10, 105–112. doi:10.1080/17583004.2018.1553435

Skaugen, G., Roussanaly, S., Jakobsen, J., and Brunsvold, A. (2016). Techno-economic evaluation of the effects of impurities on conditioning and transport of CO_2 by pipeline. *Int. J. Greenh. Gas Control.* 54, 627–639. doi:10.1016/j.ijggc.2016.07.025

Van Der Spek, M., Fout, T., Garcia, M., Kuncheekanna, V. N., Matuszewski, M., Mccoy, S., et al. (2020). Uncertainty analysis in the techno-economic assessment of CO_2 capture and storage technologies. Critical review and guidelines for use. *Int. J. Greenh. Gas Control.* 100, 103113. doi:10.1016/j.ijggc.2020.103113

Voldsund, M., Gardarsdottir, S. O., De Lena, E., Pérez-Calvo, J.-F., Jamali, A., Berstad, D., et al. (2019). Comparison of technologies for CO_2 capture from cement production—Part 1: technical evaluation. *Energies* 12, 559. doi:10.3390/en12030559

Vorrias, I., Atsonios, K., Nikolopoulos, A., Nikolopoulos, N., Grammelis, P., and Kakaras, E. (2013). Calcium looping for CO_2 capture from a lignite fired power plant. *Fuel* 113, 826–836. doi:10.1016/j.fuel.2012.12.087

Yang, Y., Zhai, R., Duan, L., Kavosh, M., Patchigolla, K., and Oakey, J. (2010). Integration and evaluation of a power plant with a CaO-based CO_2 capture system. *Int. J. Greenh. Gas Control.* 4, 603–612. doi:10.1016/j.ijggc.2010.01.004

Ylätalo, J., Ritvanen, J., Arias, B., Tynjälä, T., and Hyppänen, T. (2012). 1-Dimensional modelling and simulation of the calcium looping process. *Int. J. Greenh. Gas Control.* 9, 130–135. doi:10.1016/j.ijggc.2012.03.008

Ylätalo, J., Ritvanen, J., Tynjälä, T., and Hyppänen, T. (2014). Model based scale-up study of the calcium looping process. *Fuel* 115, 329–337. doi:10.1016/j.fuel.2013.07.036

Conflict of Interest: The authors declare that the research was conducted in the absence of any commercial or financial relationships that could be construed as a potential conflict of interest.

frontiers in Chemical Engineering

ORIGINAL RESEARCH
published: 29 April 2021
doi: 10.3389/fceng.2021.668867

Membrane Processes for Direct Carbon Dioxide Capture From Air: Possibilities and Limitations

Christophe Castel, Roda Bounaceur and Eric Favre*

LRGP-CNRS Université de Lorraine, Nancy, France

The direct capture of CO_2 from air (DAC) has been shown a growing interest for the mitigation of greenhouse gases but remains controversial among the engineering community. The high dilution level of CO_2 in air (0.04%) indeed increases the energy requirement and cost of the process compared to carbon capture from flue gases (with CO_2 concentrations around 15% for coal power plants). Until now, solid sorbents (functionalized silica, ion exchange resins, metal–organic frameworks, etc.) have been proposed to achieve DAC, with a few large-scale demonstration units. Gas-liquid absorption in alkaline solutions is also explored. Besides adsorption and absorption, membrane processes are another key gas separation technology but have not been investigated for DAC yet. The objective of this study is to explore the separation performances of a membrane unit for CO_2 capture from air through a generic engineering approach. The role of membrane material performances and the impact of the operating conditions of the process on energy requirement and module production capacity are investigated. Membranes are shown to require a high selectivity in order to achieve purity in no more than two stages. The specific energy requirement is globally higher than that of the adsorption and absorption processes, together with higher productivity levels. Guidelines on the possibilities and limitations of membranes for DAC are finally proposed.

Keywords: membrane, gas, carbon dioxide, engineering, air, capture

OPEN ACCESS

Edited by:
Adele Brunetti,
National Research Council (CNR), Italy

Reviewed by:
Zeinab Abbas Jawad,
Qatar University, Qatar
Giuseppe Genduso,
King Abdullah University of Science and Technology, Saudi Arabia
Adolfo Iulianelli,
Institute for Membrane Technology, Italy

****Correspondence:***
Christophe Castel
christophe.castel@univ-lorraine.fr

Specialty section:
This article was submitted to Separation Processes, a section of the journal Frontiers in Chemical Engineering

Received: *17 February 2021*
Accepted: *06 April 2021*
Published: *29 April 2021*

Citation:
Castel C, Bounaceur R and Favre E (2021) Membrane Processes for Direct Carbon Dioxide Capture From Air: Possibilities and Limitations. Front. Chem. Eng. 3:668867. doi: 10.3389/fceng.2021.668867

INTRODUCTION

Drastic reductions in CO_2 emissions are urgently needed in order to face climate change concerns (Field and Mach, 2017). Among the portfolio of strategies that can be deployed to mitigate greenhouse gases in the atmosphere, Carbon Capture and Storage (CCS) is considered a key technology (Lackner, 2003). CCS consists of first capturing CO_2 from concentrated sources (power plants, cement factories, blast furnaces, refineries) that typically emit around 1 million tons of CO_2 per year or more per site. The CO_2 is then concentrated, compressed, transported in a pipe, and injected into appropriate geological formations for long-term storage (depleted reservoirs, saline aquifers). CCS is actively investigated through numerous R&D (Research & Development) projects, with a strong emphasis on the capture step, which accounts for 60–80% of the cost of the overall CCS chain (Steeneveldt et al., 2006). More specifically, an energy-efficient capture process is of major importance, in order to minimize the impact of secondary carbon emissions; a maximum of 2 GJ per ton of recovered CO_2 (thermal basis) is often taken as the target (Figueroa et al., 2008). A broad range of capture processes has been investigated for CCS. Absorption in a chemical solvent is usually considered the best available technology today, with several pilot units installed and tested

on real flue gases (Davidson and Metz, 2005). Adsorption and membrane processes are expected to play also an important role as second-generation technologies (Favre, 2007; Merkel et al., 2010). A different strategy, namely CCU (Carbon Capture and Use), is also being intensively investigated more recently in the place of carbon storage; it consists of using CO_2 as a feedstock for chemicals or fuel production (such as methanol, methane, dimethylether, and polycarbonates). The challenge of CCU strongly differs from that of CCS because a cost-effective hybrid separation/reaction process (a classical chemical engineering problem) has to be designed (Senftle and Carter, 2017). The carbon footprint of CCU is also an issue.

Besides carbon capture from flue gases, direct air capture (DAC) has been proposed more recently (Keith, 2009). The topic remains controversial among the scientific community, mostly because of the higher thermodynamic barrier due to the lower concentration of CO_2 in air. There is in fact a factor of 300 between CO_2 concentration in flue gases (typically 15% for coal power plants) and air (400 ppm). This necessarily generates a larger specific energy requirement that depends on the type of capture technology but is not clearly quantitatively established yet (House et al., 2011). Moreover, the energy and materials costs of moving large quantities of air through an absorbing structure are also expected to result in large capture costs. Nevertheless, DAC is being increasingly investigated in the scientific community and some companies have started demonstration units for different applications (greenhouses, carbonated beverages, etc.) (Lackner, 2016; Keith et al., 2018). CO_2 recovered from DAC can be used either for direct use or for chemical or biochemical transformation. **Figure 1** summarizes the overall framework of CCS, CCS, and DAC.

Similar to CCS, DAC requires an efficient, energy-intensive process in order to be practically applied (rectangle in dotted line on **Figure 1**). The capture performances are, however, very different from CCS because no clear and fixed purity and recovery targets are defined (Senftle and Carter, 2017). Adsorption processes based on different solid sorbents are considered the best technology today (Sanz-Pérez et al., 2016). A large number of solid sorbents, including polymer-impregnated resins (Chen et al., 2013), ion exchange resins (Wright et al., 2010), amine-functionalized cellulose (Gebald et al., 2014), MOFs (Verdegaal et al., 2016), and activated carbons (Hauchhum and Mahanta, 2014), among others, have been proposed. Because of the key impact of energy requirement, several sorbent regeneration strategies are explored in terms of process and operating conditions. Besides the classical Pressure Swing Adsorption (PSA) option, temperature, vacuum, moisture swing, electro, and, for some very specific adsorbents, photo-switch regeneration have been proposed (Wurzbacher et al., 2012; Lyndon et al., 2013; Wang et al., 2013; Wilcox, 2020). Specific energy requirements for DAC cover a broad range, from 1.3 up to 8 GJ per ton of recovered CO_2 (Keith et al., 2018).

Besides adsorption processes, gas absorption into reactive liquids has been proposed for a long time (Tepe and Dodge, 1943; Greenwood and Pearce, 1953), especially for pre-purification through air separation. Different solvents (alkali, ionic liquids) are currently investigated as a potential DAC technology (Baciocchi et al., 2006; Keith et al., 2018). The high energy requirement of the process, ranging from 2.1 to 10.7 GJ per ton of CO_2, remains an issue (Kiani et al., 2020).

Table 1 summarizes the different gas separation technologies, their respective advantages and drawbacks, and the current state-of-the-art technologies for DAC.

Surprisingly, membrane processes, showing attractive performances for carbon capture from flue gases (Favre, 2007; Merkel et al., 2010), have not been investigated for DAC up to

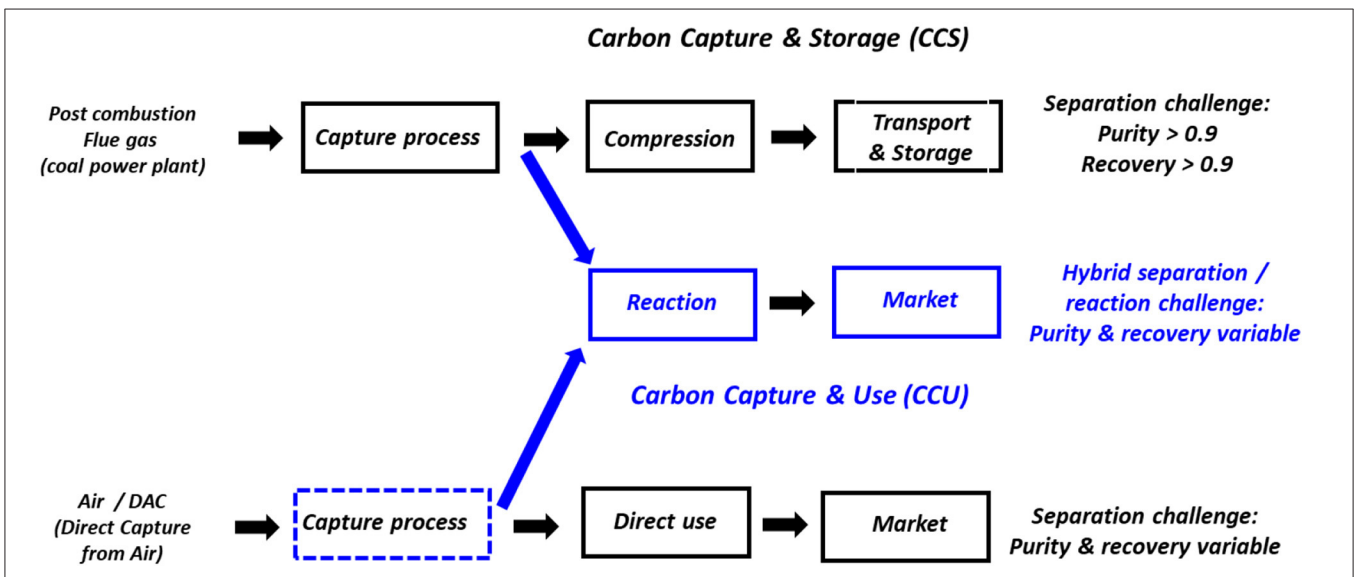

FIGURE 1 | Simplified representation of Carbon Capture and Storage (CCS), Carbon Capture and Use (CCU), and Direct Air Capture (DAC). DAC can be used either for direct use of CO_2 or chemical transformation and requires a capture process. The dotted blue rectangle shows the scope of this study.

TABLE 1 | Overview of the different gas separation processes and current state-of-the-art technologies for DAC application.

Separation process	Advantages and drawbacks	Technological options for DAC	References
Cryogeny	Mature technology Too high energy requirement for DAC	No study reported for DAC	–
Adsorption	Mature process High energy efficiency achievable High purity possible Best available technology for DAC today Cyclic process needing regeneration	Amine grafted sorbents (silica) Amine monolith MOF Ion exchange sorbent (with moisture swing regeneration)	Sanz-Pérez et al., 2016 Verdegaal et al., 2016 Wang et al., 2013
Absorption	Mature process Thermal regeneration, Low energy requirement in some cases Requires a regeneration step	KOH Amine solvents Electrolytes (with electroconversion)	Keith et al., 2018 Kiani et al., 2020
Membranes	Emerging process for gas separations Efficient membrane material and power energy requirement Not applicable to diluted feeds No economy of scale No regeneration step needed Can achieve process intensification	No study reported for DAC	–

now. Except for a proof of concept study on a Fixed Site Carrier Membrane for CO_2 capture from air (Rahaman et al., 2012) and some reports on CO_2 elimination from air for space (Hwang et al., 2008) or air separation pre-purification applications (Wu et al., 2019), no research addressed a generic analysis of the possibilities and limitations of a membrane unit for DAC. The purity, recovery, specific energy requirement, or treatment capacity of membrane processes for DAC application remain essentially unknown.

This study intends to fill that gap, through an engineering parametric study covering the impact of materials performances and operating conditions. A single-stage process has been taken for simulations for not only the sake of simplicity but also because multistage processes, including multicompression and/or vacuum operation, are usually used when increased purity and recovery are needed. The specificity of DAC, with no recovery target and the need for simple, one-step air-blowing technologies, suggests to first clearly define the purity, energy, and productivity of a single-stage membrane process. It is expected that the results detailed in this paper will help to better evaluate the best place and role of membranes for DAC purposes, be it for standalone or hybrid technologies (i.e., pre- or post-concentration of an absorption or adsorption process).

FRAMEWORK OF THE STUDY

Overall Framework

As explained in the introduction section, a large majority of research studies on carbon capture have been applied to flue gas treatment in a CCS framework. In that case, a CO_2 outlet concentration (i.e., purity) of 90% or more and a recovery of 90% or more are taken as specifications (Steeneveldt et al., 2006). Within that context, the possibilities of membrane processes have been investigated through a great number of studies, and either two-stage or hybrid membrane/cryogeny processes, with different types of design, have been proposed (Favre, 2007; Figueroa et al., 2008; Merkel et al., 2010).

The DAC context is very different in that the feed CO_2 concentration is very low (400 ppm) and no purity or recovery target is defined. Moreover, CO_2 can be either used *per se* after capturing from air (algae ponds, greenhouses, carbonated beverages, etc.) or transformed into a given chemical product or fuel (**Figure 1**). Consequently, it is not possible to fix for DAC a precise CO_2 purity, together with recovery constraints. This brings the need for very large flexibility that will be explored in this study. Membrane processes are known to show a strong parametric sensitivity and it is very useful to generate master curves where the interplay between purity, energy requirement, and productivity are linked together (Baker, 2004; Favre, 2017).

More specifically, the engineering methodology applied hereafter is sketched in **Figure 2** and it has been proposed and applied for different membrane gas separations (Castel et al., 2018). The separation performances of a membrane process (single-stage) will be systematically simulated for feed air conditions (simplified to a binary CO_2/N_2 mixture in the first step, but extended to $N_2/CO_2/O_2/H_2O$ in the second step). The outlet CO_2 purity and the associated energy requirement and overall specific fluxes will be computed for different membrane materials and operating conditions. This set of data will offer the opportunity to perform technico-economical analyses in future studies.

Membrane Materials

Industrial membrane gas separations are almost exclusively based on thin-film polymeric asymmetric or composite materials today (Baker and Low, 2014). In the first step, the separation performances of different polymeric membranes will be studied based on a so-called trade-off approach (Robeson, 2008). A series

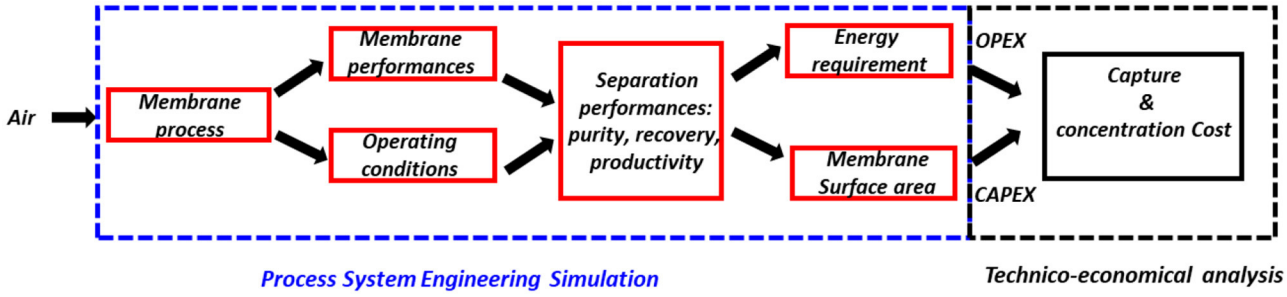

FIGURE 2 | Sketch of the overall framework of the study. The separation performances of a capture process for DAC (i.e., dotted blue rectangle, which corresponds to the capture box in **Figure 1**), based on a single-stage membrane separation unit, are explored. The impact of membrane performances and operating conditions will be systematically covered in order to evaluate the specific energy requirement and production capacity of a membrane process fed by air. These key data are needed for further technico-economical studies of DAC (black box on the right) but this task will not be performed here.

of polymeric materials and the corresponding characteristics, namely permeance and selectivity, are shown in **Table 2**. Globally speaking, it can be seen in **Figure 3** that a trade-off exists between permeance, which impacts membrane surface area, and selectivity, which impacts the CO_2 outlet purity. The different material characteristics taken for simulation purposes in this study are indicated in **Figure 3**.

In the second step, high-performance non-polymeric materials, showing performances beyond the trade-off limit of polymers, should also be investigated. Numerous materials have been reported (e.g., zeolites, carbon molecular sieves, graphenes, metal–organic frameworks, liquid membranes, fixed-site carrier membranes, etc.) to achieve that target (Skoulidas et al., 2002; Geim, 2009; Gascon and Kapteijn, 2010). An exhaustive analysis of the impact of the characteristics of these different membrane families is beyond the scope of this study. For the sake of simplicity, one of the most promising recently reported materials, showing record performances in terms of CO_2/N_2 selectivity ($\alpha = 680$) and CO_2 permeance ($P_{CO2} = 2{,}500$ GPU), will be taken (Li et al., 2013; Yuan et al., 2017). The potential interest of advanced materials for DAC, be it for purity or energy efficiency, will thus be evaluated.

Separation Performances Simulation

When the feed conditions and membrane performances are fixed, a classical process simulation study, historically developed by Weller and Steiner (1950), can be performed. The methodology has been largely reported in previous studies (Belaissaoui et al., 2014; Bounaceur et al., 2017; Favre, 2017) and will be simply summarized here.

Basically, the membrane process is supposed to be under steady-state and isothermal conditions. Flow conditions are postulated (such as perfectly mixed, cross plug flow, co- or counter-current plug flow) and the differential mass balance of the different permeants can be solved, together with a mass transfer expression. Constant permeance and no flux coupling are assumed, which is in agreement with previous studies (Pan and Habgood, 1978; Kaldis et al., 2000). The overall set of hypotheses has been already validated and it is expected to be representative of the CO_2/N_2 gas pair. The methodology can also be extended to multicomponent feed mixtures (Kaldis et al., 2000). For practical purposes, cross plug flow or counter-current flow are most often used for simulations because they are close to the real performances of industrial modules (Favre, 2007; Merkel et al., 2010).

A very interesting feature of the above approach is that the system is completely governed by four dimensionless numbers (material selectivity α^*, pressure ratio ψ, module stage cut θ, dimensionless surface area **S**) enabling generic process solutions to be obtained (Weller and Steiner, 1950):

$$\alpha^* = \frac{P_{CO2}}{P_{N2}}$$
$$\psi = \frac{p''}{p'}$$
$$\theta = \frac{Q_p}{Q_{in}}$$
$$S = \frac{A.\,\mathbf{P}_{CO2}.\,p'}{Q_{in}},$$

where **P** stands for membrane permeance, p' for upstream (retentate) pressure, p'' for downstream (permeate) pressure, Q_p for permeate flowrate, Q_{in} for feed flowrate, and A for the membrane surface area. Stage cut θ and pressure ratio ψ ranging, by definition, from 0 to 1, an exhaustive set of process solutions can be obtained through numerical resolution. The corresponding dimensionless surface area **S** can then be used to calculate the real membrane surface area A (in m^2), for a given feed flow rate, membrane permeance, and upstream pressure.

The stage-cut value will impact the CO_2 recovery ratio R through: $R = \frac{Q_p.\,y}{Q_{in}.\,x_{in}} = \frac{\theta.\,y}{x_{in}}$.

The typical engineering resolution framework is shown in **Figure 4**. The number of variables to be defined is minimal because module geometry is not required in the resolution at this stage; the permeance data, feed composition, and operating conditions (pressure ratio, stage cut) are sufficient for the outlet compositions and flowrates to be determined. In the second step, process solutions based

TABLE 2 | Examples of polymeric membrane materials with CO_2 permeance and CO_2/N_2 selectivity performances.

Membrane material	P_{CO2} (GPU)	CO_2/N_2 selectivity (α)	References	
Poly[bis(2-2(methoxyethoxy)ethoxy)]phosphazene	250	62.5	Robeson, 2008	#1
Polyactive™	1,100	52	Brinkmann et al., 2017	#2
Polaris™	2,000	30	Merkel et al., 2010	#3
PIM-1	2,300	25	Robeson, 2008	#4
Polytrimethylsilylpropyne	29,000	10.7	Robeson, 2008	#5

Polaris™ and Polyactive™ membranes are commercially available with selectivity and permeance data provided by the suppliers. For the other materials, permeance is estimated from permeability data with a 1-μm active layer thickness [in that case, 1 GPU is equivalent to 1 Barrer permeability with 1 Barrer = $10^{-10}cm^3(STP).cm.cm^{-2}.s^{-1}.cm\ Hg^{-1}$].

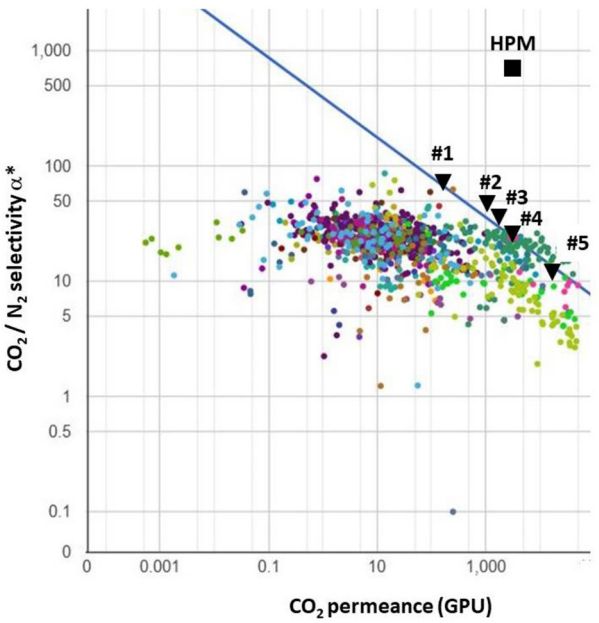

FIGURE 3 | CO_2/N_2 gas pair trade-off curve [from Robeson (2008), adapted]. Polymeric membrane materials listed in **Table 2** are indicated (#1–#5). The filled square [HPM, High-Performance Material (Li et al., 2013; Yuan et al., 2017)] corresponds to a recently reported inorganic material used for simulation purposes.

on feed compression and/or vacuum pumping can be investigated in order to obtain explicit module productivity (π), which corresponds to the specific CO_2 transmembrane flux (i.e. mol $CO_2.m^{-2}.s^{-1}$) and energy requirement (E) data, based on the following expressions (Favre, 2007; Bounaceur et al., 2017), with γ the adiabatic expansion coefficient of the gas mixture (i.e., ratio of the pressure over volume heat capacity):

$$\text{Compression}: E = \frac{\gamma.RT}{\theta.\,y.(\gamma-1)} \cdot \left(\left(\frac{p'}{p_{atm}} \right)^{\frac{\gamma-1}{\gamma}} - 1 \right)$$

$$\text{Vacuum pumping}: E = \frac{\gamma.RT}{y.(\gamma-1)} \cdot \left(\left(\frac{p_{atm}}{p''} \right)^{\frac{\gamma-1}{\gamma}} - 1 \right)$$

RESULTS

Purity/Recovery Trade-Off for CCS and DAC Membrane Process

In the first step, the impact of module conditions has been investigated, in order to select the most efficient option for simulation purposes. For carbon capture from flue gases, the cross plug flow or counter-current flow is taken, because these hydrodynamic conditions offer the best performances when purity ($y = 0.9$) and recovery ($R = 0.9$) targets are fixed. The DAC framework is very different. The target compound (CO_2) is diluted and no specific recovery is needed. Moreover, pushing recovery R will logically decrease the retentate concentration (x_{OUT}), which impacts the driving force. For a diluted feed mixture, a larger recovery will thus induce vanishing CO_2 fluxes together with a decreasing outlet purity (y). Then, it can be anticipated that a low recovery R (i.e., a low module stage cut θ) should be favored, so that the outlet concentration y is not too decreased and the specific CO_2 flux remains large enough. **Figure 5** shows a comparison between permeate purity y and recovery ratio R for different operating (pressure ratio) conditions. Carbon capture from flue gas and DAC are compared, with a baseline case corresponding to the Polaris membrane (**Table 2**).

A maximal CO_2 purity of around 1% is achievable for DAC (i.e., $y = 0.01$), providing a vanishing pressure ratio and stage cut is applied. A decreasing permeate purity value is obtained as soon as the recovery and/or pressure ratio is increased. It can be noted at this stage that, for DAC, the need to push purity and the fact that no recovery is fixed suggest the usage of a low module stage cut θ. In that case, the impact of the flow conditions is negligible. The simple, perfectly mixed case could thus be taken for simulation purposes (Favre, 2017). This peculiarity, which strongly differs from classical membrane gas separation applications, is specific to DAC and it results from the fact a maximal purity is needed and no recovery target is fixed.

Separation Performances of a Carbon Capture Polymeric Membrane

Because maximizing purity is of major importance in DAC, the upper outlet concentration that can be obtained by a single-stage module has been computed in the second step. Based on the low stage-cut assumption detailed in the previous section,

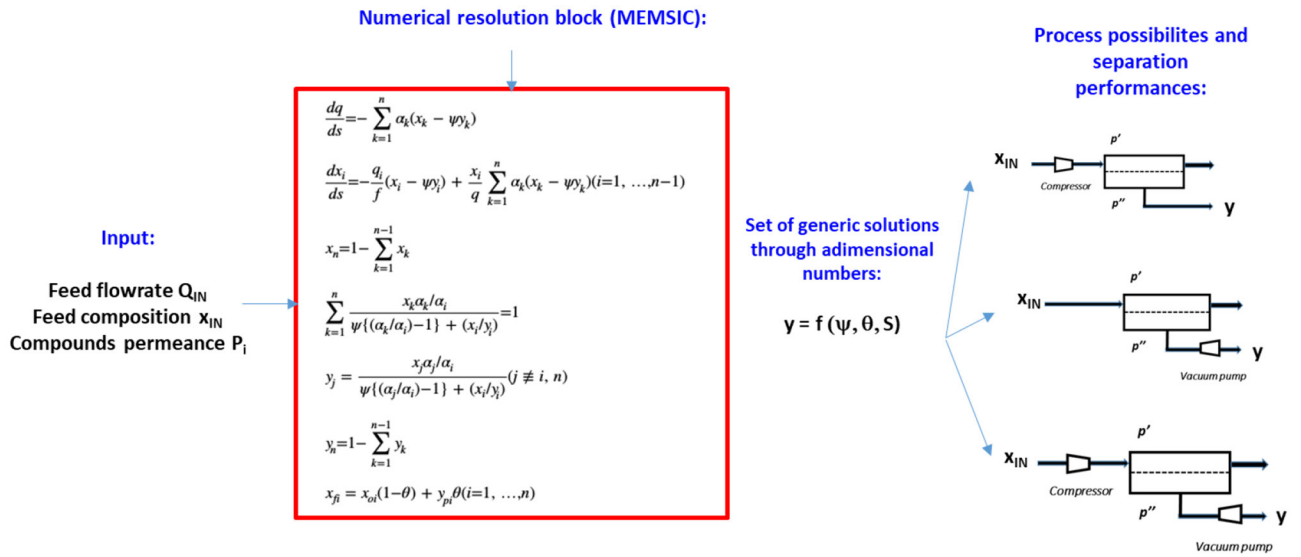

FIGURE 4 | Simplified representation of the engineering methodology which is applied in this study. Q stands for air or flue gas feed flowrate, x_{IN} for inlet mole fraction, p″ for permeate pressure, p′ for retentate pressure. ψ is the module pressure ratio, θ the module stage cut, and **S** the dimensionless surface area. For DAC, the objective is to get for each set of operating conditions the CO_2 outlet (permeate) concentration y, the CO_2 recovery ratio R, and the associated energy requirement E and membrane productivity π.

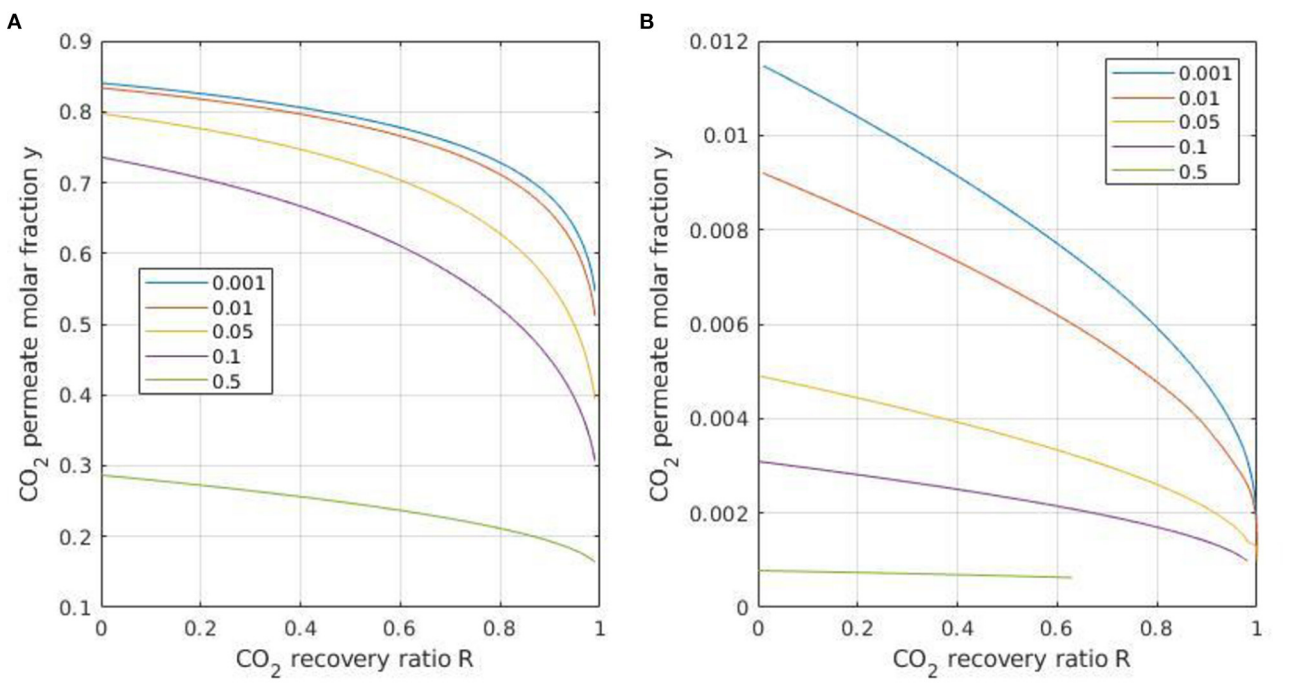

FIGURE 5 | Permeate purity y as a function of recovery ratio R for different pressure ratios (indicated in the rectangle box) for a flue gas feed mixture (x_{IN} = 0.15) **(A)** and air feed (x_{IN} = 400 ppm) **(B)**. Polaris membrane performances (#3 in **Table 2**), cross plug flow conditions.

the maximal y value can be calculated as soon as membrane performances and pressure ratio are fixed.

Figure 6A shows the results for different polymeric membranes. It can be seen that even the best polymeric membrane materials enable a CO_2 purity in the range of 2% (y = 0.02) to the best. The interest to use highly selective materials and low pressure ratio is clear. A very low pressure ratio corresponds, however, to a large energy requirement. The energy requirement

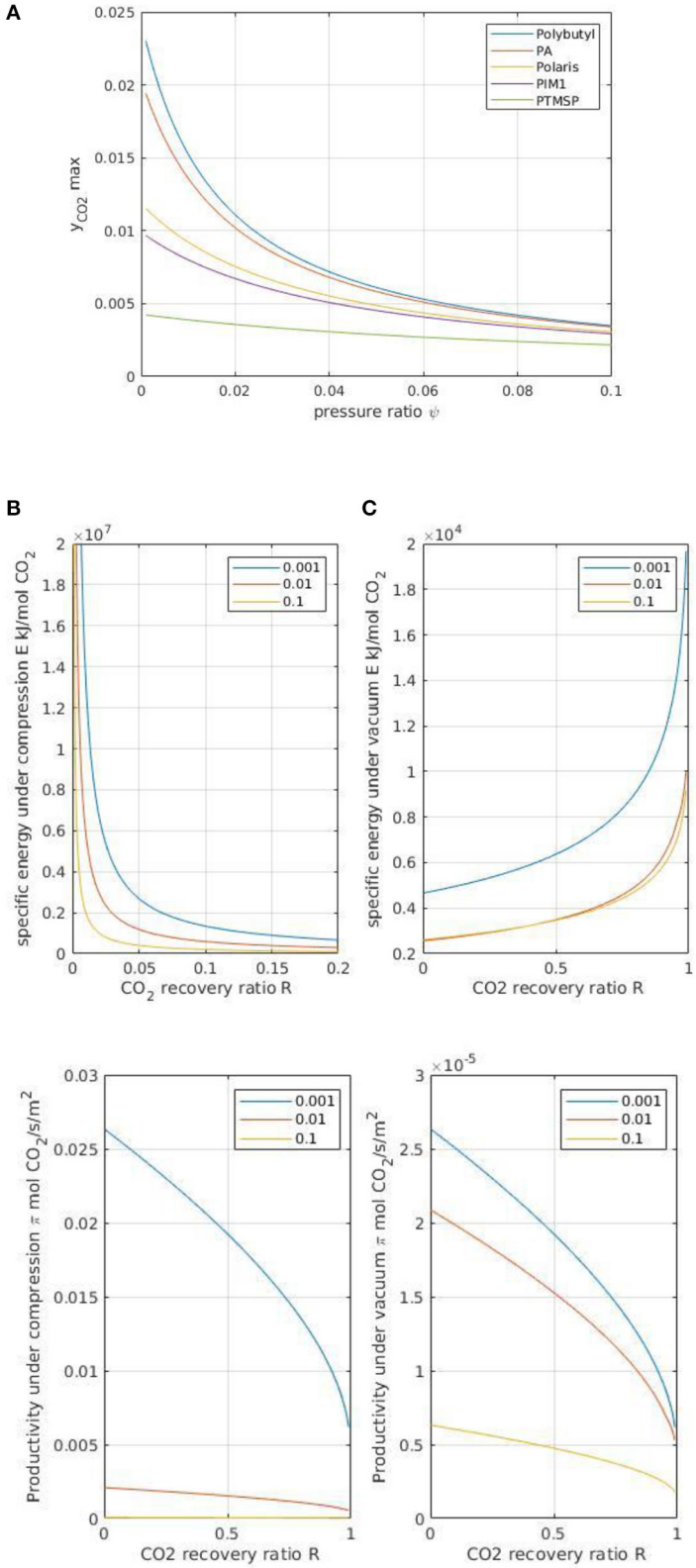

FIGURE 6 | (A) Maximal permeate purity y as a function of module pressure ratio (ψ) for different polymeric membrane materials (listed in **Table 2**). **(B)** Specific energy requirement E (expressed in kJ per mol of recovered CO_2) for a single-stage module under feed compression and vacuum pumping conditions and for different module pressure ratios (ψ). Polaris membrane, cross plug flow conditions. **(C)** Module productivity π (expressed in mol of recovered CO_2 per m^2 surface area) for a single-stage module under feed compression or vacuum pumping conditions and for different module pressure ratios (ψ). Polaris membrane, cross plug flow conditions.

and the specific membrane surface area for feed compression and vacuum pumping are also shown in **Figures 6B,C**. These sets of data summarize the interplay between the CO_2 outlet purity y, the energy requirement E (which plays a key role in OPEX), and the membrane surface area A (which plays a key role in CAPEX). A technico-economical analysis can be performed based on these, as indicated in **Figure 2**. More specifically, the increasing energy requirement with feed dilution is confirmed; compared to CCS with coal power plant flue gases, where a specific energy requirement of around 220 kWh per ton of recovered CO_2 is achievable, the minimal energy requirement for DAC with a polymeric membrane is around 18,000 kWh per ton of CO_2 when a highly selective polymeric membrane is operated under vacuum pumping conditions. Vacuum pumping should thus be favored in order to minimize E; this is however at the expense of an increased membrane surface area A (**Figure 6C**). From a practical point of view, it is important to stress that it is difficult to achieve a vacuum level below 1–10 mBar at an industrial scale with classical primary vacuum pumps. For a strict vacuum pumping strategy, this limitation has to be taken into account and it translates into a pressure ratio lower limit of around 0.01. A 0.001-pressure ratio level could possibly be achieved with high-performance leak-proof vacuum systems, but this target is challenging from a technological point of view. The specific energy requirement of vacuum pumping is indeed around three orders of magnitudes lower than compression, together with an increase of around five orders of magnitude in specific surface area. The strong impact of pressure ratio on module performances is confirmed. The best cost-effective solution can be identified as soon as membrane, compressor, vacuum pump, and electricity costs are defined. This interesting technico-economical study is beyond the scope of this paper, but it could be performed based on the data set shown in **Figure 6**.

Separation Performances of Advanced Membrane Materials (HPM)

Given the key role played by membrane selectivity, the separation performances of the most selective, non-commercially available material have been further investigated. For the sake of simplicity, a recently reported material has been taken for simulation purposes with a record CO_2/N_2 selectivity ($\alpha = 680$) and CO_2 permeance ($\mathbf{P}_{CO2} = 2{,}500$ GPU).

The results are shown in **Figure 7**, where they are compared to that from the Polaris membrane (i.e., the carbon capture membrane currently commercially available). The increase of CO_2 purity with a high selectivity membrane material (HPM) is clear (**Figure 7A**). A maximum value of around 14% (i.e., closed to the CO_2 of coal-power-plant flue gas) can be achieved for a very low module pressure ratio.

The purity–recovery trade-off is shown in **Figure 7B** for Polaris and HPM. The impact of concentration polarization, which is expected to be significant only for highly permeable and selective membranes, has also been added for the sake of comparison (Favre, 2017). The negligible impact of this phenomenon on Polaris membrane is confirmed; numerous process simulation studies previously conducted (Baker, 2004;

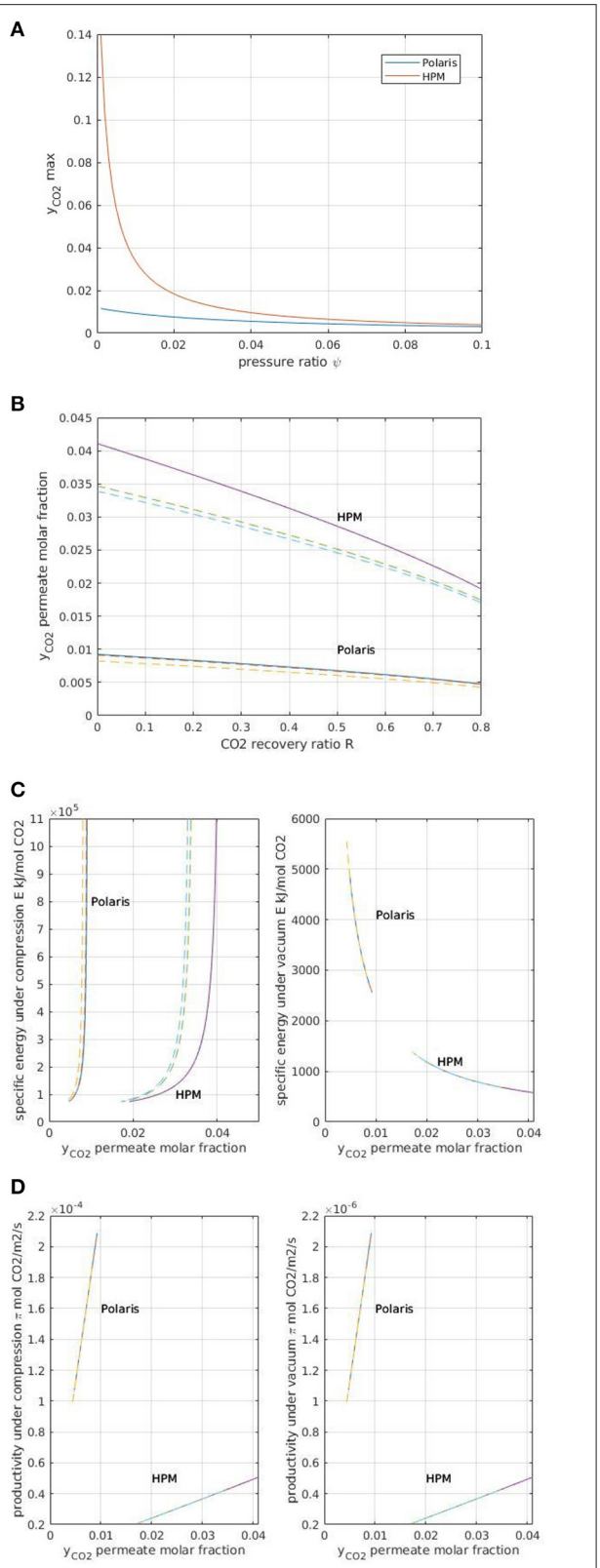

FIGURE 7 | (A) Maximal permeate purity y as a function of module pressure ratio (ψ) for an advanced membrane material HPM ($\alpha = 680$, $\mathbf{P}_{CO2} = 2{,}500$ GPU) in comparison with Polaris membrane. **(B)** Purity (y) vs. recovery

(Continued)

FIGURE 7 | (R) for DAC with Polaris and HPM membranes. Continuous lines correspond to the classical simulation framework detailed in the text section (section Overall Framework). Dotted lines correspond to a rigorous simulation taking into account concentration polarization effects on the retentate side (gas-phase mass transfer coefficient 10^{-1} m.s^{-1}, gas-phase velocity 1 m.s^{-1}). **(C)** Specific energy requirement E (expressed in kJ per mol of recovered CO_2) for a single-stage module under feed compression and vacuum pumping conditions for Polaris and HPM membranes. Module pressure ratio 0.01. Continuous lines, classical simulation framework; dotted lines, simulations taking into account concentration polarization effects on the retentate side. **(D)** Module productivity π (expressed in mol of recovered CO_2 per m^2 surface area) for a single-stage module under feed compression or vacuum pumping conditions and for Polaris and HPM membranes. Module pressure ratio 0.01. Continuous lines, classical simulation framework; dotted lines, simulations taking into account concentration polarization effects on the retentate side.

Favre, 2007, 2017) which did not take into account this effect are thus validated. For HPM however, concentration polarization, corresponding to the occurrence of a non-negligible mass transfer resistance in the gas phase (retentate side), should be taken into account. Because pushing CO_2 purity is likely to be of great interest for DAC, high selectivity and high permeance membrane materials are expected to be necessary. These results show that, in that case, the concentration polarization effect should be included in the simulation studies. Experimental and simulation studies indeed suggest a 100 selectivity/1,000 GPU permeance threshold for this phenomenon to be significant (Lüdtke et al., 1998; Mourgues and Sanchez, 2005).

The advantages of HPM in terms of specific energy requirement are shown in **Figure 7C**. For feed compression, HPM enables a higher purity to be attained compared to the Polaris membrane for a similar specific energy requirement. This result is typical of a low module stage cut, where permeate purity can be tuned mostly by changing the module pressure ratio. A specific purity/energy requirement curve is obtained, with a shift toward higher purities when a more selective membrane is used. A completely different behavior is obtained for vacuum pumping. In that case, a significantly higher purity is obtained with HPM, together with a much lower energy requirement. The interest to select a vacuum pumping strategy when energy efficiency has to be maximal is thus confirmed (Favre, 2007, 2017; Belaissaoui et al., 2014).

Figure 7D compares the specific productivity of Polaris and HPM membranes as a function of CO_2 purity. It is shown that the increased purity obtained by the HPM membrane is associated with significantly lower productivity. Increasing selectivity indeed systematically induces a larger membrane surface area requirement due to the faster decrease in the driving force as the permeating purity increases (Baker, 2004). This somehow counterintuitive relationship led to the promotion of high permeance rather than very high selectivity membranes for CCS application (Baker, 2004; Merkel et al., 2010). Interestingly, the feed compression and vacuum pumping curves (**Figure 7D**) show a similar pattern except for a factor of 100 in terms of specific productivity. This peculiar behavior results from the specific conditions of DAC: with a very low stage cut, the upstream CO_2 concentration is almost constant. So, for a given permeate concentration (i.e., CO_2 purity y), the driving force between feed compression and vacuum pumping will simply depend on the pressure ratio. The two orders of magnitude between the two figures are thus a direct consequence of the pressure ratio, namely the value of 0.01.

Influence of Oxygen, Water, and Other Air Compounds

In the last step, the impact of air compounds (other than nitrogen and carbon dioxide) has been studied. It is in fact important to know whether oxygen or water (which are present in the air feed for DAC application) are found in the enriched carbon dioxide flow rate (i.e., permeate outlet of a membrane module). Depending on the target application of the captured CO_2, it can be necessary to remove oxygen or humidity, or ensure a threshold value; this holds particularly for CCU, where catalytic conversion can be, in some cases, sensitive to oxygen or wet CO_2 feed.

In order to evaluate the composition of the CO_2 outlet stream, a series of simulations have been performed with a multicomponent feed stream corresponding to air (N_2 79%, O_2 21%, CO_2 400 ppm, dry basis), saturated in humidity at 25C. A Polyactive^{TM} membrane has been taken for simulation purposes because permeance data for these compounds have been reported (Brinkmann et al., 2017); the results are shown in **Figure 8**. Because polymeric membranes always show a very high permeability toward water and a larger oxygen permeability than nitrogen permeability, the permeate is enriched in oxygen and collects almost integrally the water feed flux. This point has to be stressed, both for CO_2 chemical transformation and for hybrid processes (humidity can impact adsorption processes for instance, and these results show that a membrane unit installed before a PSA system will generate a wet CO_2 stream). Taking into account again the hypothesis that low stage cut conditions are more appropriate for DAC, it can be concluded that a single-stage membrane CO_2 stream with a classical CO_2 selective polymeric membrane will contain around 29% oxygen, 30% water, 40% nitrogen, and up to 1% CO_2. This set of information can be of interest when membrane processes are considered for DAC applications, be it for CCU or direct use (**Figure 1**).

It is likely that non-polymeric membranes will show different behaviors. Unfortunately, the permeance of oxygen and water is most often not reported in studies on advanced carbon capture materials.

Synthesis

Based on the set of simulations detailed above, the different ranges of permeate compositions and process performances have been described. From a practical point of view, the limited CO_2 purity level which is attainable can be anticipated to be too low for several target applications. The single-stage option should then be discarded, and multistaged processes must be considered (Favre, 2017). A typical membrane cascade used to increase purity for a fast compound is shown in **Figure 9**. A large spectrum of connection possibilities and module conditions can be investigated so that the most efficient design is selected. Because a high purity is needed, a simple permeate to feed connection, with no recycling loop, is likely to be of interest

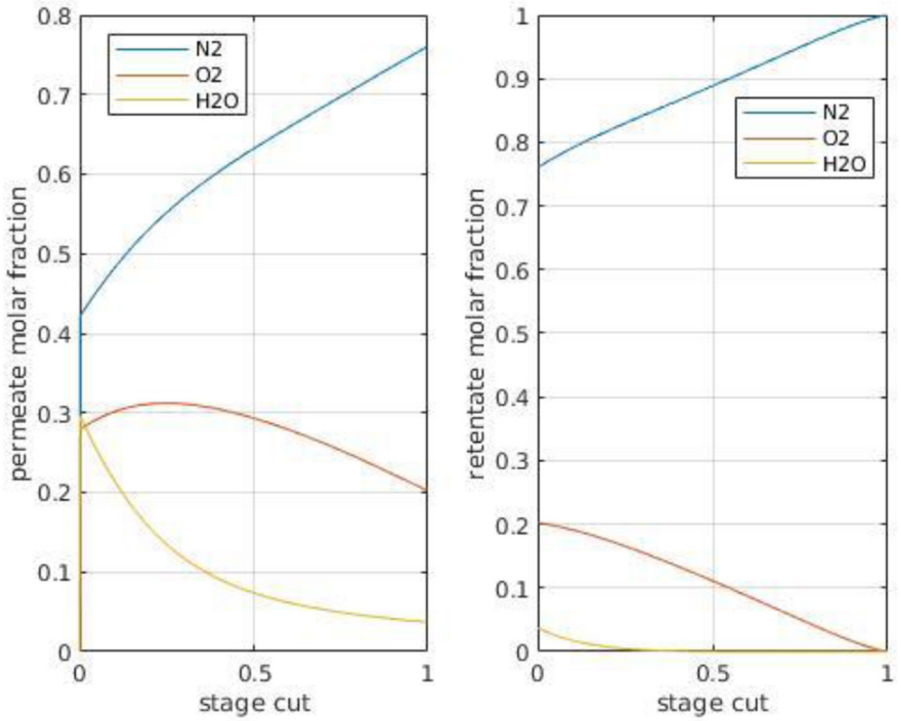

FIGURE 8 | Retentate (x_{out}) and permeate (y) compositions for different air compounds as a function of module stage cut with a Polyactive membrane (#2 in **Table 2**). Permeance in GPU: CO_2: 1,100, N_2: 28.5, O_2: 77.8, H_2O: 2,000 (Brinkmann et al., 2017). Pressure ratio (ψ) 0.01, cross plug flow conditions.

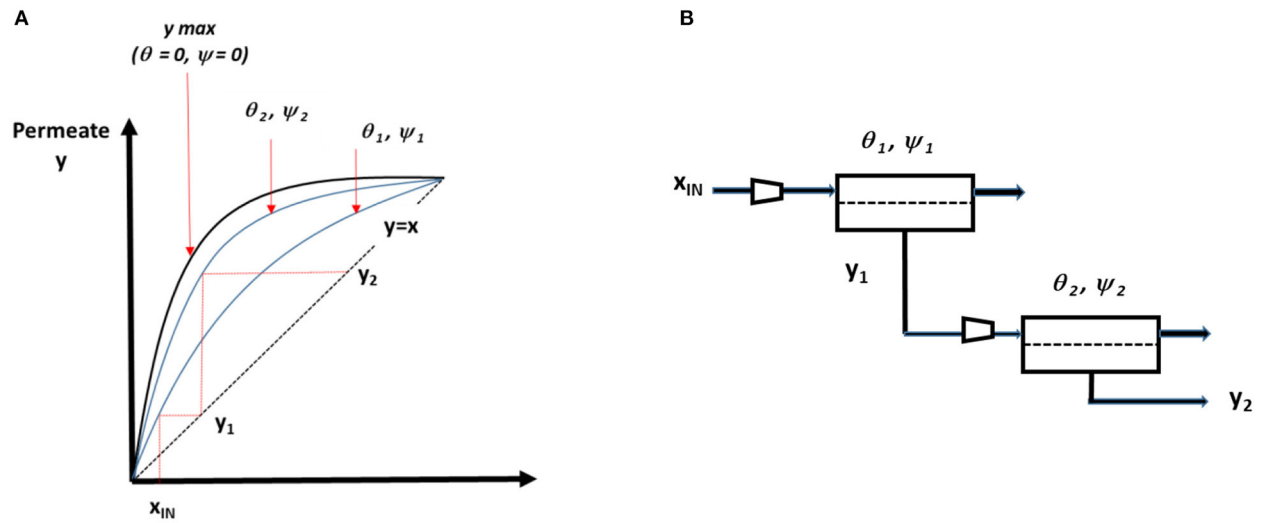

FIGURE 9 | Generic composition curve of a multistage membrane process for DAC and the corresponding two-stage process design. Simulations enable the permeate composition to be predicted for a set of pressure ratio, stage cut, and membrane performances. The maximal purity, shown by the upper bold line on graph **(A)** is obtained for vanishing pressure ratio (i.e., maximal energy requirement) and vanishing stage cut (i.e., minimal productivity). Different purity performances can be obtained for each set of ψ and θ. CO_2 purity can gradually increase as a function of each module outlet (permeate) and operating conditions. An infinite number of solutions are possible for a given target composition (y_2 for the two-stage example shown). The best set of ψ and θ values can be identified by process optimization methods if a cost function is defined. **(B)** Example of a multistage membrane process.

(Baker, 2004). Basically, each set of module pressure ratio and stage cut will generate a specific process separation performance, as shown on the graph in **Figure 9**. Taking the θ, ψ pair as a degree of freedom for each membrane stage, an increased CO_2 purity will be obtained according to the step-by-step construction shown in the figure. Taking 2 and 12% as the upper one-stage

TABLE 3 | Tentative comparison of key performance indicators of CCUS and DAC processes, based on existing studies.

Application	Process	CO_2 Purity (y)	Capture ratio (R)	Energy requirement* (E)		Process capacity (C) (kg $CO_2.m^{-3}.s^{-1}$)**	References
				GJ.ton^{-1} (Heat)	kWh.ton^{-1} (Power)		
CCUS from flue gas	Advanced solvents	0.9–0.99	0.8–0.9	2.5	–	5.10^{-2}	Steeneveldt et al., 2006; Favre and Svendsen, 2012
	Membranes	0.8–0.9	0.8–0.9	–	300	0.2	Favre, 2007; Merkel et al., 2010
Direct CO_2 capture from air (DAC)	Adsorption	0.3–0.9	0.5	6–7	–	10^{-5}–2.10^{-4}	Kulkarni and Sholl, 2012
			–	2–5	400	–	Kiani et al., 2020
	Absorption	0.9–0.99	0.5	10.7	1,400	3.10^{-4}	Kiani et al., 2020
	Commercial membrane (Polaris, 1 stage)	0.025	<0.1	–	18,000 >100,000	2.10^{-3}*** (vacuum) 2*** (compression)	This study
	Advanced membrane (HPM, 1 stage)	0.2	<0.1	–	3,000 >100,000	5.10^{-4}*** (vacuum) 0.5*** (compression)	This study

Taking a 2.7 conversion factor between heat and power (1 J power basis = 2.7 J thermal basis), 1 GJ heat basis corresponds to ~100 kWh.
***For absorption and adsorption processes, the productivity data indicated in the table are limited to the feed stage and do not include the volume of the regeneration (purge) unit.*
****For a 5,000 m^{-1} module specific surface area.*

purity level for polymeric and advanced membrane materials (**Figures 6A**, **7A**), respectively, purities around 50 and 98% could be theoretically obtained with a two-stage process. Nevertheless, because these calculations correspond to a minimum pressure ratio (that is a maximal energy requirement) and a minimal stage cut, a more realistic set of conditions should be selected. This suggests a systematic process synthesis study to be achieved in order to identify the most cost-effective two-stage solution for different CO_2 purity levels.

In the last step, a tentative comparison between the key performance indicators of membrane processes and absorption and adsorption processes is proposed and shown in **Table 3**. A synoptic graph showing the range of performances of DAC, CCS, and biomass is also shown in **Figure 10**. In **Table 3**, CCUS and DAC are considered so that the impact of CO_2 feed dilution is highlighted. Besides the separation performances, namely CO_2 purity (y) and recovery (R), existing data on energy requirement (E) and specific production capacity, expressed on a volume basis (C, expressed in kg $CO_2.m^{-3}.s^{-1}$) have been gathered. Production capacity C is of major interest in order to evaluate the footprint of the process. For membrane processes, C can be obtained from module productivity π as soon as a specific membrane surface area is defined; a typical value of 5,000 $m^2.m^{-3}$ has been taken for the membrane gas separation modules (Baker, 2004). The objective is to picture, roughly, the pros and cons of the different CO_2 capture processes. It is obvious that, for DAC, very few studies and data are available and the numbers indicated in the table should not be considered definitive. Given a large number of possibilities and process options, it is likely that different performance levels could be achieved in the near future.

It is interesting to note, however, that DAC energy efficiency and productivity performance are always far lower than post-combustion carbon capture. The very broad range of performance indicators for the different DAC processes should also be highlighted. For membrane processes, the very high energy requirement of compression is probably not acceptable (unless strategies such as energy recovery systems are used); vacuum pumping should thus be favored, ideally in combination

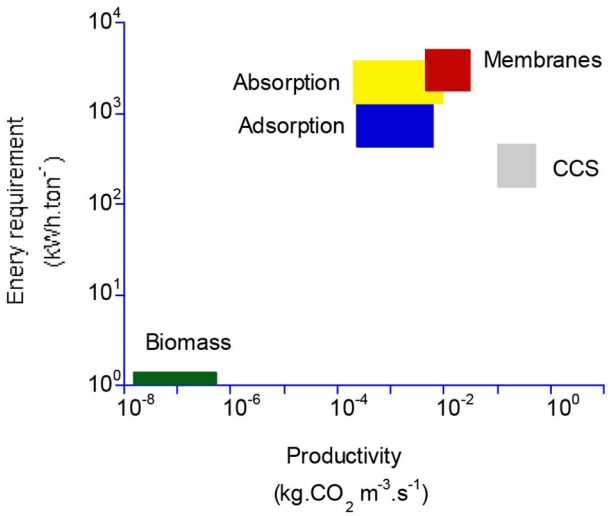

FIGURE 10 | Tentative map showing the energy and productivity performances of different DAC processes, compared to biomass and CCS. The range of performances for each technology is based on a very limited number of studies and should not be considered definitive. The very broad range of the two indicators is noticeable. Compared to biomass productivity in terms of carbon storage (Xu et al., 2014), DAC technologies offer a strong increase at the expense of a very large energy requirement.

with high-performance materials. In the latter case, the energy requirement is close to absorption processes, and the productivity is in the same range as that of the absorption columns. The major limitation of membrane processes compared to adsorption and absorption is the low achievable purity. To that extent, multistage processes should be investigated. It might be that a two-stage process, making use of high-performance membrane materials and an optimal set of operating conditions, offers attractive performances in terms of purity/energy/productivity.

In the last step, a preliminary estimate of the cost of the membrane processes for DAC has been made, based on a cost function previously proposed for air separation or natural gas treatment (Bozorg et al., 2019, 2020). A cost of \$50 per m^2 of the membrane has been taken and a two-step process with HPM membrane (**Figure 9B**), operated under vacuum (1 to 10 mBar) with a very low stage cut (around 0.01) has been used. The overall cost is obtained to be 3–10 k\$ per ton of CO_2. This is in agreement with preliminary estimates, which predict the capture cost to be \$1,000 or more per ton using rules of thumb estimations (House et al., 2011).

CONCLUSIONS

This study intended to explore the separation performances of a single-stage membrane module for the application of Direct Air Capture. Different membrane materials and a broad range of operating conditions have been investigated through a parametric engineering study.

The main conclusions of the study are summarized hereafter. First, with the existing (commercially available) membrane materials, the maximal outlet CO_2 purity of a single-stage unit is around 2%. This calls for either multistaged processes or high-performance materials in order to achieve higher purity levels. A two-stage process with existing commercial materials could achieve, at best, a purity in the range of 50%.

Given the strong sensitivity of purity *vs.* CO_2 recovery ratio R, a low module stage cut should be favored. This strongly differs from the carbon capture framework (for which $R > 0.8$) and should correspond to a negligible impact of module hydrodynamics (plug flow or perfectly mixed flow) on separation performances. Concentration polarization effects are negligible with the current polymeric membranes for carbon capture. A low stage cut will however generate high specific feed flow rates for a target permeate production level. In that case, a module pressure drop impact, which has been neglected in this study, is likely to play a role.

The specific energy requirement E is minimized by vacuum pumping operation, but a large membrane surface area is then required. Very high membrane permeance is thus of major importance in order to minimize the size of the installations.

The minimal specific energy requirement of membrane processes for DAC with currently commercially available materials is around 18,000 $kWh.ton^{-1}$, which is very high compared to the upper range of adsorption and absorption processes.

Polymeric membranes generate a CO_2 flux with significant oxygen content and water. This has to be taken into account, depending on the target use of the CO_2. For some thermal or catalytic conversion processes, oxygen and/or water can be problematic and additional polishing steps might be needed.

High-performance materials, more recently reported with CO_2/N_2 selectivity levels way above 100, offer promising breakthrough process possibilities. The concentration polarization effect should however be systematically taken into account in order to achieve rigorous evaluations in that case. CO_2 purity can reach 12% with a single-stage process and up to 99% with a two-stage process. Moreover, the energy requirement drops down to 3,000 $kWh.ton^{-1}$ for vacuum operation, with slightly higher specific productivity than absorption and adsorption processes. A preliminary cost analysis generates an overall cost in the range of 3–10 k\$ per ton of CO_2 for a two-stage process.

PERSPECTIVES

Globally speaking, process comparisons of gas separation technologies are rather limited (Prasad et al., 1994). This study offers the first set of data for a critical comparison of membrane processes for DAC, which is a very specific and challenging application; it can also be useful for preliminary technico-economical studies. In terms of perspectives, the rather low CO_2 purity that can be produced at the permeate side (y) is likely to be unacceptable for a series of applications. With currently commercially available membranes, the 2% CO_2 concentration could be of interest for the intensification of greenhouses or algae ponds. The 12% CO_2 concentration that could be achievable with high-performance materials (such as the one detailed in this study) globally corresponds to that of a power plant flue gas and may offer more attractive performances for direct use. It might also be that it still represents too large a dilution into N_2 (inert gas). In that event, multistage membrane units or hybrid processes could be of interest. It is expected that the results reported in this study will stimulate further efforts and help to identify the best place and role of membrane processes for DAC.

DATA AVAILABILITY STATEMENT

The raw data supporting the conclusions of this article will be made available by the authors, without undue reservation.

AUTHOR CONTRIBUTIONS

All authors listed have made a substantial, direct and intellectual contribution to the work, and approved it for publication.

REFERENCES

Baciocchi, R., Storti, G., and Mazzotti, M. (2006). Process design and energy requirements for the capture of carbon dioxide from air. *Chem. Eng. Process.* 45,1047–1058. doi: 10.1016/j.cep.2006.03.015

Baker, R. (2004). *Membrane Technology and Applications*. (Chichester, NY: J. Wiley). doi: 10.1002/0470020393

Baker, R. W., and Low, T. B. (2014). Gas separation membrane materials: a perspective. *Macromolecules* 47, 6999–7013. doi: 10.1021/ma501488s

Belaissaoui, B., Le Moullec, Y., Hagi, H., and Favre, E. (2014). Energy efficiency of oxygen enriched air technologies: cryogeny vs membrane separation. *Sep. Purificat. Technol.* 125, 142–150. doi: 10.1016/j.seppur.2014.01.043

Bounaceur, R., Berger, E., Pfister, M., Ramirez Santos, A. A., and Favre, E. (2017). Rigorous variable permeability modelling and process simulation for the design of polymeric membrane gas separation units: MEMSIC simulation tool. *J. Membr. Sci.* 523, 77–91. doi: 10.1016/j.memsci.2016.09.011

Bozorg, M., Addis, B., Piccialli, V., Castel, C., Pinnau, I., and Favre, E. (2019). Polymeric membrane materials for nitrogen production from air: a process synthesis study. *Chem. Eng. Sci.* 207, 1196–1213. doi: 10.1016/j.ces.2019.07.029

Bozorg, M., Ramírez-Santos, Á. A., Addis, B., Piccialli, V., Castel, C., and Favre, E. (2020). Optimal process design of biogas upgrading membrane systems: polymeric vs. high performance inorganic membrane materials. *Chem. Eng. Sci.* 225:115769. doi: 10.1016/j.ces.2020.115769

Brinkmann, T., Lillepärg, J., Notzke, H., Pohlmann, J., Shishatskiy, S., Wind, J., et al. (2017). Development of CO_2 selective poly(ethylene oxide)-based membranes: from laboratory to pilot plant scale. *Engineering* 3, 485–493. doi: 10.1016/J.ENG.2017.04.004

Castel, C., Wang, L., Corriou, J. P., and Favre, E. (2018). Steady vs unsteady membrane gas separation processes. *Chem. Eng. Sci.* 183, 136–147. doi: 10.1016/j.ces.2018.03.013

Chen, Z., Deng, S., Wei, H., Wang, B., Huang, J., and Yu, G. (2013). Polyethylenimine-impregnated resin for high CO2 adsorption: an efficient adsorbent for CO_2 capture from simulated flue gas and ambient air. *ACS Appl. Mater. Interfaces* 5, 6937–6945. doi: 10.1021/am400661b

Davidson, O., and Metz, B. (2005). *Special Report on Carbon Dioxide Capture and Storage*. Geneva: International Panel on Climate Change.

Favre, E. (2007). carbon dioxide recovery from post combustion processes: Can gas permeation membranes compete with absorption? *J. Membrane Sci.* 294, 50–59. doi: 10.1016/j.memsci.2007.02.007

Favre, E. (2017). "Polymeric membranes for gas separation," in *Comprehensive Membrane Science and Technology*, eds E. Drioli and L. Giorno (New York, NY: Elsevier). doi: 10.1016/B978-0-12-409547-2.12743-X

Favre, E., and Svendsen, H. F. (2012). Membrane contactors for intensified post-combustion carbon dioxide capture by gas–liquid absorption processes. *J. Membr. Sci.* 407–408, 1–7. doi: 10.1016/j.memsci.2012.03.019

Field, C. B., and Mach, K. J. (2017). Rightsizing carbon dioxide removal. *Science* 356, 706–707. doi: 10.1126/science.aam9726

Figueroa, D. J., Fout, T., Plasynski, S., McIlvried, H., and Srivastava, R. D. (2008). Advances in CO2 capture technology—the U.S. Department of energy's carbon sequestration program. *Int. J. Greenhouse Gas Control* 2, 9–20. doi: 10.1016/S1750-5836(07)00094-1

Gascon, J., and Kapteijn, F. (2010). Metal-organic framework membranes–high potential, bright future? *Angew. Chem. Int. Ed.* 49, 1530–1532. doi: 10.1002/anie.200906491

Gebald, C., Wurzbacher, J. A., Borgschulte, A., Zimmermann, T., and Steinfeld, A. (2014). Single-component and binary CO_2 and H_2O adsorption of amine- functionalized cellulose. *Environ. Sci. Technol.* 48, 2497–2504. doi: 10.1021/es404430g

Geim, A. K. (2009). Graphene: status and prospects. *Science* 324, 1530–1534. doi: 10.1126/science.1158877

Greenwood, K., and Pearce, M. (1953). The removal of carbon dioxide from atmospheric air by scrubbing with caustic soda in packed towers. *Trans. Inst. Chem. Eng.* 31, 201–207. doi: 10.1021/cen-v031n042.p4324

Hauchhum, L., and Mahanta, P. (2014). Carbon dioxide adsorption on zeolites and activated carbon by pressure swing adsorption in a fixed bed. *Int. J. Energy Environ. Eng.* 5, 349–356. doi: 10.1007/s40095-014-0131-3

House, K. Z., Baclig, A. C., Ranjan, M., van Nierop, E., Wilcox, J., and Herzog, H. (2011). Economic and energetic analysis of capturing CO2 from ambient air. *Proc. Natl. Acad. Sci. U. S. A.* 108, 20428–20433. doi: 10.1073/pnas.1012253108

Hwang, H. T., Harale, A., Liub, P., Sahimia, M., and Tsotsis, T. T. (2008). A membrane-based reactive separation system for CO_2 removal in a life support system. *J. Membrane Sci.* 315, 116–124. doi: 10.1016/j.memsci.2008.02.018

Kaldis, S. P., Kapantaidakis, G. C., and Sakellaropoulos, G. P. (2000). Simulation of multicomponent gas separation in a hollow fiber membrane by orthogonal collocation—hydrogen recovery from refinery gases. *J. Membr. Sci.* 173, 61–71. doi: 10.1016/S0376-7388(00)00353-7

Keith, D. (2009). Why capture CO_2 from the atmosphere?, *Science*, 325, 1654–1655. doi: 10.1126/science.1175680

Keith, D. W., Holmes, G., Angelo, D., and Heidel, K. (2018). A process for capturing CO_2 from the atmosphere. *Joule* 2, 1573–1594. doi: 10.1016/j.joule.2018.05.006

Kiani, A., Jiang, K., and Feron, P. (2020). Techno-economic assessment for CO2 capture from air using a conventional liquid-based absorption process. *Front. Energy Res.* 8:92. doi: 10.3389/fenrg.2020.00092

Kulkarni, A. R., and Sholl, D. S. (2012). Analysis of equilibrium based TSA processes for direct capture of CO_2 from air. *Ind. Eng. Chem. Res.* 51, 8631–8645. doi: 10.1021/ie300691c

Lackner, K. S. (2003). A guide to CO_2 sequestration. *Science* 300, 1677–1678. doi: 10.1126/science.1079033

Lackner, K. S. (2016). The promise of negative emissions. *Science* 354:714. doi: 10.1126/science.aal2432

Li, H., Song, Z., Zhang, X., Huang, Y., Li, S., and Mao, Y., et al. (2013). Ultrathin, molecular-sieving graphene oxide membranes for selective hydrogen separation. *Science* 342, 95–98. doi: 10.1126/science.1236686

Lüdtke, O., Behling, R. D., and Ohlrogge, K. (1998). Concentration polarization in gas permeation. *J. Membr. Sci.* 146, 145–157. doi: 10.1016/S0376-7388(98)00104-5

Lyndon, R., Konstas, K., Ladewig, B. P., Southon, P. D., Kepert, P. C., and Hill, M. R. (2013). Dynamic photo-switching in metalorganic frameworks as a route to low-energy carbon dioxide capture and release. *Angew. Chem. Int. Ed. Engl.* 52, 3695–3698. doi: 10.1002/anie.201206359

Merkel, T., Lin, H., Wei, X., and Baker, R. (2010). Power plant post-combustion carbon dioxide capture: an opportunity for membranes. *J. Membrane Sci.* 359, 126–139. doi: 10.1016/j.memsci.2009.10.041

Mourgues, A., and Sanchez, J. (2005). Theoretical analysis of concentration polarization in membrane modules for gas separation with feed inside the hollow-fibers. *J. Membr. Sci.* 252, 133–144. doi: 10.1016/j.memsci.2004.11.024

Pan, C.-Y., and Habgood, H. W. (1978). Gas separation by permeation part I. Calculation methods and parametric analysis. *Can. J. Chem. Eng.* 56, 197–209. doi: 10.1002/cjce.5450560207

Prasad, R., Shaner, R. L., and Doshi, K. J. (1994). "Comparison of membranes with other gas separation technologies," in *Polymeric Gas Separation Membranes*, eds D. R. Paul and Y. P. Yampol?skii (Boca Raton, FL: CRC Press, Inc.).

Rahaman, M. S. A., Zhang, L., Cheng, L. H., Xu, L. H., and Chen, H. L. (2012). Capturing carbon dioxide from air using a fixed carrier facilitated transport membrane. *RSC Adv.* 2, 9165–9172. doi: 10.1039/c2ra20783d

Robeson, L. M. (2008). The upper bound revisited. *J. Membrane Sci.* 320, 390–400. doi: 10.1016/j.memsci.2008.04.030

Sanz-Pérez, S., Murdock, C. R., Didas, S. A., and Jones, C. W. (2016). Direct capture of CO_2 from ambient air. *Chem. Rev.* 116, 11840–11876 doi: 10.1021/acs.chemrev.6b00173

Senftle, T. P., and Carter, E. A. (2017). The holy grail: chemistry enabling an economically viable CO2 capture. Utilization and storage strategy. *Acc. Chem. Res.* 50, 472–475. doi: 10.1021/acs.accounts.6b00479

Skoulidas, A. I., Ackerman, D. M., Johnson, J. K., and Sholl, D. S. (2002). Rapid transport of gases in carbon nanotubes. *Phys. Rev. Lett.* 89:185901. doi: 10.1103/PhysRevLett.89.185901

Steeneveldt, R., Berger, B., and Torp, T. A. (2006). CO2 capture and storage: closing the knowing doing gap. *Chem. Eng. Res. Dev.* 84–A9, 739–763. doi: 10.1205/cherd05049

Tepe, J. B., and Dodge, B. F. (1943). Absorption of carbon dioxide by sodium hydroxide solutions in a packed column. *Trans. Am. Inst. Chem. Eng.* 39, 255–276.

Verdegaal, W. M., Wang, K., Sculley, J. P., Wriedt, M., and Zhou, H. C. (2016). Evaluation of metal-organic frameworks and porous polymer networks for CO_2-capture applications. *ChemSusChem* 9, 636–643. doi: 10.1002/cssc.201501464

Wang, T., Lackner, K. S., and Wright, A. B. (2013). Moisture-swing sorption for carbon dioxide capture from ambient air: a thermodynamic analysis. *Phys. Chem. Chem. Phys*. 15, 504–514. doi: 10.1039/C2CP43124F

Weller, S., and Steiner, A. W. (1950). Separation of gases by fractional permeation through membranes. *J. Appl. Phys*. 21, 279–283. doi: 10.1063/1.1699653

Wilcox, J. (2020). An electro-swing approach. *Nat. Energy* 5, 121–122. doi: 10.1038/s41560-020-0554-4

Wright, A. B., Lackner, K. S., and Ginster, U. (2010). *Method and Apparatus for Extracting Carbon Dioxide from Air*.

Wu, D., Yi, C., Wang, W., Wang, Y., Yang, B., and Qi, S. (2019). Membrane separation process modeling for CO_2 partial removal in prepurification of air separation units. *Chem. Eng. Commun*. 12, 1676–1688. doi: 10.1080/00986445.2019.1570162

Wurzbacher, J. A., Gebald, C., Piatkowski, N., and Steinfeld, A. (2012). Concurrent separation of CO_2 and H_2O from air by a temperature- vacuum swing adsorption/desorption cycle. *Environ. Sci. Technol*. 46, 9191–9198. doi: 10.1021/es301953k

Xu, B., Yang, Y., Li, P., Shen, H., and Fang, J. (2014). Global patterns of ecosystem carbon flux in forests: a biometric data-based synthesis. *Glob. Biogeochem. Cycles* 28, 962–973. doi: 10.1002/2013GB004593

Yuan, S., Zou, L., Qin, J. S., Li, J., Huang, L., Feng, L., et al. (2017). Construction of hierarchically porous metal–organic frameworks through linker labilization. *Nat. Commun*. 8:15356. doi: 10.1038/ncomms15356

Conflict of Interest: The authors declare that the research was conducted in the absence of any commercial or financial relationships that could be construed as a potential conflict of interest.

LIST OF SYMBOLS

A	Effective membrane surface [m^2]
C	Process production capacity [kg $CO_2.m^{-3}.s^{-1}$]
E	Specific energy requirement [$J.mol^{-1}$ or $kWh.ton^{-1}$]
p	Pressure [Pa]
P	Permeance [$mol.s^{-1}.Pa^{-1}$ [SI] or GPU]
Q	flow rate [$mol.s^{-1}$]
R	perfect gas constant [8.314 $J.mol^{-1}.K^{-1}$]
R	CO_2 recovery ratio [–]
S	Dimensionless surface area [–]
T	Temperature [K]
x	Feed or retentate mole fraction [–]
y	Permeate mole fraction [–]
$\alpha*$	Membrane material selectivity [-]
π	Membrane module productivity [mol $CO_2.m^{-2}.s^{-1}$]
ψ	Pressure ratio [-]
θ	Stage cut [-]
Subscripts	
Atm,	Atmospheric
i	Component
IN	Relative to inlet
OUT	Relative to outlet
P	Permeate
Superscripts	
$'$	upstream (retentate)
$''$	downstream (permeate)
Acronyms	
CAPEX	Capital Expenses
CCS	Carbon Capture & Storage
CCU	Carbon Capture & Use
DAC	Direct Air Capture
GPU	Gas Permeation Unit
HPM	High Performance Material
MOF	Metal Oxide Frameworks
OPEX	Operating Expenses
PIM	Polymer of Intrinsic Microporosity
PSA	Pressure Swing Adsorption
R&D	Research & Development

Advantages of publishing in Frontiers

OPEN ACCESS
Articles are free to read for greatest visibility and readership

FAST PUBLICATION
Around 90 days from submission to decision

HIGH QUALITY PEER-REVIEW
Rigorous, collaborative, and constructive peer-review

TRANSPARENT PEER-REVIEW
Editors and reviewers acknowledged by name on published articles

Frontiers
Avenue du Tribunal-Fédéral 34
1005 Lausanne | Switzerland

Visit us: www.frontiersin.org
Contact us: frontiersin.org/about/contact

REPRODUCIBILITY OF RESEARCH
Support open data and methods to enhance research reproducibility

DIGITAL PUBLISHING
Articles designed for optimal readership across devices

FOLLOW US
@frontiersin

IMPACT METRICS
Advanced article metrics track visibility across digital media

EXTENSIVE PROMOTION
Marketing and promotion of impactful research

LOOP RESEARCH NETWORK
Our network increases your article's readership